DEPROGRAMMING SENESCENCE BY GENOMIC STABILIZING MOLECULES *IN VIVO*

Miss Sakawdaurn Yasom

จุฬาลงกรณ์มหาวิทยาลัย
Chulalongkorn University

A Dissertation Submitted in Partial Fulfillment of the Requirements
for the Degree of Doctor of Philosophy in Biomedical Sciences
Inter-Department of Biomedical Sciences
GRADUATE SCHOOL
Chulalongkorn University
Academic Year 2021
Copyright of Chulalongkorn University

การแก้ไขความชราในสัตว์ทดลองโดยโมเลกุลเพิ่มความเสถียรของจีโนม

น.ส.สกาวเดือน ยะสม

จุฬาลงกรณ์มหาวิทยาลัย
Chulalongkorn University

วิทยานิพนธ์นี้เป็นส่วนหนึ่งของการศึกษาตามหลักสูตรปริญญาวิทยาศาสตรดุษฎีบัณฑิต
สาขาวิชาชีวเวชศาสตร์ (สหสาขาวิชา) สหสาขาวิชาชีวเวชศาสตร์
บัณฑิตวิทยาลัย จุฬาลงกรณ์มหาวิทยาลัย
ปีการศึกษา 2564
ลิขสิทธิ์ของจุฬาลงกรณ์มหาวิทยาลัย

Thesis Title	DEPROGRAMMING SENESCENCE BY GENOMIC STABILIZING MOLECULES *IN VIVO*
By	Miss Sakawdaurn Yasom
Field of Study	Biomedical Sciences
Thesis Advisor	Professor APIWAT MUTIRANGURA, M.D., Ph.D.

Accepted by the GRADUATE SCHOOL, Chulalongkorn University in Partial Fulfillment of the Requirement for the Doctor of Philosophy

..... Dean of the GRADUATE SCHOOL
(Associate Professor YOOTTHANA CHUPPUNNARAT, Ph.D.)

DISSERTATION COMMITTEE

..... Chairman
(Assistant Professor AMORNPUN SEREEMASPUN, M.D., Ph.D.)

..... Thesis Advisor
(Professor APIWAT MUTIRANGURA, M.D., Ph.D.)

..... Examiner
(Professor SUTHILUK PATUMRAJ, Ph.D.)

..... Examiner
(Professor PITHI CHANVORACHOTE, Ph.D.)

..... External Examiner
(Associate Professor Siwanon Jirawatnotai, Ph.D.)

จุฬาลงกรณ์มหาวิทยาลัย
Chulalongkorn University

สกาวเดือน ยะสม : การแก้ไขความชราในสัตว์ทดลองโดยโมเลกุลเพิ่มความเสถียรของจีโนม. (DEPROGRAMMING SENESCENCE BY GENOMIC STABILIZING MOLECULES *IN VIVO*) อ.ที่ปรึกษาหลัก : ศ. ดร.อภิวัฒน์ มุทิรางกูร

ภาวะชราเป็นกลไกทางธรรมชาติของสิ่งมีชีวิตทุชนิดที่เกิดขึ้นตามเวลา โดยเกิดเองตามธรรมชาติและเป็นกระบวการที่เซลล์หลีกเลี่ยงไม่ได้ ภาวะชราของเซลล์เป็นผลมาจากการสะสมของความเสียหายในระดับเซลล์ โดยที่เซลล์ชราไม่สามารถซ่อมแซมตนเองได้ในอัตราเร็วที่เพียงพอเมื่อเทียบกับความเสียหายที่เกิดขึ้นและสะสมในเซลล์ตามกาลเวลา จากผลการศึกษาพบว่าการลดลงของการเติมหมู่เมททิลทั่วทั้งจีโนม (genome-wide หรือ global hypomethylation) และการลดลงของการเติมหมู่เมททิลบนลำดับดีเอนเอที่ตำแหน่งอะลู หรือ บี1 (Alu or B1 elements) สามารถใช้เป็นตัวบ่งชี้ภาวะชราของเซลล์ โดยไม่เพียงแต่พบในภาวะชราของเซลล์แต่ยังพบในรายงานการศึกษาระดับคลินิกของโรคที่เกี่ยวข้องกับภาวะชราในเซลล์มนุษย์อีกด้วย จากหลักฐานการศึกษาวิจัยไม่นานมานี้พบว่าการมีหมู่เมททิลลบนลำดับดีเอนเอที่ตำแหน่งอะลูในระดับสูง (Alu hypermethylation) สามารถกระตุ้นการแบ่งตัวของเซลล์เพาะเลี้ยงของสัตว์เลี้ยงลูกด้วยน้ำนมและเซลล์ยีสต์ และยังสามารถเพิ่มอัตราการรอดชีวิตของเซลล์เพาะเลี้ยงเมื่อเลี้ยงเซลล์ในสภาวะที่มีสารออกฤทธิ์ทำลายดีเอ็นเอ (DNA-damaging agents) นอกจากนี้ มีการศึกษาของโปรตีนเอชเอ็มจีบี 1 ส่วนบ็อกซ์เอ (Box-A of high mobility group box 1 (HMGB1) ซึ่งเป็นโปรตีนตัวหนึ่งในนิวเคลียสที่โดยปกติทำหน้าที่จับและกำหนดโครงสร้างความโค้งงอของสายดีเอ็นเอ (DNA chaperone protein) พบว่าโปรตีนส่วนบ็อกซ์เอนี้ ทำหน้าที่เป็นโปรตีนเพิ่มความเสถียรให้จีโนม (genomic stabilizing protein) โดยการสร้างช่องว่างบนสายดีเอ็นเอ ที่เรียกว่า physiologic replication-independent endogenous DNA double-strand breaks (phy-RIND-EDSBs) และภายหลังได้ปรับเปลี่ยนชื่อเป็น youth-associated genome stabilizing DNA gaps (Youth-DNA-GAPs) โดยประโยชน์ของช่องว่างบนสายดีเอ็นเอหรือ Youth-DNA-GAPs นี้ ช่วยลดแรงตึงบนสายดีเอ็นเอทำให้จีโนมเสถียรมากขึ้น การศึกษาเพิ่มเติมพบว่าโปรตีนเอชเอ็มจีบี 1 ส่วนบ็อกซ์เอเพิ่มการแบ่งตัวและลดการทำลายดีเอ็นเอของเซลล์เพาะเลี้ยงของสัตว์เลี้ยงลูกด้วยน้ำนม การลดลงของระดับของโปรตีนเอชเอ็มจีบี 1 ส่วนบ็อกซ์เอส่งผลให้ระดับของช่องว่างบนสายดีเอ็นเอ (Youth-DNA-GAPs) ลดลงพร้อมทั้งพบการทำลายดีเอ็นเอเพิ่มขึ้นในเซลล์ชราอีกด้วย การศึกษาครั้งนี้ได้ใช้โมเดลหนูทดลองแก่ที่เกิดจากการเหนี่ยวนำด้วยสาร ดี-กาแลคโตส ซึ่งสามารถกระตุ้นให้เกิดทำลายดีเอ็นเอและนำไปสู่ภาวะแก่ชราของอวัยวะต่างๆ ได้แก่ ตับและสมองทำงานบกพร่องเนื่องมาจากเซลล์มีความความเครียดออกซิเดทีฟมากเกินไป เช่นเดียวกับที่พบในภาวะชราตามธรรมชาติ นอกจากนี้ ในการศึกษาครั้งนี้ได้ใช้โมเดลหนูทดลองแผลเบาหวานชนิดที่ 1 ซึ่งกระตุ้นด้วยสารสเตรปโตโซโตซินอีกด้วย ผลการศึกษาพบว่าโปรตีนเอชเอ็มจีบี 1 ส่วนบ็อกซ์เอ สามารถใช้รักษาความผิดปกติของการทำงานของตับที่พบในหนูแก่ทั้งสองโมเดล ทำให้จำนวนเซลล์แก่ในตับลดลง โดยพบการลดลงของ SA-β-gal และโปรตีนที่บ่งชี้ภาวะชราระดับเซลล์ $p16^{INK4A}$ และ p21 ซึ่งสอดคล้องกับการลดลงของโปรตีนที่บ่งชี้ภาวะที่ดีเอ็นเอถูกทำลาย γ-H2A.X ในเซลล์ตับและยังส่งผลให้การทำงานของสมองในหนูแก่ดีขึ้นอีกด้วย การรักษา

สาขาวิชา	ชีวเวชศาสตร์ (สหสาขาวิชา)	ลายมือชื่อนิสิต .....
ปีการศึกษา	2564	ลายมือชื่อ อ.ที่ปรึกษาหลัก .....

จุฬาลงกรณ์มหาวิทยาลัย
Chulalongkorn University

6087799920 : MAJOR BIOMEDICAL SCIENCES
KEYWORD: Cellular senescence DNA damage Aging Epigenetics DNA hypomethylation Diabetic wound healing

Sakawdaurn Yasom : DEPROGRAMMING SENESCENCE BY GENOMIC STABILIZING MOLECULES *IN VIVO*. Advisor: Prof. APIWAT MUTIRANGURA, M.D., Ph.D.

Aging is the inevitable, time-dependent, natural process in all living cells, resulting from the accumulation of cellular damage with insufficient cell repair. Global hypomethylation and Alu (B1) hypomethylation become aging indicators, which are commonly found not only in cellular aging but also in human clinical studies of age-related diseases. Much evidence indicates that Alu (B1) hypermethylation could promote both mammalian and yeast cell growth and considerably increase cell survival by reducing the susceptibility to DNA-damaging agents. Also, Box-A of high mobility group box 1 (HMGB1), a DNA chaperone protein with different roles, is reported to be a genomic stabilizing protein by promoting physiologic replication-independent endogenous DNA double-strand breaks (phy-RIND-EDSBs). Phy-RIND-EDSBs, also called youth-associated genome stabilizing DNA gaps (Youth-DNA-GAPs), are beneficial DNA gaps, releasing DNA tension to promote genomic stability. Box-A of HMGB1 protein increased cell proliferation and declined DNA damage in mammalian cells. The decrease in HMGB1 protein level results in the reduction of phy-RIND-EDSBs (Youth-DNA-GAPs) and the high frequency of DNA damage, found in aging cells. Recently, D-galactose (D-gal)-induced animal is widely used as a pre-clinical aging model, that exhibits cellular aging phenotypes and impaired aging organ functions in liver and brain, due to excessive oxidative stress. D-gal induction also contributes to systemic DNA damage accumulating in many organs as found in naturally aging. Consistently, a type 1 diabetic rat model induced by streptozotocin (STZ) is widely employed as a mimetic model for the study of diabetic wounds, which also demonstrates the defects in wound repair and the increased DNA damage. Herein, we reported that Box-A of HMGB1 treatment in D-gal-induced and naturally aging rats alleviated the age-related phenotypes; abnormal liver function parameters, a presence of senescence-associated β-galactosidase (SA-β-gal), the expressions of aging marker protein $p16^{INK4A}$ and p21, DNA damage marker γ-H2A.X protein in the aging rat liver. These led to the restoration the impaired aging liver functions and aging brain by showing the improved cognitive functions in two aging rat models. In

Field of Study:	Biomedical Sciences	Student's Signature .....
Academic Year:	2021	Advisor's Signature .....

ACKNOWLEDGEMENTS

I would like to express my sincere gratitude to my thesis advisor, Professor Dr. Apiwat Mutirangura, for his guidance and intellectual advice, which allowed me to complete this precious research work in the Center of Excellence in Molecular Genetics of Cancer and Human Disease, Faculty of Medicine, Chulalongkorn University. He has always been a mentor and supporter to give me a great experience in the scientific world and a positive attitude toward life during the Ph.D. study. Moreover, I would like to thank the funding supported by The 100th Anniversary Chulalongkorn University for Doctoral Scholarship, Chulalongkorn University.

I also wish to express my deep gratitude to my colleagues and friends in the Faculty of Medicine, Chiang Mai University, and Mahidol University for facilitating and collaborating throughout the research projects. In addition, I would like to thank my lab member(s) for the collaboration in animal work, especially in the histological parameter assessment. Finally, I greatly appreciate the generous support from my family members, particularly my mother and my younger sister, for understanding my research work and patiently being by my side during the Ph.D. candidate's lifetime.

Sakawdaurn Yasom

จุฬาลงกรณ์มหาวิทยาลัย
CHULALONGKORN UNIVERSITY

TABLE OF CONTENTS

Page

ABSTRACT (THAI) iii

ABSTRACT (ENGLISH) iv

ACKNOWLEDGEMENTS v

TABLE OF CONTENTS vi

CHAPTER I 1

LITERATURE REVIEW 1

1. Age-Related DNA Hypomethylation Induces Genomic Instability and Diseases 1

2. DNA Methylation Status Influences on DNA Damage in Aging and Cell Growth 4

3. Box-A of HMGB1 Protein, a Promising Candidate to Reduce Genomic Instability in Aging 12

4. D-Galactose-Induced Aging Animals, an Imitated Natural Aging Model, and Naturally Aging Animals with Defective Liver and Cognitive Functions 20

5. Wound Healing Impairment in Diabetes Relevant to Global Hypomethylation and DNA Damage 23

CHAPTER II 27

RESEARCH CONCEPT 27

1. Research questions 27

2. Hypotheses 27

3. Objectives 27

CHAPTER III 29

MATERIALS AND METHODS 29

CHAPTER IV 43

RESULTS AND DISCUSSION 43

PART 1: A novel formula of gene/Ca-P nanoparticle delivery *in intro* and *in vivo* study. 43

PART 2: Box A of HMGB1 treatment in two aging rat models 52

จุฬาลงกรณ์มหาวิทยาลัย
Chulalongkorn University

PART 3: Box A of HMGB1 intervention in a micropig model.....66
PART 4: Box A of HMGB1 treatment in diabetic rat wound 67
CHAPTER V 86
CONCLUSION.....86
A summary figure for B1 siRNA intervention in a model of diabetic rat wound. ..87
REFERENCES 100
VITA.....102

จุฬาลงกรณ์มหาวิทยาลัย
Chulalongkorn University

CHAPTER I

LITERATURE REVIEW

1. Age-Related DNA Hypomethylation Induces Genomic Instability and Diseases

Decreasing methylation level found throughout a whole genome in aging cells causes genomic instability (Pal S and Tyler JK, 2016) which contributes to age-associated disorders (Wilson AS, *et al*, 2007) depicted as a diagram in **Figure 1-1**. Age-related epigenetic deregulation shows not only hypermethylation in certain specific gene promoters resulting in the silence of tumor-suppressor genes in various cancers (Finkel T, *et al*. 2007, Pal S and Tyler JK, 2016). But also, global hypomethylation existing along DNA is positively associated with advancing age (Jung M and Pfeifer GP, 2015). DNA methylation is one of the epigenetic regulation processes within a cell transferring a methyl group (CH_3-) into a 5-carbon position of the cytosine ring of the DNA strand by an action of DNA methyltransferases (Moore LD, *et al*, 2013). Recently, the study of methylation status comparison between newborn and centenarian DNA unveiled the increase in the hypomethylated Cytosine-phosphate-Guanine (CpG) throughout centenarian genome content compared with the neonate (Heyna H, *et al*, 2012). The findings emphasized that the paramount of increasing genome-wide hypomethylation might associate with an occurrence of age-related diseases accompanied by aging phenotypes and should be further investigated.

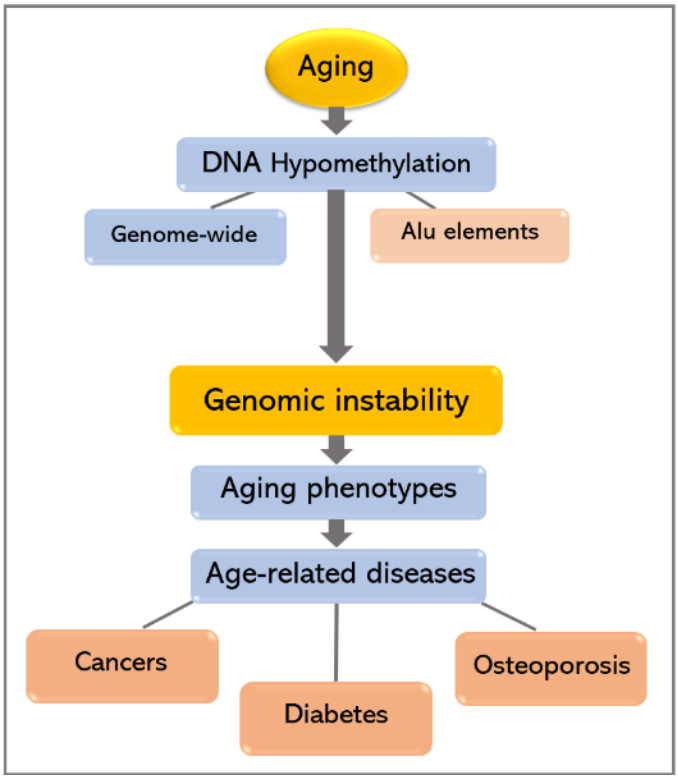

Figure 1-1: Global hypomethylation and *Alu* hypomethylation in aging cells resulting in genomic instability contributes to aging phenotypes and age-related diseases; for instance: cancers, diabetes, and osteoporosis.

Many studies demonstrated that this epigenetic mark in the short-interspersed elements (SINEs), especially *Alu* retrotransposon elements, plays a critical role in genomic stability (Mustafina OE, 2013). *Alu* elements are the most abundant

mobile element found in the human DNA as high as ~10^6 copies per human genome. Additionally, the position of CpG resided in *Alu* elements is up to 33% of total CpG sites, that plays a major part in DNA methylation status (Kramerov DA, *et al*, 2005). According to the study by Jintaridth P and Mutirangura A, the correlation of hypomethylation status of some certain interspersed repetitive sequences (IRSs) with increased age has been reported (Jintaridth P and Mutirangura A, 2010). The methylation status of *Alu*, long interspersed element (LINE)-1, and human endogenous retrovirus-K (HERV-K) from human peripheral blood mononuclear cells of 177 individuals aged 20 to 88 years was characterized. The finding showed that the increase in hypomethylation levels of *Alu* elements (r=0.452, P<0.001) and HERV-K (r=0.326, P<0.001), but not LINE-1 (r=0.145, P=0.055), was associated with advancing age as demonstrated in **Figure 1-2**. Hence, hypomethylation of IRSs, particularly *Alu* elements, is age-dependent process and could be one of major contributors to cause cellular vulnerability.

Moreover, an increase in *Alu* hypomethylation in aging cell also results in genomic instability leading to age-related diseases (Jung M and Pfeifer GP, 2015). The study by

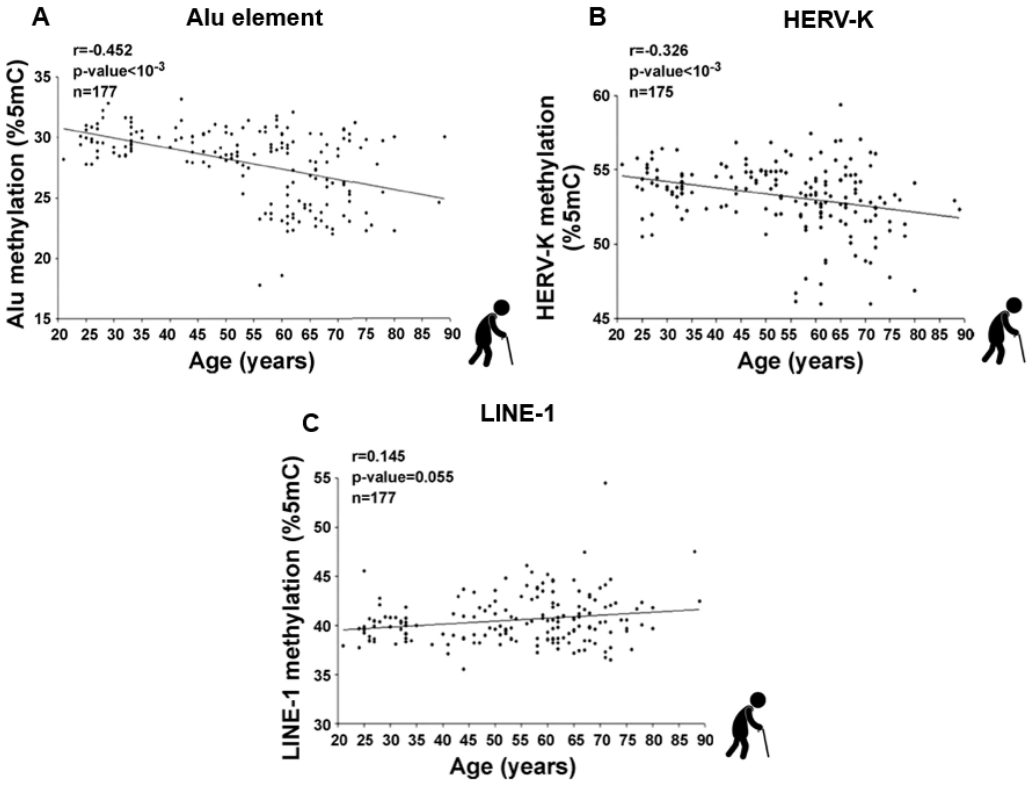

Jintaridth P and Mutirangura A, Physiol Genomics, 2010

Jintaridth P. and colleagues revealed that the decrease in the methylation status of *Alu* elements in white blood cells of post-menopausal women with osteoporosis was positively associated

Figure 1-2: The significant negative associations between age and methylation levels of each interspersed repetitive sequence including *Alu* element (r=-0.452, P<0.001) and HERV-K (r=-0.326, P<0.001) were observed (A and B, respectively). There was no significant correlation between LINE-1 methylation level and advancing age (r=0.145, P=0.055).

with advancing age together with the lowering of bone mass density (P<0.05) (Jintaridth P, *et al*, 2013). Correspondingly, they also reported that the same age patients with osteopenia and osteoporosis demonstrated the significant higher *Alu* hypomethylation than age-matched healthy individuals (P=0.0005 and P=0.003, respectively). The results highlighted that *Alu* hypomethylation correlated with one of age-related phenotypes as the lowering of bone mass density which is an age-independent phenomenon.

In addition, the correlation between diabetes mellitus (DM), one of the most common diseases in the elderly population worldwide (Kirkman MS, *et al*, 2012), and the alteration of DNA methylation has also been reported (Rönn T and Ling C, 2015). Epigenetic changes, particularly loss of DNA methylation, in diabetes are caused by oxidative stress resulting in pathogenesis of type 2 diabetes (Rönn T and Ling C, 2015). Interestingly, the recent study revealed that the decrease in *Alu* methylation levels was found in white blood cells obtained from DM patients in comparison with normal control (Thongsroy J, *et al*, 2017). As demonstrated in **Figure 1-3**, DM patients, pre-DM, and normal controls which are classified by fasting blood glucose (N=80 each group) or hemoglobin A1c (HbA1c) (N=85, 113, and 42, respectively) were determined the levels of *Alu* methylation. The results showed that the higher

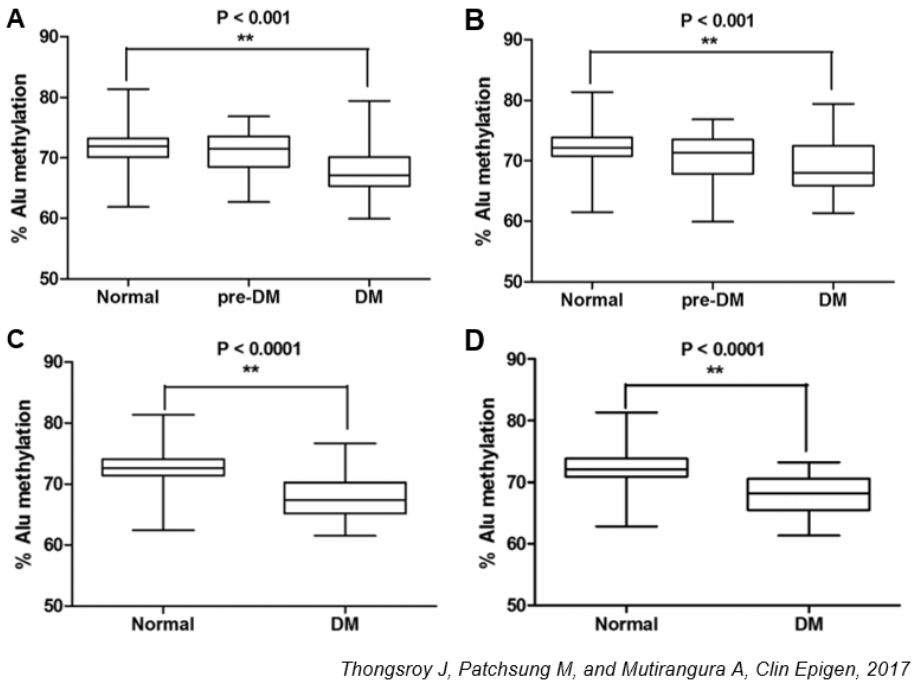

Figure 1-3: The levels of *Alu* methylation were significantly correlated with diabetes classified either fasting blood sugar (**A**) or HbA1c (**B**) (P<0.001) in age-dependent manner. Age-matched *Alu* methylation levels were also significantly associated with diabetic indicators (**C** and **D**, P<0.0001).

Alu hypomethylation was detected in the DM group (P<0.001) when compared to the normal controls as exhibited in **Figure 1-3 A** and **B**. Additionally, they also investigated the association between Alu methylation levels and diabetes after age adjustment as displayed in **Figure 1-3 C** and **D**. The findings showed that increased *Alu* hypomethylation was observed in DM patients (P<0.0001) compared with normal group in age-independent manner. Interestingly, the significant negative correlations between *Alu* methylation and blood pressure including systolic pressure (r^2=-0.3465, P=0.0012) and diastolic pressure (r^2=-0.3056, P=0.0045) were observed in DM patients classified by HbA1c (Thongsroy J, *et al*, 2017).

Hence, it is believed that the epigenetic deregulation as *Alu* hypomethylation, which directly has an influence on global hypomethylation, leads to genomic instability in aging contributing to a pathogenesis of some certain age-related diseases.

2. DNA Methylation Status Influences on DNA Damage in Aging and Cell Growth

Compiling many studies involved in aging, epigenetic modification as *Alu*

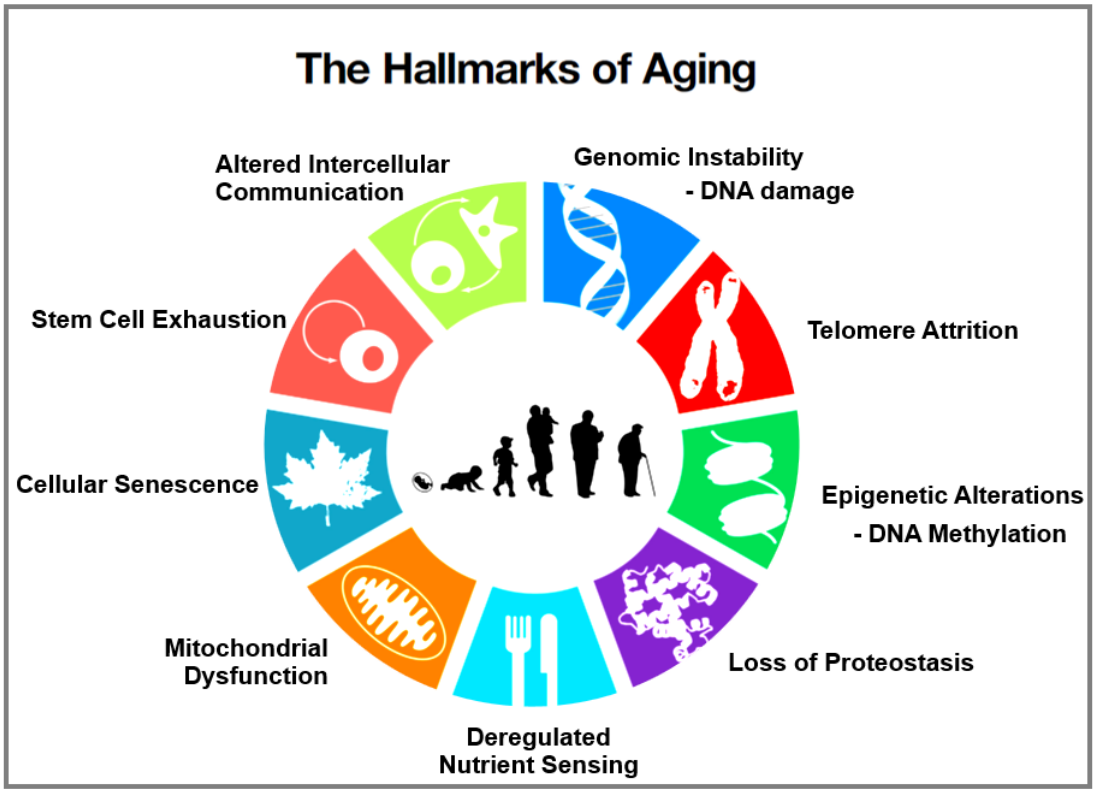

Lopez-Otin C, et al. Cell, 2013

hypomethylation plays a critical role in underlying mechanism to induce genomic instability, eventually resulting in cellular aging (Pal S and Tyler JK, 2016, Lopez-Otin C, *et al*, 2013). Aging is a natural spontaneous process that accumulates detrimental changes in molecular,

cellular, tissue, and organ levels over time. It is believed that the age-related changes are mainly caused by the collective cellular damage as well as the insufficient cellular repair process in aging cells (Lopez-Otin C, *et al*, 2013). Both of genomic instability and epigenetic alterations, which are defined as common features of the hallmarks of aging (**Figure 1-4**), are responsible for the primary causes of cellular damage and are also profoundly linked to each other (Wilson AS, *et al*, 2007, Lopez-Otin C, *et al*, 2013). DNA lesions, which are caused by either endogenous or exogenous sources, are naturally found in a common cellular fate and repaired by various DNA repair mechanisms (Tubbs A and Nussenzweig A, 2017). Hence, the aging process can indicate the imbalance of DNA damage and DNA repair including high frequencies of DNA lesions with insufficient DNA repairs.

Figure 1-4: Common features of the hallmarks of aging. Genomic instability resulting from DNA damage and epigenetic modification, especially DNA methylation, which are primary causes of cellular damage are responsible for main underlying mechanisms of the aging process. In response to the cellular aging process, an inevitable mechanism as cellular senescence also provides cellular survival.

Since DNA is used as the template for transcription and translation, the stabilization of DNA is a crucial process thorough life for maintaining DNA strength affecting on health and lifespan. As mentioned previously, endogenous, and exogenous agents can induce the DNA lesions as demonstrated in **Figure 2-5** (Tubbs A and Nussenzweig A, 2017). The sources of endogenous DNA comprise reactive oxygen species (ROS), replication errors as well as spontaneous hydrolytic reactions. The DNA is also exposed to chemical, physical, biological ingredients and UV lights, for instance. The highest DNA damage found in cells (per cell per day) is a DNA single-strand break (SSB) which occurs as high as 55,000 positions. In contrast to a DNA double-strand break (DSB), the frequency of this type of DNA damage is found approximately 25 positions per cell per day which is lower but more dangerous than the SSB. The second most abundant DNA damage found in cells is the abasic site or apurinic/apyrimidinic site, AP site (approximately 12,000/6 00 positions per cell per day for apurinic sites and apyrimidinic sites, respectively). Normally, AP sites spontaneously occur in the DNA or can be activated by the exposure to many sources of DNA damage. However, AP sites can also be triggered as intermediates in base excision repair pathway. In BER pathway, two types of enzymes involved in the process include a variety of DNA glycosylases to recognize and cleave a damaged base and an AP endonuclease to cleave the AP site forming a single-strand break (SSB). These DNA damages, which cause genomic instability, are generally repaired by several distinct mechanisms consisting of base excision repair (BER), nucleotide

จุฬาลงกรณ์มหาวิทยาลัย
Chulalongkorn University

excision repair (NER), single-strand break repair (SSBR), and homologous recombination (HR) (Tubbs A and Nussenzweig A, 2017). The other type of accumulating DNA damages that can be induced by reactive oxygen species (ROS) is 8-oxoguanine, also called 8-oxo-2'-deoxyguanosine, or 8-hydroxyguanine (8-OHdG) (Cheng KC, *et al*, 1992). Under oxidative stress condition, guanine (G) base can be interacted with ROS becoming 8-hydroxyguanine and leading to mismatch with adenine (A) base instead of cytosine (C) base. Because of G to T and C to A substitutions from 8-hydroxyguanine, a removal of 8-OHdG from the DNA can be assisted by oxoguanine glycosylase (OGG) enzyme in base excision repair (BER) mechanism (Tubbs A and Nussenzweig A, 2017).

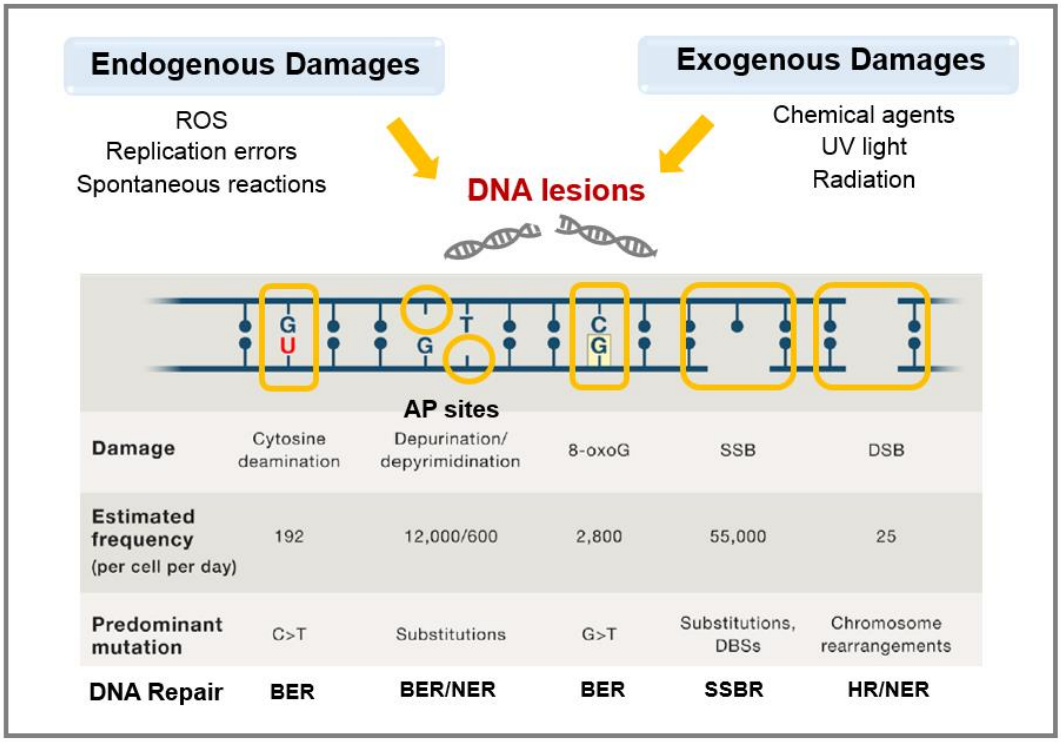

Damage	Cytosine deamination	Depurination/ depyrimidination	8-oxoG	SSB	DSB
Estimated frequency (per cell per day)	192	12,000/600	2,800	55,000	25
Predominant mutation	C>T	Substitutions	G>T	Substitutions, DBSs	Chromosome rearrangements
DNA Repair	BER	BER/NER	BER	SSBR	HR/NER

Adapted from Lopez-Otın C, et al. Cell, 2013 and Anthony Tubbs, et al. Cell, 2017

Figure 1-5: Prominent DNA damages caused by endogenous and exogenous sources are found in normal cells and can contribute to cellular aging. The three most abundant DNA damages include DNA single-strand break (SSB), apurinic/apyrimidinic (AP) site, and 8-oxoguanine (8-oxoG), respectively.

As stated previously, the *Alu* hypomethylation was significantly related to both of a severity of type 2 DM (Thongsroy J, *et al*, 2017) and osteoporosis (Jintaridth P, *et al*, 2013), which are age-associated diseases. These findings emphasized that *Alu* methylation level obviously plays some certain specific roles in cellular aging phenotypes underlying age-related

diseases. More recently, it has been reported that hypermethylated *Alu* elements induced by Alu siRNA could prevent genomic instability (Patchsung M, *et al*, 2018). The study aimed to specifically enhance the methylation level of *Alu* elements using Alu siRNA transfection in HeLa cells and human embryonic kidney (HEK) 293 cells. They reported that Alu siRNA

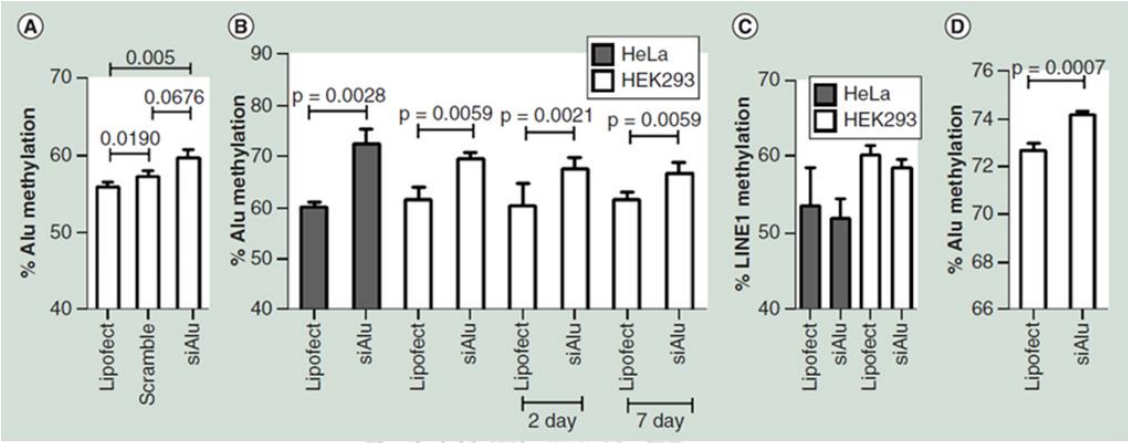

Patchsung M, et al, Epigenomics, 2018

transfection system significantly increased *Alu* methylation compared to the Lipofectamine-negative control (P=0.005) as shown in **Figure 1-6 A**. Correspondingly, the same results of Alu siRNA transfection were observed in both HeLa cells and HEK293 cells (P=0.0028 and P=0.0059, respectively) compared to negative controls and the methylated *Alu* elements sustainably increased (P=0.0059) even in 7 days after Alu siRNA transfection (**Figure 1-6 B**). Alu siRNA transfection specifically promoted the methylation level of Alu elements due to no significant changes in LINE-1 methylation levels in both cell types (**Figure 1-6 C**). Similarly, Alu siRNA transfection significantly increased the percentage of Alu methylation in periodontal ligament fibroblasts when compared to lipofectamine transfection control (P=0.0007, **Figure 1-6 D**) (Patchsung M, *et al*, 2018).

Figure 1-6: Alu hypermethylation by Alu siRNA transfection. (**A**) The percentage of Alu methylation after Alu siRNA transfection compared with the Lipofectamine and siRNA (scramble) negative controls. (**B**) The percentage of Alu methylation in HeLa cell (grey bar) and HEK293 cell (white bar) at 24 hours, 2 days, and 7 days after Alu siRNA transfection. (**C**) The percentage of LINE-1 methylation in HeLa cell and HEK293 cells after Alu siRNA transfection.

In addition to specific methylated Alu enhancement, Patchsung M and colleagues also investigated the correlation between increased *Alu* methylation and cell proliferation after Alu siRNA transfection using 3-[4,5-dimethylthiazol-2-yl]-2,5 diphenyl tetrazolium bromide or MTT assay, absolute cell count, and population doublings. Interestingly, Alu siRNA

transfection significantly encouraged cell proliferation of HEK293, and periodontal ligament cells determined by MTT assay (**Figure 1-7 A** and **C**, respectively). Consistently, the absolute cell count of HEK293 cells was enumerated for three days after Alu siRNA transfection and the result showed that the significant higher cell number when compared with control cell number (**Figure 1-7 B**). Expectedly, population doublings of Alu siRNA transfected periodontal ligament cells were examined at 13^{th} and 14^{th} passages and demonstrated the significant increase in population doublings (P=0.0005 and P=0.0003, respectively) as shown in **Figure 1-7 D** (Patchsung M, *et al*, 2018).

In accordance with the study by Rerkasem K. *et al*., the levels of total *Alu* and LINE-1 methylation were determined in peripheral mononuclear cells obtained from 249 volunteers aged 20 years ± 6 months (Rerkasem K. *et al*, 2015). They also explored the correlation of specific IRS methylation status and the participant's phenotypes at birth. According to WHO standard, the designated catch-up growth (CUG) when infant weight during the first year was >0.67 of the standard index. The findings revealed that the CUG group had the significant higher percentage of the mean total Alu methylation than the non-CUG group as shown in **Figure 1-8 A**, (39.61% and 33.66% respectively, P<0.0001). On the contrary, the mean level of LINE-1 methylation was not related to the CUG parameter as displayed in **Figure 1-8 B.** The accumulating data indicated that Alu methylation status directly involved in not only aging phenotypes, but also cell proliferation and human growth rate.

จุฬาลงกรณ์มหาวิทยาลัย
Chulalongkorn University

As mentioned earlier, the preceding study unveiled that *Alu* hypermethylation contributed to prevent DNA damages *in vitro* study (Patchsung M, *et al*, 2018). The percentage of cell survival was elucidated after Alu siRNA transfection and hypermethylated *Alu* confirmation in HEK293 and periodontal ligament (PDL) cells when exposed to DNA damage agents. Intriguingly, *Alu* hypermethylation significantly reduced the susceptibility to DNA damage and enhanced the percentage of cell survival in both HEK293 cells (**Figure 2-9 A** and **C**) and PDL cells (**Figure 2-9 B** and **D**) when exposed to methyl methane sulphonate (MMS) and H_2O_2 at the higher concentrations (1.0 to 2.0 mM and 100 to 150 µM, respectively) compared to control

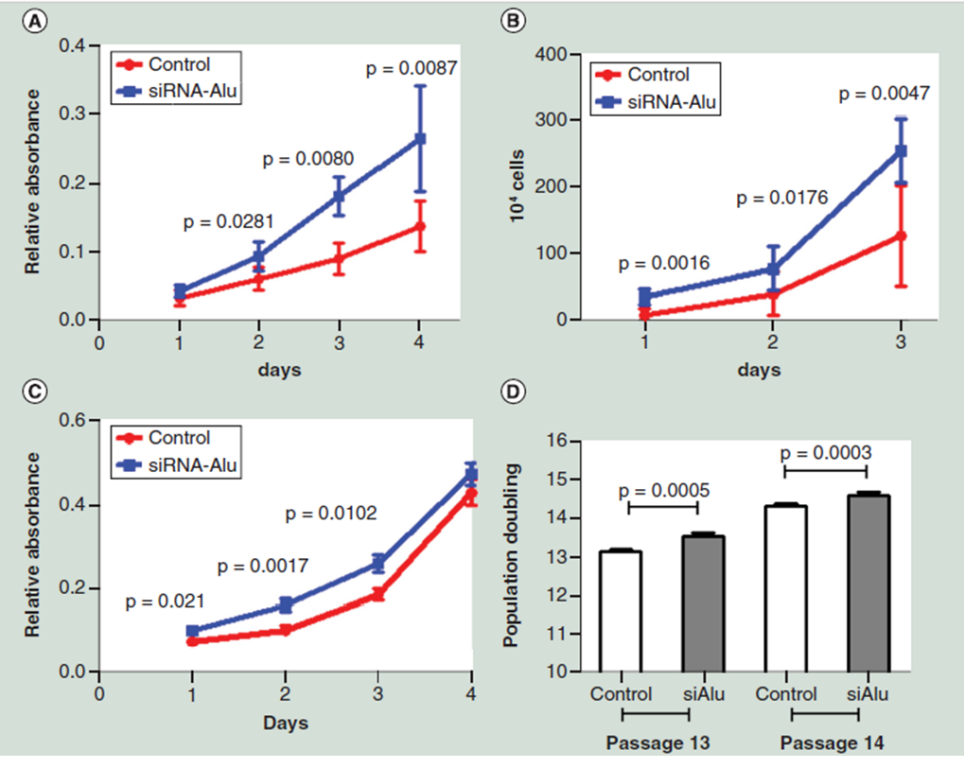

Patchsung M, et al, Epigenomics, 2018

Figure 1-7: Assessment of MTT assay (**A** and **C**), absolute cell count (**B**), and population doublings (**D**) to investigate the effect of Alu siRNA transfection on cell proliferation in HEK293 cell (**A** and **B**) and periodontal ligament cell (**C** and **D**).

cells. Moreover, they also determined the levels of endogenous DNA damages including 8-hydroxy-2'-

guanosine (8-OHdG) and abasic (AP) site after Alu siRNA transfection in HEK293 cells. As expected, the levels of 8-OHdG and AP site were significantly reduced in Alu siRNA transfected cells when compared with the control cells (P=0.005 and 0.0152, respectively) (Patchsung M, *et al*, 2018).

Therefore, it might be concluded that an increase in DNA methylation, particularly *Alu* elements, is considerably responsible for strengthening the genome and could improve aging phenotypes as genomic instability in many previous studies (Jung M and Pfeifer GP, 2015, Pal S and Tyler JK, 2016, Lopez-Otin C, *et al*, 2013, Patchsung M, *et al*, 2018). Even though, the *Alu* methylation status is apparently linked to aging phenotypes *in vitro* study, it is needed to be further investigated whether an improved *Alu* methylation status also alleviates aging phenotypes and/or restores the physiological functions of aging organs using an aging animal model.

Figure 1-8: Comparisons of the percentage of total Alu methylation levels (**A**) and LINE-1 methylation levels (**B**) between CUG and non-CUG in 249 individuals (20-year-old of age). (CUG, catch-up growth)

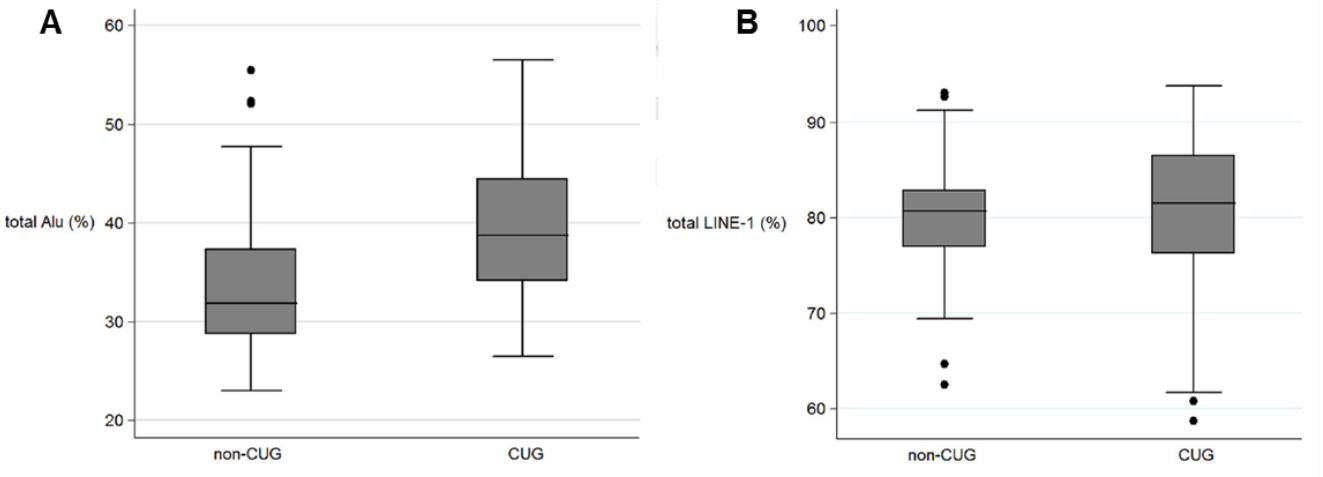

Rerkasem K. et al, PLoS ONE, 2015

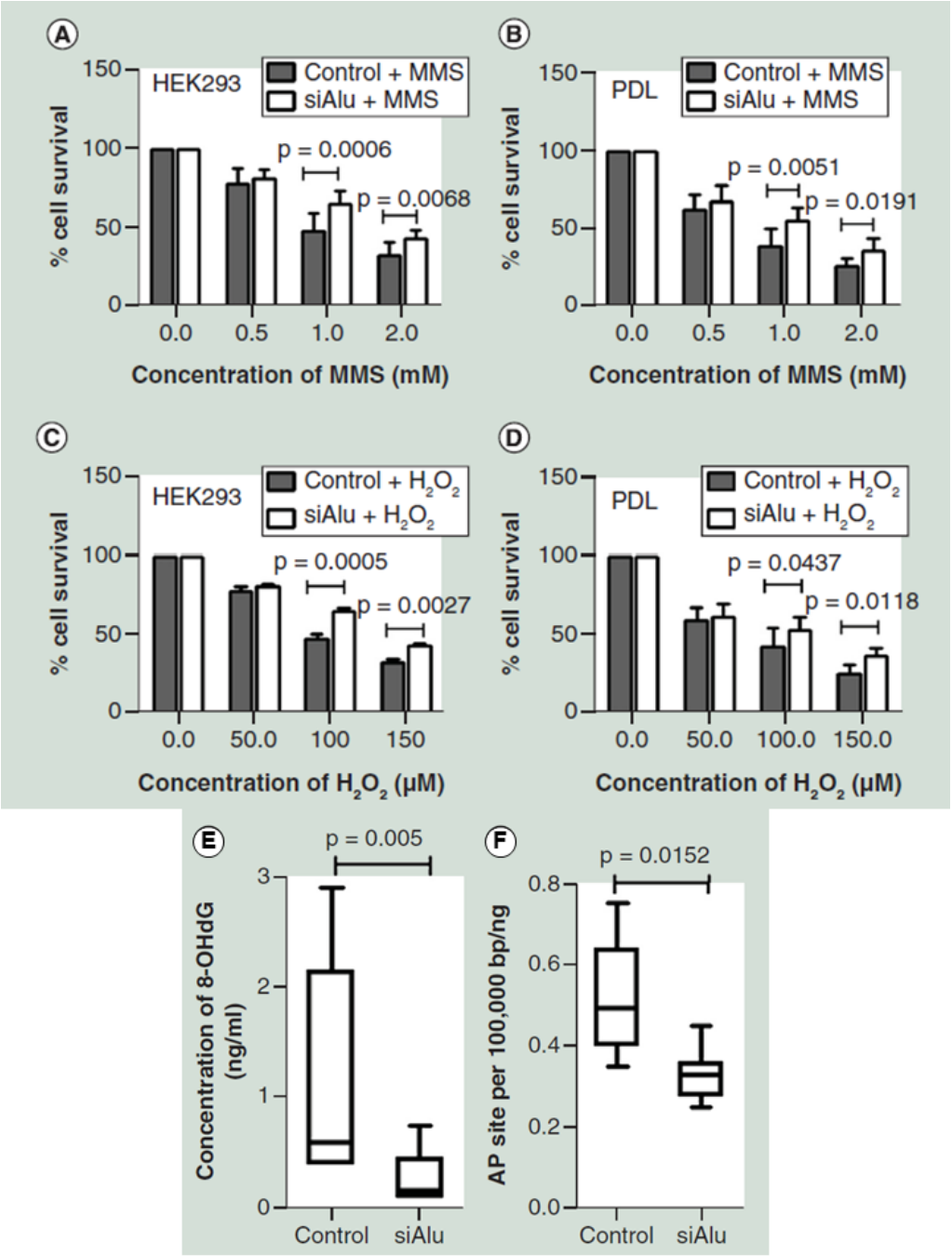

Patchsung M, et al, Epigenomics, 2018

Figure 1-9: Alu hypermethylation in both HEK293 and PDL cells significantly decreased the susceptibility to DNA damage agent exposure. (**A**) and (**B**) The percentages of cell survival were detected in Alu hypermethylated HEK293 and PDL cells after 48-hour MMS exposure. (**C**) and (**D**) The percentages of cell survival in Alu hypermethylated HEK293 and PDL cells were examined when exposed to the increasing concentrations of H_2O_2. (**E**) and (**F**) The levels of endogenous DNA damage, 8-OHdG (ng/ml) and AP site (per 100,000bp/ng) after Alu

siRNA transfection in HEK293 cells compared to control cells. (MMS: Methyl methane sulfonate)

3. Box-A of HMGB1 Protein, a Promising Candidate to Reduce Genomic Instability in Aging

High-mobility group box 1 protein (HMGB1) is the most abundant nonhistone protein, which non-specifically binds to DNA sequence and acts as an architectural factor of the chromatin in the nucleus with a dual function outside the cell (Kang R, *et al*, 2014). Human HMGB1 protein contains 215 amino acid residues including Box-A (aa 9-79) and Box-B (aa 89-162) along with the terminal acidic tail (186-215) that has also a conserved sequence across all mammals, **Figure 1-10** (Ugrinova I and Pasheva E, 2016). There are two DNA binding domains located in Box-A and Box-B respectively, and an acidic tail containing glutamic and aspartic acids with histone H1 binding activity (Ugrinova I and Pasheva E, 2016). As demonstrated in **Figure 1-10**, Box-A of HMGB1 contains not only DNA binding motif, which is located at the nuclear localization sites (NSL)-1 (aa 28-44), but also a sirtuin-1 (SIRT-1) binding domain, [SIRT-1, a protein is bound to the DNA and responsible for histone deacetylation involved in DNA repair and DNA stability (Hwang JS, *et al*, 2015)]. Similarly, Box-B of HMGB1 has a DNA-binding motif located at the NSL2 (aa 179-185) and plays the same role as a BOX-A of HMGB1 protein in DNA-bending and binding activity as depicted in **Figure 1-11** (Ugrinova I and Pasheva E, 2016, Kang R, *et al*, 2014).

In addition to a DNA chaperone function, HMGB1 remarkably participates in DNA replication, DNA repair, and V(D)J recombination inside the nucleus (Mitsouras K, *et al*, 2002, Štros M, 2010, Ugrinova I and Pasheva E, 2016). In contrast to the nuclear functions, the HMGB1 protein also considerably plays a different role in extracellular functions. The Box-B of HMGB1 is capable of stimulating an inflammatory response when released from the cell due to Toll-like receptor (TLR)-4 binding activity domain (aa 89-108), whereas the Box-A of HMGB1 has an antagonistic extracellular function by competing with HMGB1 binding to its receptors contributing to attenuate a pro-inflammatory cytokine induction both *in vitro* and in vivo studies (Yang H, *et al*, 2015, Kang R, *et al*, 2014). The first receptor for HMGB1 protein discovered in 1995 is a receptor for advanced glycation end products (RAGE), which has been identified the binding activity not only to advanced glycation end products (AGEs), but also a variety of diversely molecules as HMGB1, DNA, RNA, etc. Because of the capacity of Box-A of HMGB1 to RAGE binding with a lack of TLR4-binding domain, the Box-A of HMGB1

induces the RAGE activation without an inflammatory signal transduction (Ugrinova I and Pasheva E, 2016).

จุฬาลงกรณ์มหาวิทยาลัย
Chulalongkorn University

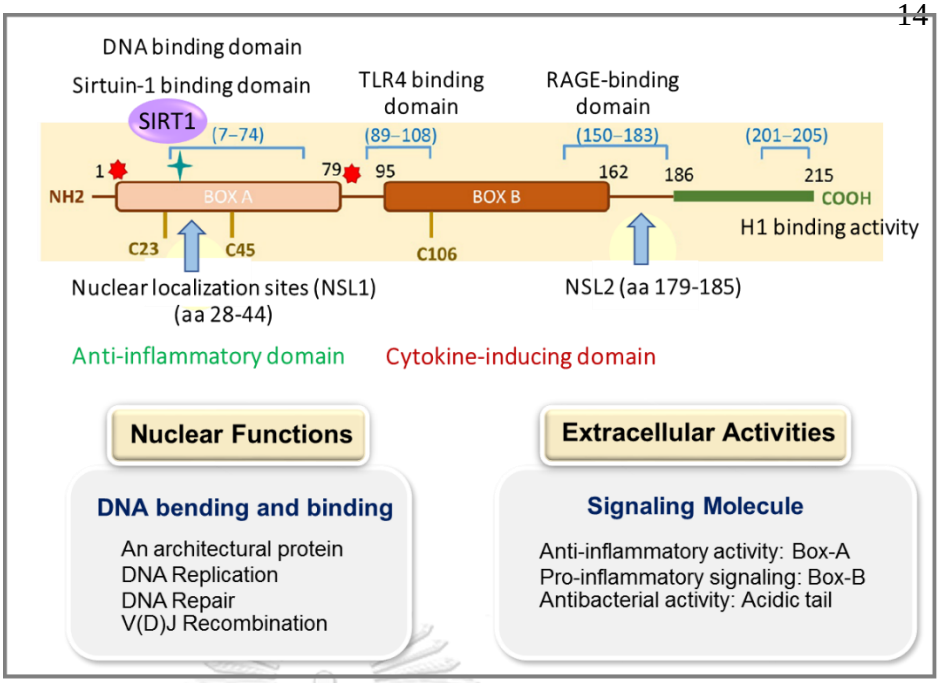

Yang H., et al, Molecular Medicine, 2015

Ugrinova I.,et al, Advances in Protein Chemistry and Structural Biology, 2017

Figure 1-10: HMGB1 protein structure and functions. Two boxes of HMGB1 protein contains two DNA binding domains including the NSL1 located in Box-A (aa 28-44) and the NSL2 resided in Box B (aa 179-185). Box-A of HMGB1 also includes SIRT1-binding motif and pro-inflammation antagonistic activity, whereas Box-B of HMGB1 consists of TLR4-binding domain. A number of Box-A and Box-B of HMGB1 nuclear and extracellular functions have been elucidated.

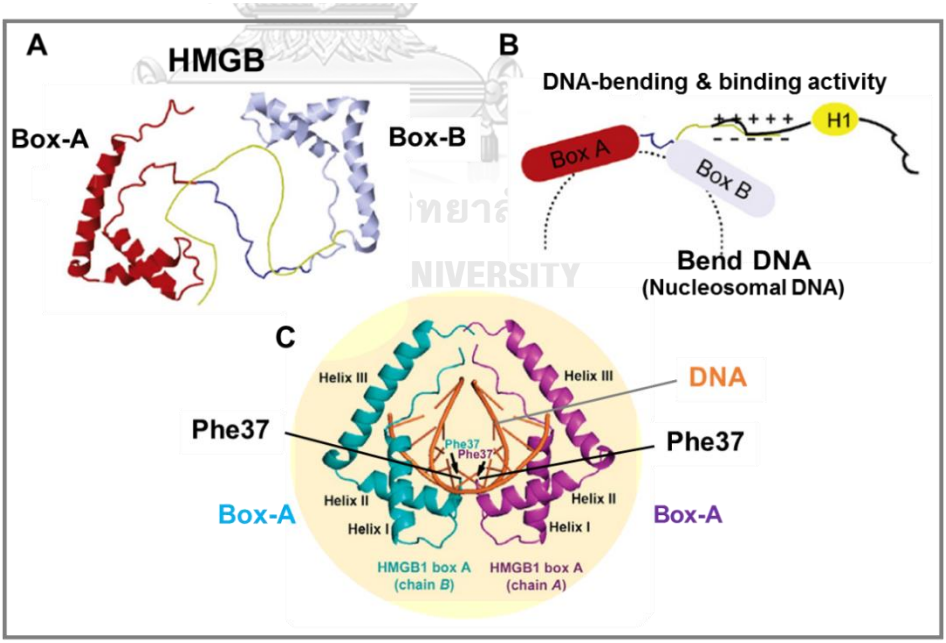

Yang H., et al, Molecular Medicine, 2015

Ugrinova I.,et al, Advances in Protein Chemistry and Structural Biology, 2017

Figure 1-11: The illustration of HMGB1 protein folding structure and its DNA interaction. (**A**) Two folded helical structures of Box-A and Box-B of HMGB1 protein. (**B**) The DNA-bending and binding activity of Box-A (Red) and Box-B (Light blue) of HMGB1 with histone H1 (Yellow) binding capacity of the acidic C-terminal. (**C**) Two symmetric Box-A domains incorporate to bend DNA (Orange strand) at Phe37 positions.

In 2005, the preceding study reported that Nhp6A/B, a protein belonging to HMGB1 superfamily in yeast and related to mammalian HMGB1, and HMGB1 proteins mediated genome stability (Giavara S, *et al*, 2005). The distinctive percentage of cell survival between Nhp6A/B deleted yeast (*nhp6a/b*) and wild-type strain (*NPH6A/B*) was compared during advancing age (represented by numbers of bud removed). As shown in **Figure 1-12 A**, the percentage of Nhp6A/B-deleted yeast cell survival was remarkably declined when compared to the wild-type strain in advancing age. In addition, the production of thymine dimers was immediately observed in the wild-type and Nhp6A/B-deleted yeast (*nph6a/b*) strains after UV exposure, as indicated **in Figure 1-12 B**. Correspondingly, *nph6a/b* strain markedly increased in thymine dimer formation compared to the wild-type strain. Hence, it could be concluded that the Nhp6A/B protein regulated yeast life span and protected the cells from DNA damage resulting in the maintenance of genomic stability (Giavara S, *et al*, 2005).

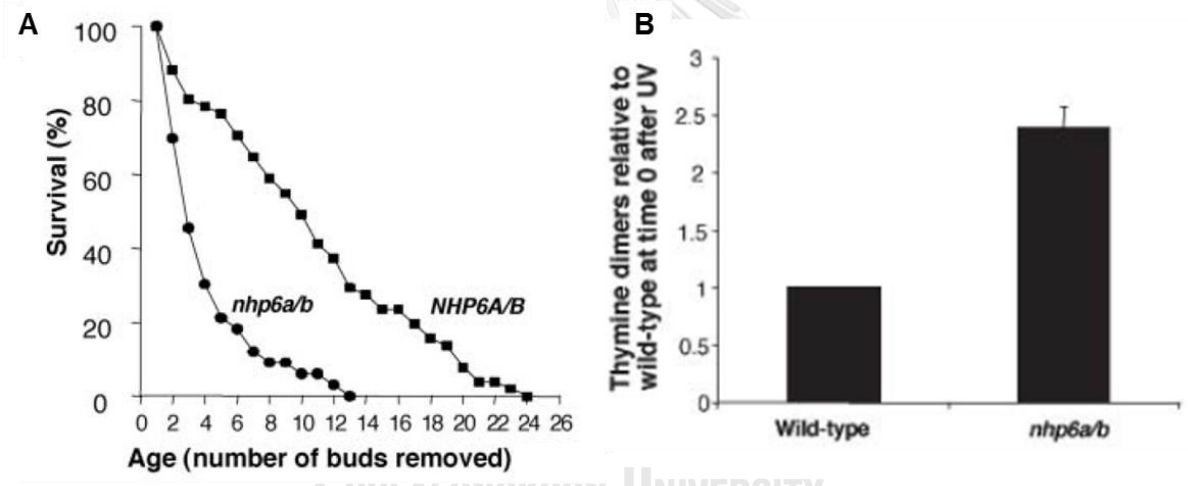

CHULALONGKORN UNIVERSITY

Giavara S, et al. Current Biology, 2005

Figure 1-12: The beneficial role of Nhp6A/B protein, a HMGB1 superfamily in yeast, on the cell survival and the DNA damage response. (**A**) The *nhp6a/b* (Nhp6A/B-deleted) yeast cells showed sharply reduced the percentage of cell survival compared to the wild-type strain (*NHP6A/B*) during replicative age. (**B**) The comparison of thymine dimer production between the wild-type and the *nhp6a* strains after UV exposure at time 0.

In addition to this, there have been reported that physiologic replicative-independent endogenous double-strand break (phy-RIND-EDSB) is significantly relevant to genomic stability in both yeast (Thongsroy J, *et al*, 2013, Pongpanich M, *et al*, 2014) and human (Pornthanakasem W, *et al*, 2008, Kongruttanachok N, *et al*, 2010). The previous report revealed that RIND-EDSBs are preferably located in the human hypermethylated genome (Pornthanakasem W, *et al*, 2008), therefore aging human cells should be prone to display a

lower number of RIND-EDSBs in the hypomethylated genome. In contrast to physiologic EDSBs, it is believed that RIND-EDSBs involved in DNA repair process and spontaneously occurred without radiation or DNA-damaging substance exposure (Kongruttanachok N, *et al*, 2010, Thongsroy J, *et al*, 2013, and Pongpanich M, *et al*, 2014). Correspondingly, RIND-EDSBs, that are highly retained in heterochromatin, are thought to uncorrelated with γH2A.X, a pathologic EDSB indicator (Kongruttanachok N, *et al*, 2010). The recent study by Thongsroy J and colleagues unveiled that HMGB1 protein family in yeast cell as Nhp6A protein and human HMGB1 protein were significantly correlated with physiologic EDSBs as demonstrated in **Figure 1-13** (Thongsroy J, *et al*, 2013). The results showed that deletions of each of the seven genes in the HMGB family in yeast cells had an impact on the reduction of the levels of RIND-EDSBs; however, the yeast strains with *nhp6aΔ*, *rox1Δ*, *ixr1Δ*, and *hmo1Δ* significantly decreased physiologic RIND-EDSB levels (**Figure 1-13 A**). Likewise, the significant depletion of HMGB1 protein expression using HMGB1 siRNA transfection (**P<0.001) in mammalian HeLa cells was positively related to the significant lowering of RIND-EDSB levels compared to control siRNA treated cells (*P<0.05) as shown in **Figure 1-13 B** and **C**. (Thongsroy J, *et al*, 2013) Surprisingly, the more recent study in 2018 revealed the strong relationship between the levels of RIND-EDSBs and cell viability in advancing age of yeast cells (r=0.94, P<0.0001) (Thongsroy J, *et al*, 2018). These findings emphasized the strong correlation between HMGB1 protein and numbers of physiologic RIND-EDSBs in both yeast and mammalian cells, which had also an influence on genomic stability in cellular aging.

จุฬาลงกรณ์มหาวิทยาลัย

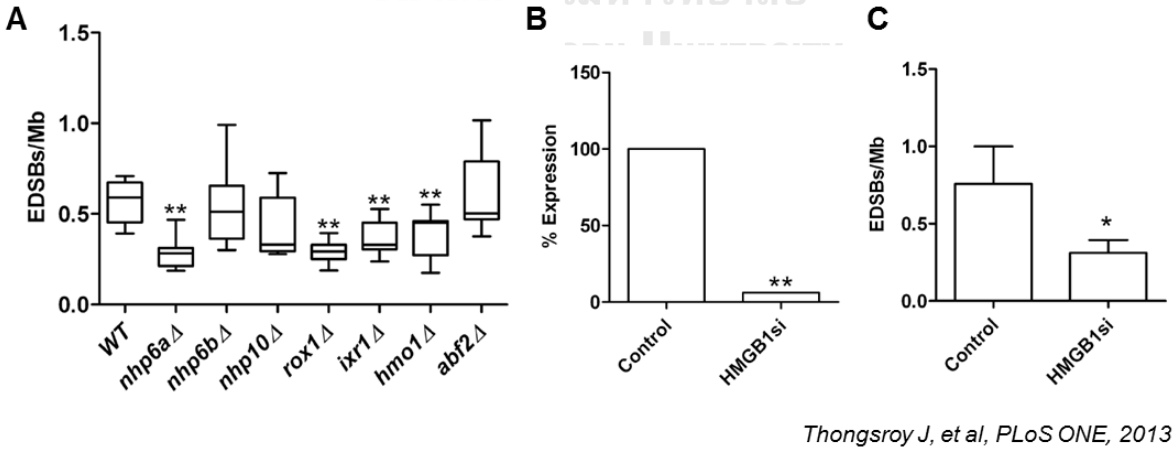

Figure 1-13: Physiologic RIND-EDSB levels detected in the HMGB1 protein family mutant yeasts and HMGB1-gene silencing mammalian cells. (**A**) The levels of RIND-EDSBs were measured in mutant yeast cells including *nhp6aΔ, nhp6bΔ, nhp610Δ, rox1Δ, ixr1Δ, hmo1Δ*, and

abf2Δ strains. The percentage of HMGB1 mRNA expression (**B**) and numbers of RIND-EDSBs (**C**) were determined after HMGB1 siRNA transfection compared with control siRNA transfection in HeLa cells. (*P<0.05 and **P<0.001)

Consistently, the recent study by Settayanon S and Mutirangura M (unpublished data, 2017) revealed that the mutant yeast cells, which were deleted either *nhp6a* or *hmo1* gene (*nhp6aΔ* and *hmo1Δ*) showed the significantly increased endogenous DNA damages including AP sites (P<0.0001 and P<0.0001) and 8-OHdG (P<0.0001 and P<0.0001) when compared with wild-type yeast strain (**Figure 1-14 A** and **B**). Furthermore, the endogenous DNA damages were also investigated in human embryonic kidney 293 (HEK293) cells transfected with either HMGB1 or Box-A of HMGB1 plasmids compared to plasmid control (PC) transfection. Importantly, the levels of AP sites were strongly reduced in Box-A of HMGB1 plasmid-transfected HEK293 cells (P=0.0046) compared with transfected control cells (**Figure 1-14 C**). The levels of 8-OHdG were also significantly diminished in HMGB1 plasmid-transfected HEK293 cells (P=0.006) and remarkably declined in Box-A of HMGB1 plasmid-transfected cells (P=0.0007) when compared to the control (**Figure 1-14 D**). Additionally, HEK293 cell viability and proliferation after Box-A of HMGB1 plasmid transfection were significantly

จุฬาลงกรณ์มหาวิทยาลัย
Chulalongkorn University

increased compared with transfected control cell (**Figure 1-14 E** and **F**) (Settayanon S and Mutirangura M, unpublished data, 2017).

Figure 1-14: The measurement of AP site and 8-OHdG levels in *nhp6aΔ* and *hmo1Δ* mutant yeast strains compared with the wild-type strain (**A**) in HMGB1 plasmid- and Box-A of HMGB1 plasmid-transfected HEK293 cells compared with the plasmid control (PC) transfection (**B**). The cell viability and an absolute cell number of Box-A of HMGB1 plasmid

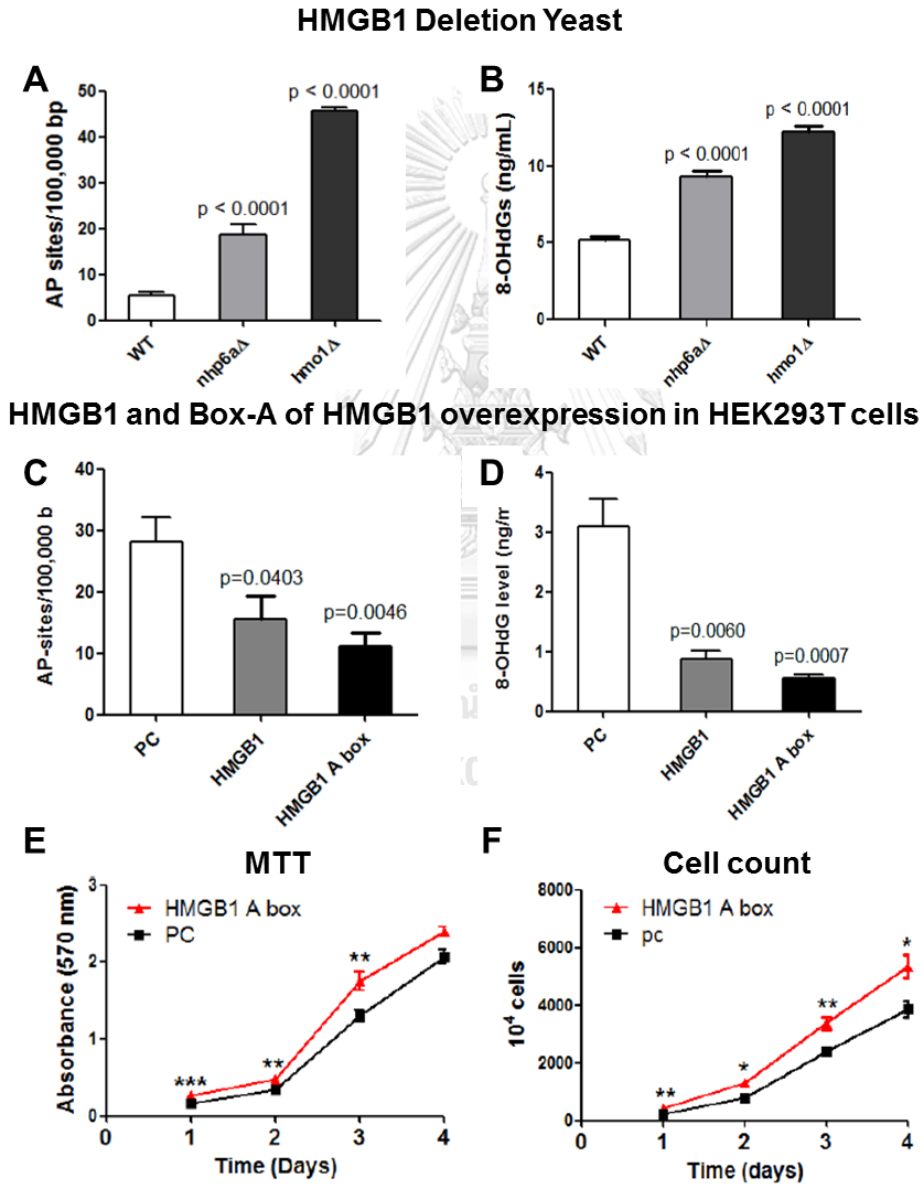

Settayanon S and Mutirangura A, Unpublished data, 2017

transfection in HEK293 cells using MTT and cell count assay compared to the transfected control cells (**E** and **F**), (*P<0.05, **P<0.01, and ***P<0.001).

Taken together, the recent study by Patchsung M and Mutirangura A (unpublished data) investigated the tolerance of HMGB1 plasmid- and Box-A of HMGB1 plasmid-transfected mammalian cells to the exposure of increasing concentrations of H_2O_2, a strongly oxidative DNA-damaging agent, or rapamycin, a mTOR and DNA double-strand break (DDB) inhibitor. The findings exhibited the significant increases in the percentage of HMGB1 plasmid-transfected HEK293 cell survival (Red line) after H_2O_2 and rapamycin exposures when compared to the control cell survival (Black line) as shown in **Figure 1-15 A** and **B** (**P<0.05 and ***P<0.001). Moreover, Box-A of HMGB1 transfection (Blue line) incredibly reduced the cell sensitivity to DNA-damaging agent and DNA repair inhibitor and prevented cell death compared with the plasmid control transfection (Black line) as demonstrated in **Figure 1-15 A** and **B** (***P<0.001) (Patchsung M and Mutirangura A, unpublished data, 2017).

Figure 1-15: The percentage of HEK293 cell survival after HMGB1 plasmid (Red line) or Box-A of HMGB1 plasmid (Blue line) transfection when exposed to a DNA-damaging agent H_2O_2 (**A**), or mTOR and DNA repair inhibitor rapamycin (**B**) (**P<0.01, and ***P<0.001).

According to many previous studies, it has been purposed that Box-A of HMGB1 protein might become a promising nuclear protein that might be able to effectively improve the

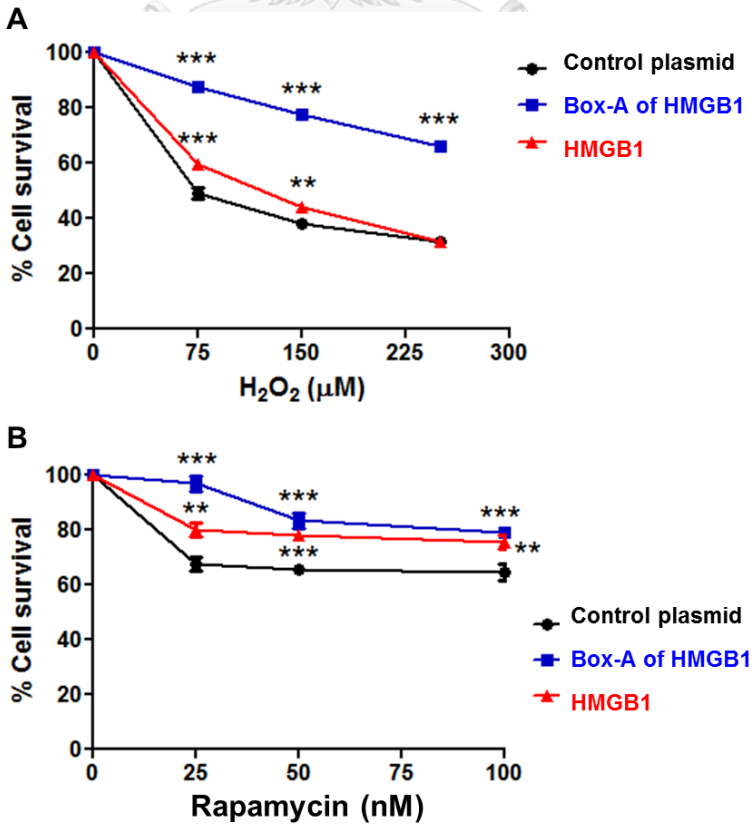

Patchsung M and Mutirangura A, Unpublished data, 2017

genomic instability and enhance the levels of physiologic RIND-EDSBs in cellular aging. Eventually, the less genomic instability in the aging cells, along with more physiologic RIND-EDSBs by enhancing Box-A of HMGB1 protein expression might potentially alleviate or reverse aging phenotypes by restoring impaired organ functions in aging animal model.

4. D-Galactose-Induced Aging Animals, an Imitated Natural Aging Model, and Naturally Aging Animals with Defective Liver and Cognitive Functions

Because of a global massive rising elderly population, age-related diseases have been largely becoming more common, including, cardiovascular disease, diabetes, and cancer (Lopez-Otin C, *et al*, 2013). There have been many attempts to understand aging process to overcome loads of age-associated diseases, so it is necessary to possess an appropriate aging model to imitate a natural aging process and can be employed as a potential tool for investigating novel anti-aging agents (Zhu ZY and Zhu GH, 2007, Ho SC, *et al*, 2003). Among all unnatural aging models, one of the most suitable and stable aging models is a D-galactose induced aging model, which was firstly discovered by Gong GQ in 1991 and has been continuously used to study in molecular level of aging process, as well as physiological level of aging organs (Ho SC, *et al*, 2003, Zhou YY, *et al*, 2015). It is well-known that long-term D-galactose induction causes excessive oxidative stress, especially reactive oxygen species (ROS), as well as increased inflammatory responses, contributing to genomic instability as DNA damage, cellular aging, and eventually organ aging (Lombard DB, *et al*, 2005, Zhou YY, *et al*, 2015, Sadigh-Eteghad S, *et al*, 2017).

Many pieces of evidence have been shown that D-galactose-induced aging could be represented aging phenotypes as found in a natural aging process at the level of organ function including aging liver, impaired cardiovascular parameters, and aging brain (Huang CC, *et al*, 2013, Zhou YY, *et al*, 2015, Sadigh-Eteghad S, *et al*, 2017, Shwe T, *et al*, 2018). As previously demonstrated by Ho SC and colleagues, three groups of mice were consecutively injected with 5%, 1% D-galactose, and phosphate-buffered saline (PBS), respectively, via subcutaneous route (once a day) for 45 days. The results showed that the levels of blood melondialdehyde (MDA), a lipid peroxidation biomarker in aging liver, were significantly increased, whereas the levels of blood superoxide dismutase (SOD), an antioxidant preventing cell damage and cellular aging, significantly reduced compared with the PBS-injected group (Ho SC, *et al*, 2003). Consistently, mice treated with D-galactose showed significant higher levels of brain MDA, as well as lowering of brain SOD compared to the control. Moreover, liver MDA levels were strongly increased in 5% D-galactose-treated mice compared to PBS-treated mice (Ho SC, *et al*, 2003). Likewise, the increased aging parameters in D-galactose-

induced animals were also supported by other groups of study; for examples, impaired cognitive functions and neurochemical changes (Zhang Q, *et al*, 2015, Sadigh-Eteghad S, *et al*, 2017, Heidari S, *et al*, 2017, Shwe T, *et al*, 2018), the increased levels of aging liver markers (Zhen YZ, *et al*, 2016, Zhou YY, *et al*, 2015, Huang CC, *et al*, 2013) and abnormal cardiac functions (Cebe T, *et al*, 2014, Liu J, *et al*, 2012).

Furthermore, the findings also revealed that the liver section area of positive-immunohistochemical staining of nuclear factor-kappa B (NF-ƙB), a central signaling molecule in inflammation, were significantly elevated in of both the D-galactose-induced aging group and naturally aging group when compared to the young control group (Ji M, *et al*, 2017). Again, this group also determined brain aging parameters including the reduced expression of proliferating cell nuclear antigen (PCNA), an essential protein involved in cell proliferation and DNA repair, and the increased expression levels of p16 and p21, effector proteins in cellular senescence (Childs BG, *et al*, 2015), in the brain tissue after D-galactose administration (**Figure 1-16**). Naturally aging group displayed the significant reduction of the mRNA expression of PCNA and the significantly decrease in the expression levels of senescence-associated molecules as p16 and p21, compared to the young control group (**Figure 1-16 A-C**). Interestingly, D-galactose induced group exhibited the parallel trends of p16 and p21 mRNA expression as found in naturally aging group when compared with the young controls (**Figure 1-16 A-C**) (Ji M, *et al*, 2017).

Additionally, D-galactose administration in animal model could considerably accelerated apparent aging phenotypes including senescence-associated β-galactosidase (SA-β-gal), senescence-associated heterochromatin-foci (SA-HF), increased senescence-associated secretary proteins (SASPs), and elevated senescence-associated signaling mediators such as p16 and p21, which were acceptably used as early and fully senescent biomarkers in aging

จุฬาลงกรณ์มหาวิทยาลัย
Chulalongkorn University

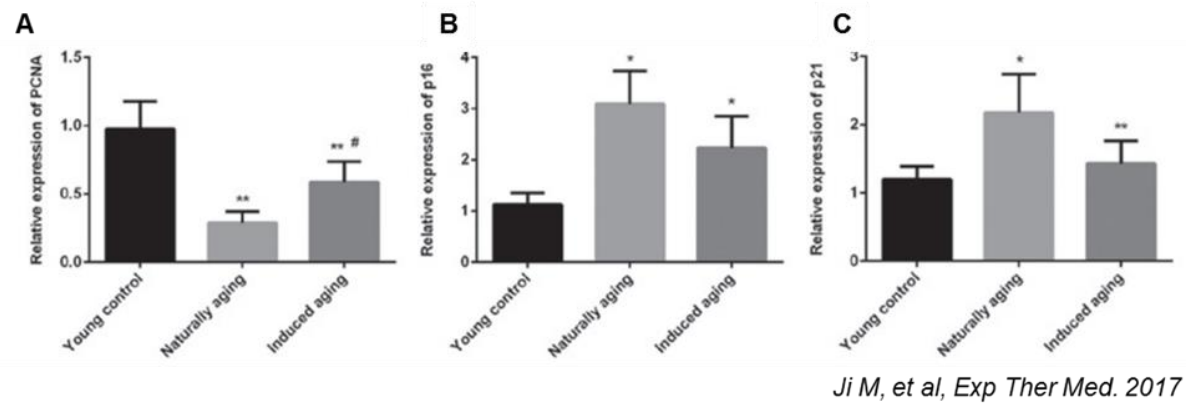

Ji M, et al, Exp Ther Med. 2017

model (Childs BG, *et al*, 2015, Liu J, *et al*, 2012, Baker DJ, *et al*, 2004).

Figure 1-16: The relative expression levels of PCNA mRNA (A), p16 mRNA (B) and p21 mRNA in the brain tissue normalized to the GAPDH level. *P<0.05 and **P<0.01 vs young control group; #P<0.05, naturally aging group. (PCNA, proliferating cell nuclear antigen)

There have been reported the robust correlation between an increased global hypomethylation and advancing age; however, genome-wide DNA methylation status, especially IRS methylation, in D-galactose-induced aging animal is incredibly limited (Zhu ZY, *et al*, 2003, Zhu ZY, *et al*, 2007, Zhou YY, *et al*, 2015). The excessive oxidative stress, which is caused by D-galactose administration, leads to the uncontrolled level of DNA damages and genomic instability and might be able to induce the significant global hypomethylation as previously demonstrated in naturally aging rat organs (**Figure 1-17**) (Vanyushin BF, *et al*, 1973).

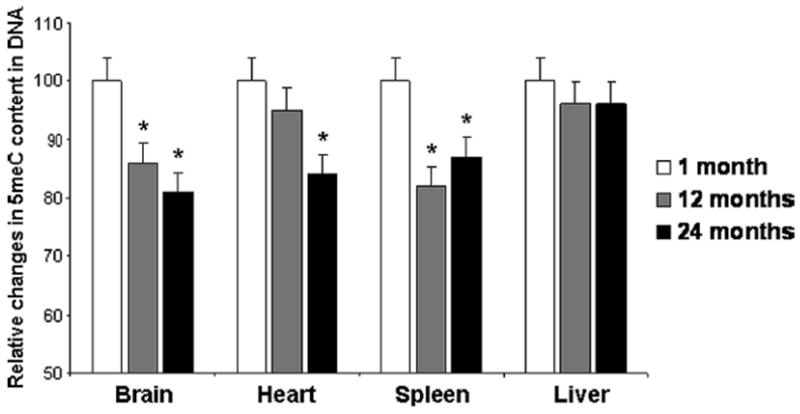

Figure 1-17: Age-associated global methylation alteration in the rat brain, heart, spleen and liver tissues. The DNA 5'methyl-cytosine (5meC) contents of 1-month-old rats were adjusted as 100%. (*P<0.05).

Herein, I hypothesize that aging phenotypes, including a common aging marker SA-β-gal, Alu (B1 element in rat) hypomethylation, impaired liver functions and brain aging in D-galactose-induced and naturally aging rat models, are able to be alleviated by overexpressing Box-A of HMGB1 protein due to reduced genomic instability and/or elevated the levels of physiologic RIND-EDSBs (or Youth-DNA-GAPs), contributing to mitigation of the deficits of physiological functions in aging rat organs.

5. Wound Healing Impairment in Diabetes Relevant to Global Hypomethylation and DNA Damage

Diabetes is an important age-associated disease caused by the inability of the body to produce insulin hormones at normal levels, resulting in high blood sugar (Testa R and Ceriello A, 2017). Diabetes is a life-threatening disease that causes systemic tissue damage and multiorgan dysfunctions, mainly chronic hyperglycemia. Kerner and Brückel (2014) In 2014, the World Health Organization reported that there were 422 million people with diabetes mellitus worldwide, and in 2012, 1.5 million patients died from diabetes (Global Report on Diabetes WHO 2016). Diabetic ulceration is one of the most common chronic wounds that has more than 70% recurrence in diabetic patients in 5 years of treatment. (Riedel et al., 2020) (Reiber et al., 1998) The most common complications in diabetic patients are foot ulcers (15%), which can be caused a high opportunity to develop chronic wound ulceration, leading to leg amputation or organ loss (up to 84%) (Giurini JM and Lyons TE, 2005, Jeffcoate WJ, *et al*, 2004). The current treatment for diabetic ulcers is a reduction in foot bearing pressure in patients with neuropathic ulcers, together with increased blood flow; however, diabetic patients with chronic wound partially responded to diabetic ulcer treatment (Jeffcoate WJ, *et al*, 2004). Chronic diabetic ulcers are thought to be caused by the presence of cellular senescence, especially vascular senescence, due to excessive oxidative stress and inadequate cell damage repair (Allyson K, *et al*, 2015, Testa R and Ceriello A, 2017). Growth factors, such as transforming growth factor-β (TGF-β) and platelet derived growth factor (PDGF), which are essential for tissue repair process, can be inhibited by senescence-releasing molecules known as senescence-associated secretory phenotype (SASP), including proinflammatory cytokines and chemokines, exacerbating the impaired wound healing mechanism (Huang JS, *et al*, 2002, Keswani SG, et al, 2004, Allyson K, *et al*, 2015). The high level of oxidative stress in diabetes results in genomic instability as increased DNA damages and eventually induces persistent cellular senescence; however, the underlying mechanism of abnormal wound healing caused by cellular senescence is necessary to be further investigated (Lombard DB, *et al*, 2005, Childs BG, *et al*, 2015).

Impaired wound healing has become a predominant complication in diabetic patients who eventually have a high risk of limb amputation. (Nunan et al., 2014) The imbalance of oxidative production and suppression due to prolonged hyperglycemia directly affects cellular signaling, cellular functions, and cell components, such as DNA strands. (Newsholme et al., 2016) Previous studies have reported the association between diabetic conditions and DNA lesions (8-oxo-deoxyguanosine, 8-OHdG; and γ-H2A.X) in clinical trials and animal studies.

(Lee & Chan, 2015) (Algire et al., 2012) Hyperglycemia-derived DNA damage in diabetes influences cell proliferation, migration, and functions in various cell types in wound areas, directly affecting the healing process. (Davis et al., 2018) (Blakytny & Jude, 2006) Correspondingly, irrecoverable DNA damage in wound-healing phases perpetuates a delayed healing process, leading to defective fibroblast maturation, fibrosis deposition, re-epithelialization, and formation of new vessel and granulation tissue in diabetes. (Blakytny & Jude, 2006) (Leoni et al., 2015) The underlying mechanism of DNA damage-induced impaired wound healing has been studied, and an alteration of epigenetic modification, such as DNA methylation in Alu elements, has been proposed.

Alu elements in humans (B1 elements in rodents) are the most abundant retrotransposon or short intersperse elements (SINEs), containing approximately 40-45% of the human and rodent genomes. (Kramerov & Vassetzky, 2005) Alu or B1 elements are located in noncoding regions and are primarily methylated, termed Alu (B1) methylation, to form heterochromatin for maintaining genome stability. (Kramerov & Vassetzky, 2005) Recent studies have focused on the DNA methylation pattern, a predominantly epigenetic modification that confers a methyl group to cytosine-phosphate-guanine (CpG) sites along the genome, in age-related conditions. (López-Otín et al., 2013) (Brunet & Berger, 2014) Changes in the DNA methylation pattern caused by a decrease in methylated CpG islands, which is known as DNA hypomethylation, in genome-wide and intergenic regions distinctively occur during the aging process. (Jintaridth & Mutirangura, 2010) (Jintaridth et al., 2013) Under certain aging-induced conditions, such as diabetes, Alu hypomethylation is correlated with prediabetic conditions, type II diabetes, and osteoporosis, and it is correlated with the presence of a high rate of DNA damage. (Thongsroy et al., 2017) In addition, our laboratory group has reported that the Alu hypomethylation levels in type 2 diabetic patients are strongly correlated with high fasting blood sugar and HbA1C compared to age-matched normal individuals, suggesting that genome-wide hypomethylation might be an implicit contributor to genome instability in diabetes. (Thongsroy et al., 2017) Notably, a relevant study has provided evidence that modulation of Alu methylation through *de novo* methylation-mediated Alu small interfering ribonucleic acids (siRNAs) using a mechanism of RNA-directed DNA methylation (RdDM) occurs in human cells. (Chalertpet et al., 2019) Moreover, *de novo* Alu methylation by Alu siRNA transfection prevents 8-OHdG and AP site DNA damage, enhances cell growth, and increases cellular tolerance to DNA damage agents in human cell lines. (Patchsung et al., 2018) However, focusing on DNA hypomethylation treatment in Alu or B1 repetitive elements in diabetes is inevitably limited. (den Dekker et al., 2019) (Pastar et al., 2021) Based on the collective

evidence showing the relationship between Alu (B1) hypomethylation and DNA damage accumulation in diabetes, we aimed to elucidate the possibility of diabetic wound treatment by reprogramming B1 hypomethylation and strengthening genome integrity to enhance cell proliferation in a preclinical study.

As mentioned earlier, Alu (in human) or B1 (in rodent) hypomethylation is believed to a potential contributor in aging process and subsequently stimulates aging phenotypes, therefore a higher level of oxidative stress in diabetic induction rat model could result in alteration of B1 methylation status and enhanced genomic instability, leading to the impairment of wound healing process (Wilson AS, *et al*, 2007, Jung M and Pfeifer GP, 2015, Thongsroy J, *et al*, 2017). Recently, type 1 diabetic animal model using streptozotocin (STZ) induction has been discovered and widely used as a pre-clinical animal model to study the pathogenesis of diabetes and diabetic wound healing as well (Aileen JK,2012, Deeds MC, *et al*, 2011). There are four main stages in wound healing process as illustrated in **Figure 1-18**, consisting of hemostasis phase, inflammatory phase, proliferative phase, and remodeling phase, respectively (Thiruvoth FM, *et al*, 2015, McLennan S, *et al*, 2006). it is possible that oxidative stress as an increased reactive oxygen species (ROS) in diabetic rat model strongly had impacts on cell signaling, particularly in the early phases, and further exacerbated cell proliferation and migration in the proliferative phase of wound repair (McLennan S, *et al*, 2006, Brem H and Tomic-Canic M, 2007).

A streptozotocin (STZ)-induced type I diabetic rat model was utilized, which is widely used and well accepted to mimic type I diabetes and successfully demonstrates characteristics of diabetes with increased DNA damage. (Furman, 2015a) (King, 2012) I transfected B1 siRNA or plasmid DNA into target cells using calcium-phosphate (Ca-P) nanoparticles. These nanoparticles act as a nonviral vector to allow inorganic gene transfer, and their composition pre-exists in cells and tissues with biocompatibility and biodegradation features. (Zhao et al., 2014) (Yin et al., 2014) Due to the low immunogenicity and toxicity of inorganic Ca-P coatings, these nanoparticles are suitable gene delivery systems and provide sufficient transfection efficiency for *in vivo* studies. (Ramamoorth & Narvekar, 2015)

จุฬาลงกรณ์มหาวิทยาลัย
Chulalongkorn University

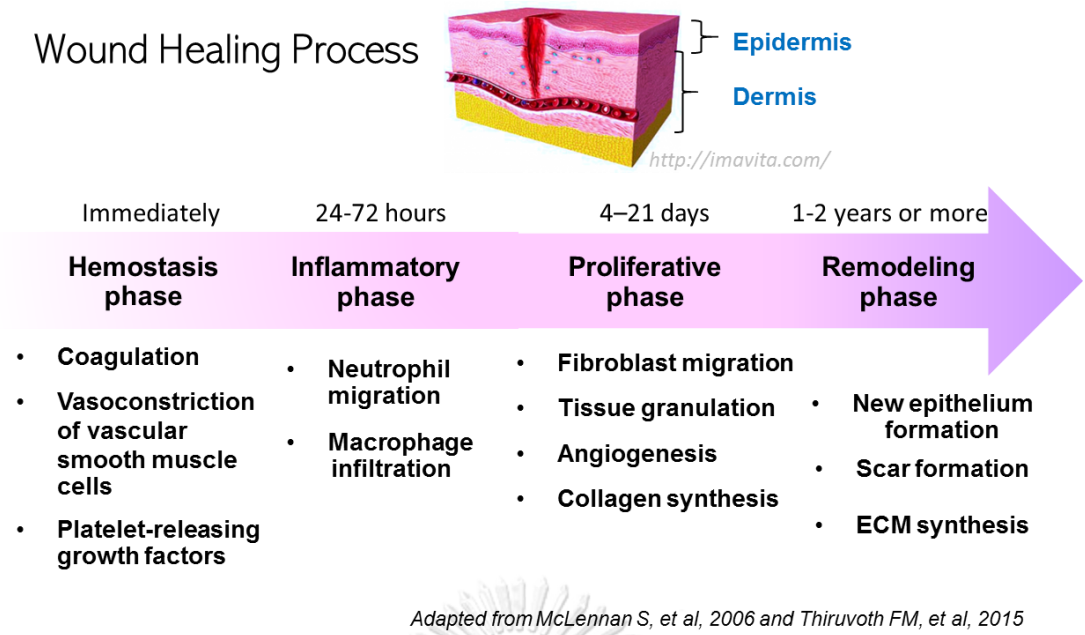

Adapted from McLennan S, et al, 2006 and Thiruvoth FM, et al, 2015

Figure 1-18: Wound healing process includes four major stages; (1) Hemostasis or coagulation phase, (2) Inflammatory phase, (3) Proliferative phase, and (4) Remodeling phase. The STZ-induced oxidative stress in diabetic rat model could contribute to a disturbance of cell signaling in mainly in 2nd and 3th phases, resulting in the delayed wound repair.

Besides cell signaling disruption by unrestrained oxidative stress, it needs to be elucidated whether genomic instability in cellular senescence as found in diabetes mainly causes the impaired wound healing (McLennan S, *et al*, 2006, Lombard DB, *et al*, 2005, Childs BG, *et al*, 2015). **Hence, I also hypothesize that the enhancement of B1 methylation level and the increased Box-A of HMGB1 protein expression level restores the genomic instability (B1 hypomethylation and DNA damage) in diabetic rat wound model, resulting in the accelerating wound repair process.**

จุฬาลงกรณ์มหาวิทยาลัย
Chulalongkorn University

CHAPTER II
RESEARCH CONCEPT

1. Research questions

1. Does Box-A of HMGB1 reverse/alleviate aging phenotypes in D-galactose-induced and naturally aging rats?

2. Does Box-A of HMGB1 promote a growth rate in a baby pig model?

3. Does Box-A of HMGB1 treatment improve impaired wound healing in diabetic rats?

4. Does B1 hypermethylation improve impaired wound healing in diabetic rats?

2. Hypotheses

Hypothesis 1

Treatment with Box-A of HMGB1 can alleviate/reverse aging phenotypes in D-galactose-induced and naturally aging rat models.

Hypothesis 2

Box-A of HMGB1 administration promotes a growth rate in a baby pig model.

Hypothesis 3

Box-A of HMGB1 intervention accelerates wound healing in diabetic rats.

Hypothesis 4

B1 siRNA treatment improve impaired wound healing in diabetic rats.

3. Objectives

Objective 1: To investigate whether Box A of HMGB1 treatment alleviates aging phenotypes in D-galactose-induced and naturally aging rats.

Objective 2: To examine whether Box A of HMGB1 intervention promotes a growth rate in baby porcine model.

Objective 3: To study if Box A of HMGB1 treatment improves impaired wound healing in diabetic rats.

จุฬาลงกรณ์มหาวิทยาลัย
Chulalongkorn University

Objective 4: To explore whether B1 siRNA treatment improves impaired wound healing in diabetic rats.

จุฬาลงกรณ์มหาวิทยาลัย
Chulalongkorn University

CHAPTER III

MATERIALS AND METHODS

Figure 3-1 sh-B1-GFP plasmid map The B1 sequence

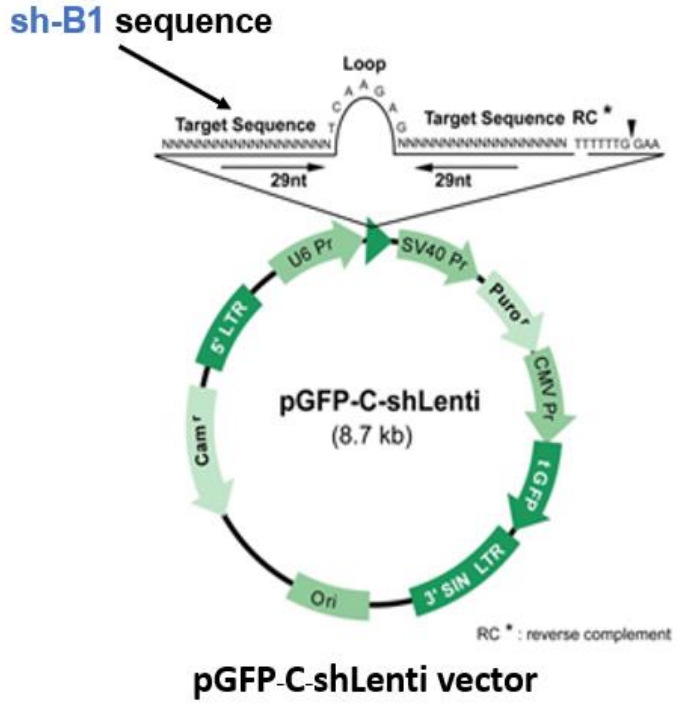

pGFP-C-shLenti vector

(5'GATCTCTGAGTTCGAGGCCAGCCTGGTCT3') was inserted into the pGFP-C-shLenti backbone vector containing chloramphenicol-resistant gene driven by CMV promoter.

จุฬาลงกรณ์มหาวิทยาลัย
Chulalongkorn University

Plasmid constructs

Short hairpin (sh)-B1-GFP plasmid containing green fluorescence protein driven by cytomegalovirus (CMV) promoter was constructed by Origene Technologies, Inc. (Rockville, MD, USA). The 29 nucleotide B1 sequence (5'GATCTCTGAGTTCGAGGCCAGCCTGGTCT3') and its reverse complement (RC) were inserted into the pGFP-C-shLenti backbone vector (plasmid size 8.7 kb) as shown in **Figure 3-1**. The sh-B1-GFP plasmid also consisted of chloramphenicol-resistant gene providing a potential selective marker in a plasmid preparation process. The pGFP-C-shLenti vector without B1 sequence insertion obtained from Origene Technologies, Inc. was used as a plasmid control in the study of sh-B1-GFP plasmid treatment. For the study of Box-A of HMGB1, the Box A of HMGB1 plasmid was constructed by Addgene (Cambridge, MA, USA) containing FLAG sequence driven by CMV promoter. The 350 nucleotides of Box-A of the HMGB1

sequence were inserted into pcDNA 3.1(+) plasmid backbone vector (plasmid size 5.4 kb) which contained the ampicillin-resistant gene as an antibiotic selective marker (**Figure 3-2**).

Plasmid transformation and plasmid preparation

Each type of plasmid (sh-B1-GFP plasmid, scramble-GFP plasmid, Box A-GFP plasmid, Box-A of HMGB1 plasmid, and pcDNA 3.1(+) plasmid control) was transformed into *Escherichia coli* competent cells DH5-α (Invitrogen, USA) following a conventional chemical transformation protocol (Sambrook JF. *Et al*, 2002). The transformant *E. coli* with sh-B1-GFP plasmid or scramble-GFP plasmid were grown on a selective Luria-Bertani (LB) agar containing ampicillin and chloramphenicol whereas the transformant cells with Box-A of HMGB1 plasmid or pcDNA 3.1(+) plasmid were selectively cultured on an ampicillin-containing LB agar. After overnight incubation at 37˚C, a single isolated colony of transformant was picked and transferred to 5 ml of LB broth with appropriate antibiotics as a starter culture. Then, a starter culture of a single colony was incubated in a 37˚C shaking incubator, at 220 rounds per minute (rpm) for 8 hours. After incubation, the starter culture was inoculated into 250 ml of LB broth containing appropriate antibiotics (ratio 1:1,000) and further incubated at 37˚C in a shaking incubator (220 rpm) for 16-18 hours (overnight). An optical density (OD) of the overnight culture was measured using the Asys *UVM 340* spectrophotometer (Biochrom, MA, USA) at a wavelength of 600 nm to estimate the growth of bacterial cells until the OD reached 2-3.

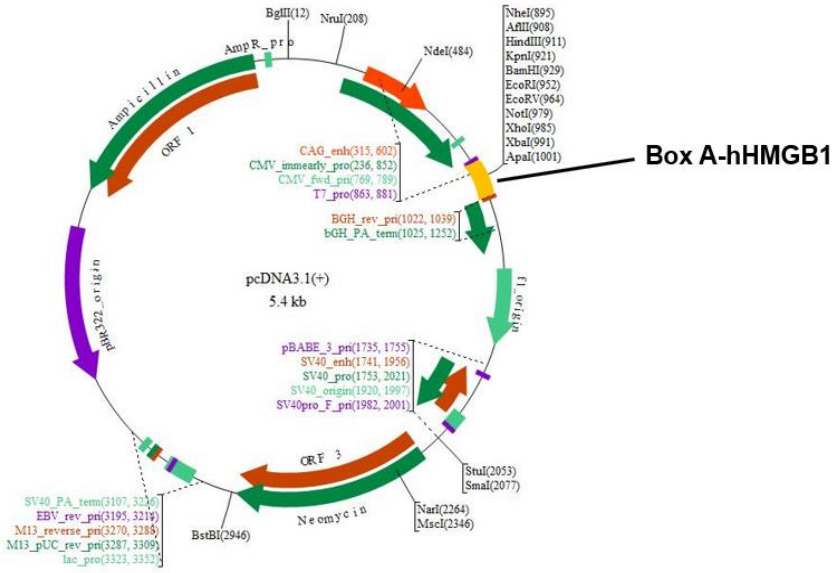

pcDNA 3.1 Flag-Box A-hHMGB1

Figure 3-2 Box-A of HMGB1 plasmid map. The 350 nucleotides of Box-A of human HMGB1 were inserted into pcDNA 3.1 (+) plasmid vector consisting of ampicillin-resistant gene driven by CMV promoter.

To harvest the transformant *E. coli*, the overnight culture was centrifuged at 5,000 g for 10 minutes and discarded the supernatant. The plasmids were extracted and purified using the GeneJet Plasmid Maxiprep Kit (Thermo Scientific, MA, USA) according to the manufacturer's instruction. The extracted plasmids were determined the purity (A260/A280) and concentration of plasmid by the Thermo Scientific™ NanoDrop 2000 spectrophotometer. The plasmids in each preparation were sequenced and aligned with each original plasmid sequence to confirm the accuracy of the plasmid sequence. After plasmid sequencing, plasmids were pooled and stored at -20˚C until use.

B1 siRNA and plasmid control preparation

The B1 siRNA [5'-AGUUUCUCUGUGUAACAGCCC-3' (sense) and 5'-GCUGUUACACAGAGAAACUCU-3' (antisense)] sequences were designed using siDirect 2.0 siRNA design software (Naito & Ui-Tei, 2012) and synthesized by U2Bio Co., Ltd. (Korea). The pLenti-C-mGFP-P2A-Puro (scramble-GFP) plasmid (Origene Technologies, Inc., CA, USA) containing green fluorescence protein (GFP) was utilized as an *in vitro* transfection control, and the pcDNA 3.1(+) plasmid containing a FLAG sequence (Invitrogen, USA) was used as a transfection control plasmid in a rat wound model. Each plasmid was transformed into competent *E. coli* (DH5α) (Invitrogen, USA). After selective bacterial culture, the plasmids were extracted and purified using the GeneJet Plasmid Maxiprep Kit (Thermo Scientific, MA, USA) according to the manufacturer's instructions. The purity (A260/A280) and concentration of the plasmids were determined using a Thermo Scientific™ NanoDrop 2000 spectrophotometer.

จุฬาลงกรณ์มหาวิทยาลัย
Chulalongkorn University

Plasmid DNA and siRNA delivery using Ca-P nanoparticles *in vitro* and *in vivo*

To deliver the B1 siRNA or the plasmid into the target cells, each type of genetic material was coated with the nanoparticle solution as previously described by Zhao *et al.* (2014) with some modifications before topical administration. (Zhao et al., 2014) The most effective plasmid ratio to nanoparticle solution for transfection was 5 µg plasmid in 100 µl of nanoparticle solution. The nanoparticle solution was comprised of 50 µl of a mixture of 0.5 M calcium chloride ($CaCl_2$) solution (Merck Millipore, USA) and 5 µg of plasmid DNA as well as 50 µl of a mixture of 0.01 M sodium carbonate (Na_2CO_3) solution (Merck Millipore, USA) and 0.01 M sodium dihydrogen phosphate monohydrate ($NaH_2PO_4 \cdot H_2O$) solution (Merck

Millipore, USA). A molar ratio of CO_3^{2-}/PO_4^{3-} of 31:1 was used. First, the plasmid was mixed with 16 µl of 0.5 M calcium chloride ($CaCl_2$) solution, and the final volume was adjusted to 50 µl using sterile dH_2O. Then, the plasmid DNA-calcium complex was added to 50 µl of a mixture of sodium carbonate solution (16 µl), sodium dihydrogen phosphate monohydrate solution (16 µl), and sterile dH_2O (34 µl). The nanoparticle-coated plasmid solution was freshly prepared before transfection or administration.

Confocal microscopy

We investigated the efficiency of transfection using the nanoparticle-coating solution and Ca-P nanoparticle-coated Box A-GFP plasmids by transfecting them into HEK293 cells ($5x10^4$ cells/well) in a 24-well plate 24 hours after cell seeding. The transfected HEK293 cells were observed, and confocal images were captured at 20X 48 hours after transfection using a confocal microscope (ZEISS LSM 800, CARL ZEISS, USA).

Animal models for aging study

All animal procedures were reviewed and approved by the Animal Care and Use Committee, Chiang Mai University, Thailand, in conformity with the Association for Assessment and Accreditation of Laboratory Animal Care (AAALAC) guidelines (Approval No. 2562/RT0013 and 09/2563). Twenty-four male Wistar rats (6-8 weeks of age) were obtained from the National Laboratory Animal Center, Mahidol University, Bangkok, Thailand, and twenty-four male Wistar rats (10 weeks of age) were purchased from Nomura Siam International, Bangkok, Thailand. After one week of acclimatization, all animals were housed in a temperature-controlled chamber (25±0.5°C) with a 12:12-hour light/dark cycle until they reached the desired ages (3 months of age for the D-gal study and at 28 months of age for the natural aging study). Standard diet and sterilized water were provided *ad libitum* All rats were monitored daily and weighed weekly. The desired aged rats of both studies were randomly assigned to subgroups by a veterinarian who was blinded to the characteristics of the rats. For the D-gal study, the first group of rats (n=16) was subcutaneously injected with D-gal (150 mg/kg, Sigma Aldrich, St Louis, MO, USA) in normal saline solution (NSS) daily for 16 weeks, and the other (normal control) group of rats (n=8) was administered NSS without D-gal in the same manner. After an 8-week D-gal injection period, the D-gal rats were randomly subdivided into two groups of 8 rats per group. Group 1: Normal rats (7 months old) were intraperitoneally injected with 100 µg of pcDNA3.1 per kg body weight (7 m→PC) once a week for 8 weeks. Group 2: D-gal rats (aging control) were intraperitoneally administered 100 µg/kg pcDNA3.1 (D-gal→PC), and Group 3: D-gal rats (treatment group) were also injected with 100 µg/kg Box A plasmid (D-gal→Box A) in the same manner. For the D-gal aging study, the rats were

subjected to a lateral tail vein bleed of approximately 300 µl at baseline (3 months of age), after 8 weeks of the D-gal or NSS injection (5 months of age), and after 8 weeks of the treatment (7 months of age). For the natural aging study, the rats were aged in a house until the age of 28 months and then randomly designated into three groups. Twenty-eight-month-old rats were injected with Box A plasmid (30 m→Box A, n=10), pcDNA3.1 (30 m→PC, n=10), and p. F38G (30 m→p. F38G, n=4) for consecutive 8 weeks. Rat blood samples were also collected before and after the treatment period (at 2 8 and 30 months of age, respectively). The rat sera were shipped to the Hematology and Biochemistry Laboratory, Small Animal Hospital, Faculty of Veterinary Medicine, Chiang Mai University, for analysis of rat liver function parameters. At the end of the treatment, the rats in all experiments were euthanized, and various rat tissues were immediately collected in 4% paraformaldehyde (PFA) (Sigma Aldrich, MO, USA) and 10% formalin buffer and snap frozen in liquid nitrogen at -80°C for subsequent analyses. All snap frozen tissues were shipped to the Faculty of Medicine, Chulalongkorn University, on dry ice. Visceral fat was weighed and reported as visceral fat per 100 g of rat bodyweight.

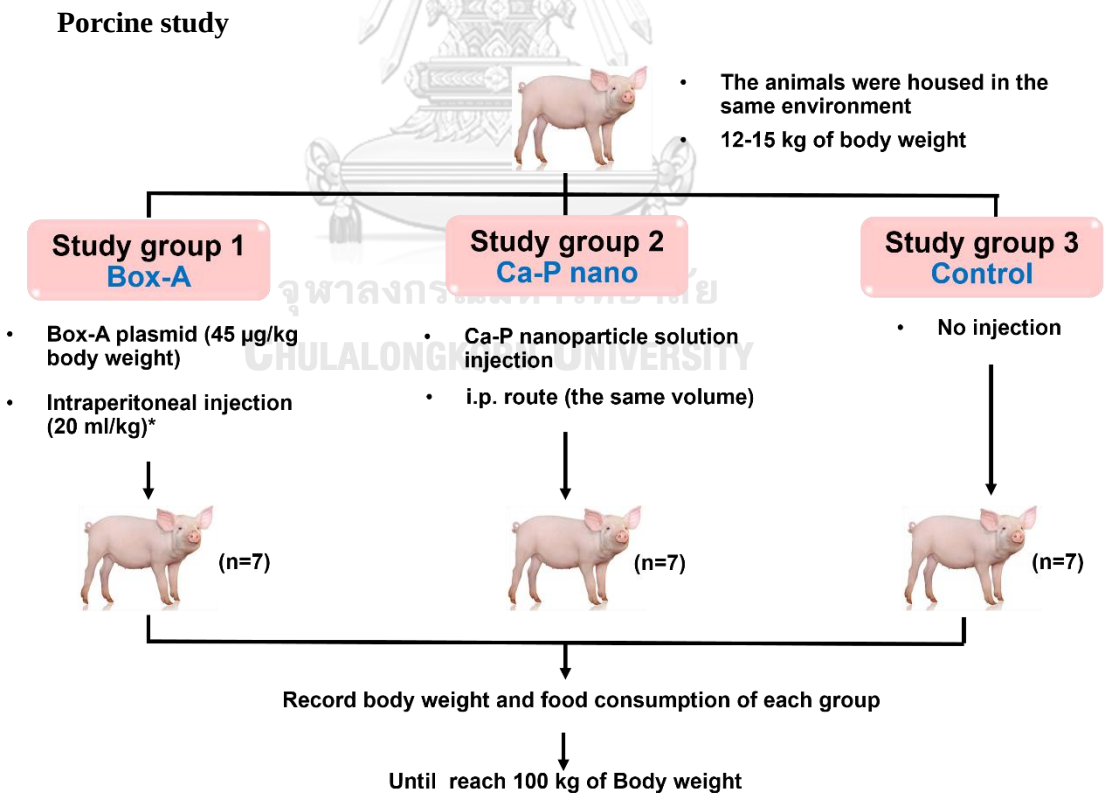

*Recommended Dose Volumes for Common Laboratory Animal, 2016

All animal procedures were approved by Mahidol University-Institute Animal Care and Use Committee (MU-IACUC), Mahidol University, Thailand, in conformity with the Association for Assessment and Accreditation of Laboratory Animal Care (AAALAC) guidelines (Protocol number: MUVS-KA 2018-11-02, approved 01/2019). After weaning, twenty-one male micropigs (21 days of age) were obtained from Betagro, Thailand. The study was conducted at a farm of the Faculty of Veterinary Medicine, Mahidol University, Kanchanaburi, Thailand. All pigs were housed in a temperature-controlled room (25±0.5°C) with a 12:12 h light/dark cycle. At the 3rd and 10th week of age, all animals were received standard vaccine regimen, including Enrofloxacin vaccine (5 mg/kg) and Classical Swine Fever vaccine (Coglapest, CEVA), respectively. After 7 days of acclimatization, all pigs were weighed and randomly divided into three groups (7 animals per group), and no difference of average body weight among three groups was observed at the starting point of the study. Pigs in all groups were fast for 9 hours before a single dose of plasmid DNA administration. The pigs in Group 1 (treatment group) were intraperitoneally injected with Box A plasmid/Ca-P nanoparticle (100 μg of Box A plasmid per kg body weight). The pigs in Group 2 were administrated with a single dose of Ca-P nanoparticle solution (without plasmid DNA) in the same volume and route of administration (a vehicle control group). No treatment was performed in the Group 3 pigs (no treatment control group). After 14 weeks of treatment period, all pigs were euthanized and porcine organs were immediately collected, including heart, liver, kidney, small intestine, muscle (sirloin), and skin, and stored at -20˚C for subsequent analyses. The porcine heart, liver, kidney, small intestine, muscle (sirloin), and skin were extracted and detected the contaminant plasmid DNA. Sirloin was also stored at -20˚C for sensory evaluation assessment.

จุฬาลงกรณ์มหาวิทยาลัย
Chulalongkorn University

Wound healing in an animal study

Diabetic rat model

Male Wistar rats (6 weeks old and 150-180 g) were obtained from the National Laboratory Animal Center, Mahidol University, Bangkok, Thailand. The Institutional Animal Care and Use Committee (IACUC) approved the animal use protocol at the Faculty of Medicine, Chulalongkorn University (approval number: 006/2561 in September 2018). Rats were maintained on a control 12:12-hour light:dark cycle and *ad libitum* fed standard normal chow and water. Animals were allowed to acclimatize for seven days before type 1 diabetes induction. Rats were then randomly divided into two groups and intraperitoneally injected with (1) a single

dose of 65 mg/kg body weight STZ (Sigma–Aldrich, USA) dissolved in 50 mM sodium citrate buffer (Alfa Aesar, USA) and (2) 50 mM sodium citrate buffer (2 mL/kg body weight). (Furman, 2015a) (King, 2012) After 7 days of STZ induction, the fasting blood sugar (FBS) levels were monitored in both groups using a glucometer and blood glucose strips (ACCU-CHEK® Roche, Germany). The STZ-induced rats with FBS greater than 250 mg/dL were considered diabetic rats, whereas the rats with FBS lower than 150 mg/dL were considered nondiabetic rats.

Excisional wound protocol

Two paired full-thickness excisional wounds were created at the dorsa of rats using an 8-mm biopsy punch and splinted with silicone rings. (Davidson et al., 2013) (Yao et al., 2014) Diabetic and nondiabetic rats were further subdivided into two groups and treated with nanocoated B1 siRNA and NSS, and the NSS-treated group represented the standard wound dressing in this study. The nondiabetic and diabetic wounds were dressed daily and treated with each type of intervention for 14 days. The wound area was measured at days 0, 3, 5, 7, 10, and 14 after the treatment and was reported as the percent wound closure rate using the following formula: percent wound closure rate = [(wound area *day 0* – wound area *day n*)/wound area *day 0*]x100 (day *n* representing days 3, 5, 7, 10, or 14). To investigate the expression of the genetic materials using Ca-P nanoparticles in rat wounds, the nanocoated pcDNA 3.1 (+) plasmid control with the FLAG-tagged protein sequence was topically applied to the wounds. After 14 days of the complete healing process, all rats were sacrificed, and the wound areas were excised and immediately collected in DNAzol reagent (Invitrogen, USA) for measurement of DNA methylation levels and in 10% formalin buffer for histological determination and immunohistochemistry staining.

จุฬาลงกรณ์มหาวิทยาลัย
Chulalongkorn University

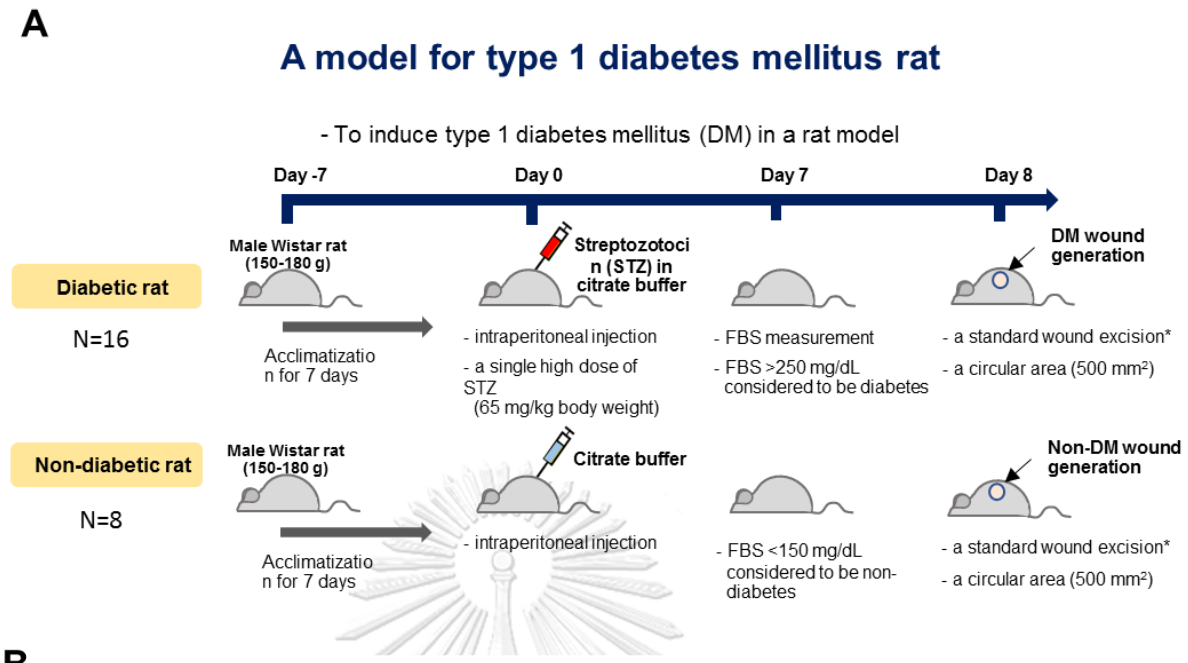
A
A model for type 1 diabetes mellitus rat
- To induce type 1 diabetes mellitus (DM) in a rat model
Day -7
Day 0
Day 7
Day 8
Diabetic rat
N=16
Male Wistar rat (150-180 g)
Acclimatization for 7 days
Streptozotocin (STZ) in citrate buffer
- intraperitoneal injection
- a single high dose of STZ (65 mg/kg body weight)
- FBS measurement
- FBS >250 mg/dL considered to be diabetes
DM wound generation
- a standard wound excision*
- a circular area (500 mm²)
Non-diabetic rat
N=8
Male Wistar rat (150-180 g)
Acclimatization for 7 days
Citrate buffer
- intraperitoneal injection
- FBS <150 mg/dL considered to be non-diabetes
Non-DM wound generation
- a standard wound excision*
- a circular area (500 mm²)

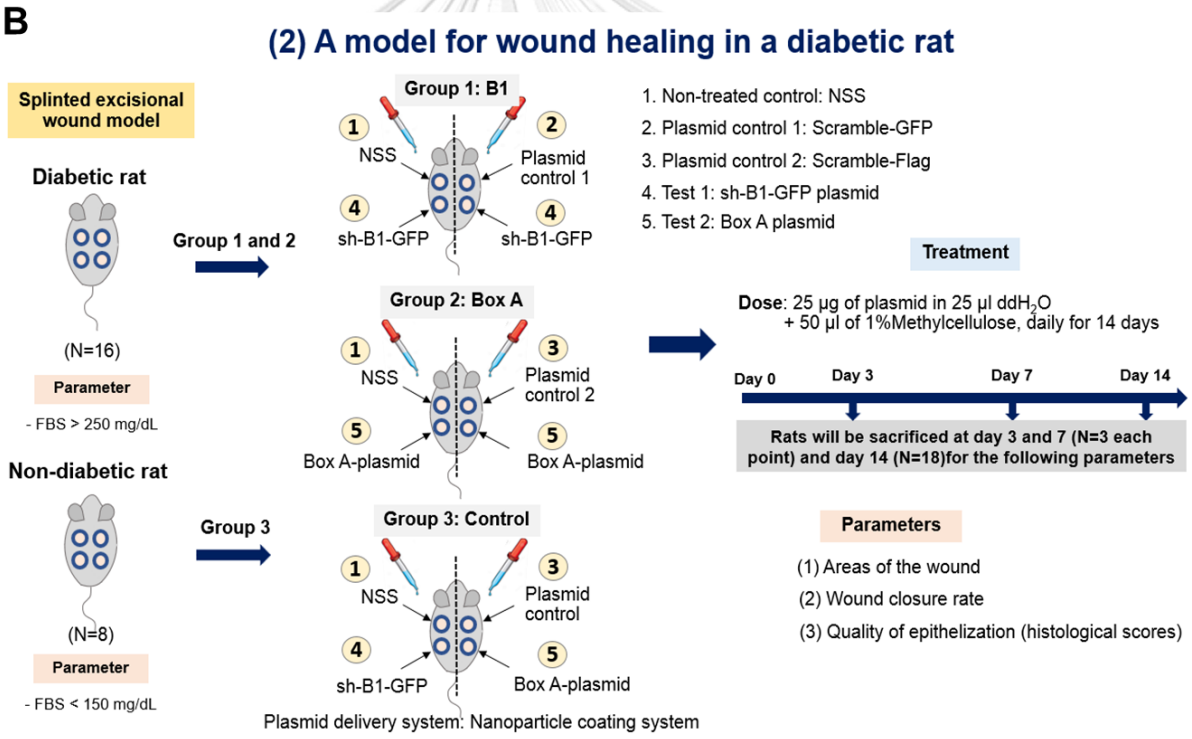
B
(2) A model for wound healing in a diabetic rat
Splinted excisional wound model
Diabetic rat
(N=16)
Parameter
- FBS > 250 mg/dL
Non-diabetic rat
(N=8)
Parameter
- FBS < 150 mg/dL
Group 1 and 2
Group 3
Group 1: B1
1 NSS
2 Plasmid control 1
4 sh-B1-GFP
4 sh-B1-GFP
Group 2: Box A
1 NSS
3 Plasmid control 2
5 Box A-plasmid
5 Box A-plasmid
Group 3: Control
1 NSS
3 Plasmid control
4 sh-B1-GFP
5 Box A-plasmid
Plasmid delivery system: Nanoparticle coating system
1. Non-treated control: NSS
2. Plasmid control 1: Scramble-GFP
3. Plasmid control 2: Scramble-Flag
4. Test 1: sh-B1-GFP plasmid
5. Test 2: Box A plasmid
Treatment
Dose: 25 µg of plasmid in 25 µl ddH2O + 50 µl of 1%Methylcellulose, daily for 14 days
Day 0
Day 3
Day 7
Day 14
Rats will be sacrificed at day 3 and 7 (N=3 each point) and day 14 (N=18)for the following parameters
Parameters
(1) Areas of the wound
(2) Wound closure rate
(3) Quality of epithelization (histological scores)

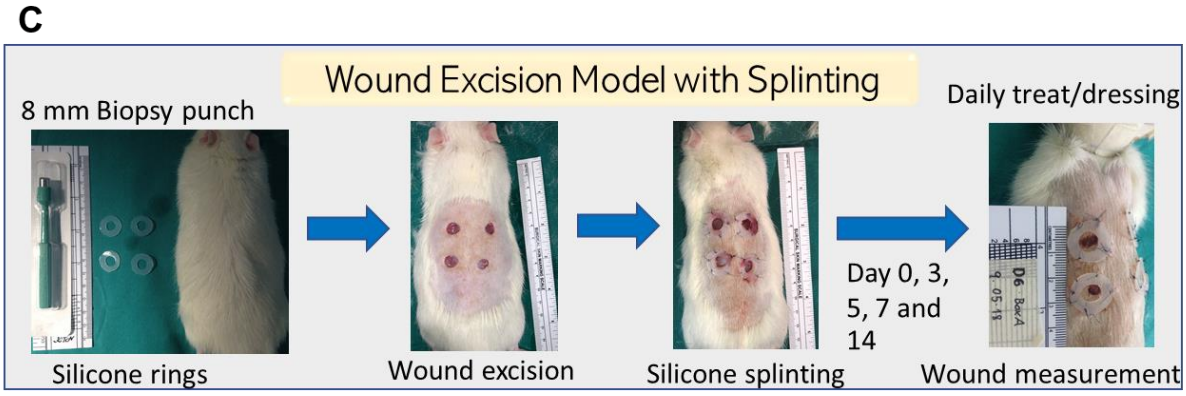

Figure 3-3 Illustrations display a method to generate type 1 diabetic rats **(A)**, the experimental design for diabetic wound healing study **(B)**, and an example of wound excision model with splinting technique **(C)**.

Morris water maze (MWM) performance

Since motor and anxiety-like behaviors could impact the results of cognitive assessment, we first evaluated the modulatory effects of our treatments on locomotor activity and anxiety throughout the experiment using an open field test. We found that there were no significant differences among all groups in the total distance traveled, average speed, and total time spent in the central zone, indicating no potential impact of any motor disorders or anxiety on cognitive assessments. Spatial learning and memory were assessed by the MWM test in both D-gal and natural aging rats at the end of the treatment period. The water maze test was performed using a circular pool 200 cm in diameter filled with water (26±1°C), following Morris's protocol of Vorhees & Williams. A 10 cm^2 escape platform was placed in the designated quadrant of the pool and submerged ~1-2 cm below the water surface. The MWM test was composed of two different sessions, including the acquisition test and the probe test. In the acquisition training test, each rat was trained to navigate to the platform four trials per day for five consecutive days. Each rat was given a trial limit of 120 s per trial and guided to the platform when it reached the time limit. The rats were left on the platform for 15 s during the intertrial interval. The escape latency time was recorded from the starting point until the rats reached the platform using the camera. In the probe test (the 6^{th} day), the platform in the target quadrant was removed, and rats were placed in a novel starting position (the opposite of the target quadrant). The time that rats spent in the target quadrant was recorded during the 120-s testing period. The data analysis was performed from the video files using SMART 3.0 software (Panlab Harvard Apparatus, Barcelona, Spain).

Determination of serum hepatic biochemical parameters

Rat serum samples were shipped to the Hematology and Biochemistry Laboratory, Small Animal Hospital, as mentioned above. Levels of serum aspartate aminotransferase (AST), alanine aminotransferase (ALT), alkaline phosphatase (ALP), total protein (TP) and albumin were measured using an Automated Clinical Chemistry Analyzer (BX-3010, Sysmex, Japan). Serum globulin levels were calculated from serum TP and albumin levels.

SA-β-Gal staining, immunohistochemical (IHC) staining and histopathological analysis

After euthanization, rat tissues were immediately dissected and fixed in fresh fixative buffer. For SA-β-gal staining on liver cryosections, tissue was stored in 4% PFA before embedding in OCT (Sakura, Tissue-Tek, Hatfield, PA, USA) and cryosectioning at 10 µm-thickness. After rehydration of the liver section in PBS, the sections were SA-β-gal stained using the Cell Signaling kit (9860, Beverly, MA, USA) with a 15-min fixation followed by 37°C incubation in the staining solution for 12 h. For IHC and histopathological analyses, tissues were fixed in 10% formalin buffer for at least 48 h. Then, the tissues were dehydrated and paraffin-embedded before 5-µm thick tissue sectioning by a microtome. Subsequently, the rat liver and pancreas sections were stained with hematoxylin & eosin (H&E) according to standard procedures for histopathological analysis. For IHC staining, rat spleen and muscle (gastrocnemius) were stained with anti-DYKDDDDK tag (FLAG) rabbit monoclonal antibody (14793, Cell Signaling, MA, USA) diluted 1:500. The mounted sections were captured using a Leica DM1000 inverted microscope with a color camera. Masson's trichrome staining was conducted to measure collagen accumulation in the liver according to the manufacturer's standard protocol (Bio-Optica, 04-010802, Malino, S.p.A. For quantification of SA-β-gal in the liver, hepatic sinusoidal space, collagen accumulation in the liver, and islets of Langerhans size, the images were analyzed using ImageJ software (n=3-4 animals per group).

จุฬาลงกรณ์มหาวิทยาลัย
Chulalongkorn University

High-Molecular weight (HMW) DNA preparation from rat WBCs for EDSB-LMPCR (DNA-GAPs)

To determine physiologic RIND-EDSB numbers, high-molecular weight (HMW) DNA was prepared as described previously (Thongsoy J, *et al*, 2013). Briefly, after buffy coat (WBC) isolation from rat EDTA blood, WBC pellets were embedded in 1% low melting point agarose at a concentration of 3-5 µg DNA per plug. Then, the embedded samples were digested in 400 ml of digestion buffer (1 mg/ml proteinase K, 50 mM Tris, pH 8.0, 20 mM EDTA, 1% sodium lauryl sarcosine) at 37˚C overnight. The plugs were rinsed in TE buffer at least 6 times for 40 minutes. EDSBs with cohesive ends were polished by incubating with T4 DNA polymerase (New England Biolabs, Beverly, MA, USA) along with dNTPs for 1 hour. Next, EDTA was added to inactivate the enzyme at a final concentration of 20 mM for 5 minutes, and

further rinsed 6 times in TE buffer for 40 minutes. The modified LMPCR linkers were prepared from oligonucleotides: 5'-AGGTAACGAGTCAGACCACCGATCGCTCGGAAGCTTACCTCGTGGACGT-3' and 5'-ACGTCCACGAG-3' (Sigma, Singapore) (Kongruttanachok N, *et al*, 2010). The linkers (50 pmol) were ligated to the polished EDSB ends in the HMW DNA preparations using T4 DNA ligase (New England Biolabs) at 25˚C overnight. The linker-ligated DNA was then extracted from the agarose plugs using a QIAquick gel extraction kit (Qiagen, Basel, Switzerland) (Kongruttanachok N, *et al*, 2010). The quantity of EDSBs were measured by real-time PCR using an ABI PRISMH 7500 system (Applied Biosystems, Carlsbad, CA, USA) with B1 primer 5′-GTTGGTGGCGCACGCCTTTA-3′, the linker primer and the Taqman probe homologous to the 3' linker sequence (6-fam) ACGTCCACGAGGTAAGCTTCCGAGCGA (tamra, phosphate) [Sigma, Singapore] (Kongruttanachok N, *et al*, 2010). DNA amplification was conducted with 0.2 mM of each primer, 0.3 mM Taqman probe, 0.025 U of HotStarTaq, 16TaqManH Universal PCR Master Mix (Applied Biosystems) and 10 ng of ligated DNA. Initial denaturation was at 95˚C for 15 minutes, followed by denaturation at 95˚C for 5 seconds, annealing at 60˚C for 5 seconds, and extension for 2 minutes at 69˚C for 45 cycles, with quantification after each extension step (Kongruttanachok N, *et al*, 2010). The numbers of EDSBs were compared with the untreated rat liver control DNA and reported in arbitrary units of B1-EDSB–LMPCR templates per genome. Control DNA digested by *EcoRV* and *AluI* (Thermo Fisher Scientific, MA, USA) and ligated with linkers was used to generate a standard curve. The PCR cycle was set as follows: 1 cycle of 50°C for 2 mins followed by 95°C for 10 mins and 60 cycles of 95°C for 15 seconds along with 60°C for 2 mins. For rat aging studies, number of DNA-GAPs was calculated from a standard curve of control DNA and reported as %DNA-GAP PCR (%DNA-GAP number of the control).

จุฬาลงกรณ์มหาวิทยาลัย
Chulalongkorn University

Rat liver protein preparation for Western blotting assay

Snap frozen liver tissues were thawed and immediately homogenized on ice using ice-cold RIPA buffer (50 mM Tris pH 7.5, 150 mM NaCl, 10 mM EDTA, 1% NP, 0.1% SDS). Fifty milligrams of each tissue were mixed with 0.5 mL RIPA buffer containing protease inhibitor cocktail (Cat. No. 11836170001, Roche Diagnostics, USA) and phosphatase inhibitor cocktail (Cat No. 4906845001, Roche Diagnostics, USA). The protein concentration of the tissue extract was measured using a BCA assay, and the protein expression level was assessed by Western blotting analysis, as described above. To quantitate a DNA damage marker in rat liver, the tissue extract was probed with primary antibody phospho-Histone H2A.X (Ser139) (1:1000, rabbit mAb, Cell Signaling, cat: 9718). For a detection of ageing marker and upstream

signaling protein expression, the liver protein was probed with primary antibodies, including $p16^{INK4A}$ (1:1000, rabbit mAb, ABClonal, cat: A0262), p21 Waf1/Cip1 (1:1000, mouse mAb, Santa Cruz, cat: sc-6246), and p53 (1:1000, rabbit mAb, Cell Signaling, cat: 32532), respectively.

DNA extraction and bisulfite DNA modification

Rat wound DNA in DNAzol reagent was extracted using a standard protocol of tissue genomic DNA extraction. (Chomczynski et al., 1997) Briefly, 25-30 mg of rat wound tissue in 1 ml of DNAzol reagent was homogenized in a tissue homogenizer (IKA ULTRA-TURRAX dispersers, Sigma–Aldrich, USA) followed by a tissue genomic DNA extraction protocol according to the manufacturer's instruction. The extracted rat genomic DNA was dissolved in 8 mM NaOH, and genomic DNA concentration and purity were detected by a NanoDrop 2000 spectrophotometer (Thermo Scientific™, USA). The rat genomic DNA was stored at -20 °C until bisulfite DNA modification was performed. Rat genomic DNA (400 ng) was subjected to sodium bisulfate DNA modification according to the manufacturer's instruction manual (EZ DNA Methylation-Gold™ Kit, Zymo Research, CA, USA).

Measurement of B1 methylation by B1-Combined Bisulfite Restriction Analysis (B1-COBRA)

To determine the DNA methylation levels of B1 elements in the rat wound area, bisulfite-treated rat wound DNA was subjected to B1-PCR amplification using a PCR mixture, containing 1X PCR buffer (Qiagen, Germany), 1 mM $MgCl_2$ (Qiagen, Germany), 0.2 mM dNTPs (Promega, USA), 25 U HotStarTaq DNA Polymerase (Qiagen Germany), and 0.2 µM B1-Forward (5'-YGYAYGYYTTTAATYYYAGYAAT-3') and B1-Reverse (5'-CCCTRRCTRTCCTRRAACTCA-3') primer pairs. B1-PCR was amplified using the following protocol to generate a 98 bp amplicon: 95 °C for 15 minutes; 35 cycles of 95 °C for 45 seconds, 53 °C for 45 seconds, and 72 °C for 45 seconds; and final extension of 72 °C for 10 minutes. For B1-COBRA, the B1-PCR products were subsequently subjected to the digestion of 2 units of TaqI restriction enzyme (Thermo Scientific, MA, USA) at 65 °C for 16 hours. The digested B1-PCR products were then analyzed by 8% acrylamide gel electrophoresis and stained with SYBR green (Lonza, Basel, Switzerland). Rat dermal fibroblast (RDF) DNA was subjected to bisulfite DNA modification, B1-COBRA, and TaqI digestion by similar protocols as the experimental samples, and it was used as a rat genomic internal control DNA.

CHULALONGKORN UNIVERSITY

The methylation of B1-COBRA was assessed by detection of band intensity using Image Quant software (GE Health care®, UK). (Thongsroy et al., 2017) (Patchsung et al., 2018)

Determination of B1 methylation level

The B1 methylation level was assessed by calculating the digested B1-PCR products after TaqI digestion, and four different product sizes (98, 78, 54, and 44 bp) were detected and used to differentiate the B1 methylation status. Two forms of B1 methylation were reported, including B1 loci with methylated CpGs (mC) and B1 loci with unmethylated CpGs (uC). The formula of B1 methylation calculation was designated by the band intensity per amplicon size (bp) as follows: A = 98/98, B = 78/74, C = 54/54, and D = 44/42. The band intensities of each sample were normalized by using the average intensity of the internal RDF DNA as mentioned above. The B1 methylation level was calculated from the percentage of methylated band intensity divided by the total mC and uC band intensities as follows: [(A+C+D)/2(A+B+D) x 100]. (Thongsroy et al., 2017) (Patchsung et al., 2018)

Histopathological analysis of diabetic wound healing study

After wound collection, the wounds were fixed in 10% neutral buffered formalin for at least 48 hours. The tissues were then dehydrated and paraffin-embedded before 3-μm thick tissue sectioning by a microtome. Subsequently, the tissue sections were stained with H&E and Giemsa for tissue histopathology and immune cell infiltration, respectively. The histopathological evaluation was blindly performed and interpreted by two pathologists. Tissue granulation and re-epithelization were investigated in the observed areas of healing wounds and reported as the overall histological score as follows: 1= normal tissue; 2= mature fibroblasts; 3= immature fibroblasts; 4= mild inflammation; and 5= granulation tissue.

Immunohistochemistry for FLAG, 8-OHdG, and γH2A.X staining

Paraffin-embedded sections (3-μm) were deparaffinized and subjected to antigen retrieval by proteinase K (DAKO, CA) incubation for 2 min. To elucidate the transfection efficiency of Ca-P nanoparticles after FLAG-tagged plasmid control/Ca-P transfection in diabetic wounds, the wound sections were incubated with 1:500 anti-FLAG (DYKDDDDK) rabbit monoclonal antibody (Cell Signaling, MA) followed by incubation with HRP-conjugated anti-rabbit secondary antibody (DAKO, CA). For DNA damage determination, the wound sections were incubated with a 1:8,000 dilution of polyclonal goat anti-8-OHdG antibody (Merck Millipore) or a 1:100 dilution of rabbit anti-γH2A.X antibody (Abcam) followed by

incubation with HRP-conjugated anti-goat or rabbit secondary antibody (DAKO, CA). Subsequently, the sections were counterstained with hematoxylin.

Confocal microscopy

To investigate the efficiency of transfection using nanoparticle-coating solution, Ca-P nanoparticle-coated scramble-GFP plasmids were transfected into HEK293 cells ($5x10^4$ cells/well) in a 24-well plate 24 hours after cell seeding. The transfected HEK293 cells were observed, and images were acquired at 20X 48 hours after transfection using a confocal microscope (ZEISS LSM 800, CARL ZEISS, USA).

Statistical analysis

The data were expressed as the mean ± SEM. One-way ANOVA was performed to test the difference between the groups followed by post hoc analysis. $P<0.05$ was considered statistically significant using GraphPad Prism version 9.

จุฬาลงกรณ์มหาวิทยาลัย
Chulalongkorn University

CHAPTER IV

RESULTS AND DISCUSSION

PART 1: A novel formula of gene/Ca-P nanoparticle delivery *in intro* and *in vivo* study.

Plasmid/Ca-P nanoparticle transfection and optimization in cell culture.

The plasmid-encapsulated Ca-P nanoparticles successfully delivered and expressed green fluorescent protein (GFP) in HEK293 cells. I transfected the GFP plasmid/Ca-P nanoparticle complex into 5x104 HEK293 cells, and GFP expression was observed at 72 hours after transfection (**Figure 4-1**). Furthermore, the scramble-GFP, sh-B1-GFP, and Box A-GFP plasmid-encapsulated Ca-P nanoparticles (1 µg plasmid/100 µl Ca-P nanoparticle solution, upper panel from left to right) was transfected into the cells. Therefore, it suggests that the novel formula of Ca-P nanoparticles effectively delivered genetic materials in the varied sizes of plasmid in a cell culture system.

However, the study in a rat model required a higher concentration of plasmid per Ca-P nanoparticle solution, the ratio of plasmid concentration per Ca-P nanoparticle solution was validated by increasing from 1 to 10 µg of scramble-GFP plasmid/100 µl Ca-P nanoparticle solution including 1, 2, 5, and 10 µg, respectively. At 48 hours after the transfection, the 5 µg of plasmid/100 µL Ca-P nanoparticle solution ratio exhibited the highest numbers of GFP-producing HEK cells (**Figure 4-2**).

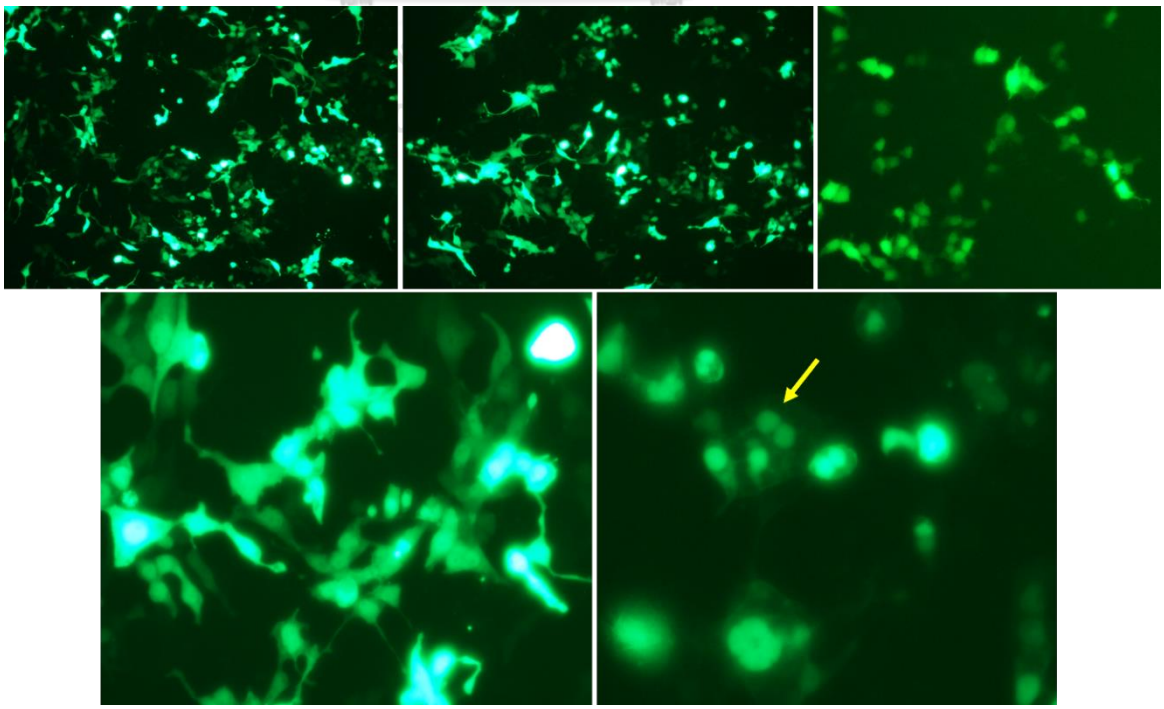

Figure 4-1. GFP-expressing HEK293 cells after 72 hours of plasmid/Ca-P nanoparticle transfection. Cells ($5x10^4$) were transfected with scramble-GFP, sh-B1-GFP, Box A-GFP plasmid-encapsulated Ca-P nanoparticles (1 µg plasmid/100 µl Ca-P nanoparticle solution), upper panel from left to right. At 72 hours after transfection, representative images were acquired using a fluorescence microscope at 10X and 20X magnifications (Zeiss LSM 800, Carl Zeiss, USA). The green color shows the GFP produced by the transfected HEK293 cells. The yellow arrow (right, lower panel) indicated GFP protein accumulated in the nucleus of Box A-GFP plasmid-transfected cells.

To investigate when the transfected cells produced GFP by the Ca-P nanoparticle transfection system, a total of $5x10^4$ cells were transfected with nanoparticle-coated Box A-GFP plasmid (5 µg plasmid/100 µl Ca-P nanoparticle solution) and recorded the time-lapse after the transfection initiation by a confocal microscope. At 10 hours after the Ca-P/plasmid transfection, the initiation of GFP production was observed within the transfected cells. The representative image was captured using a confocal microscope at 48 hours after transfection (**Figure 4-3**).

จุฬาลงกรณ์มหาวิทยาลัย
Chulalongkorn University

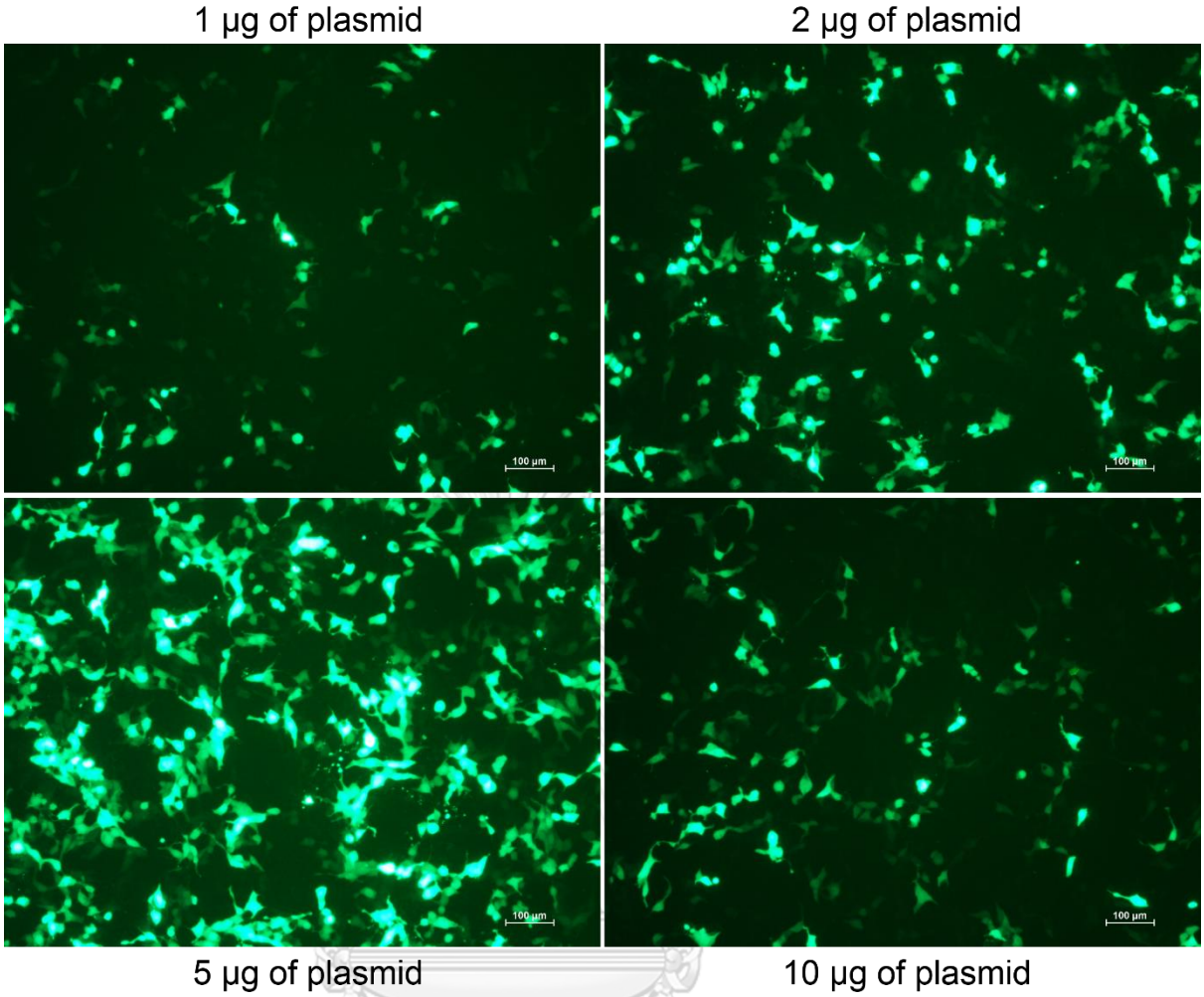

Figure 4-2 Plasmid-Ca P nanoparticle solution transfection optimization for *in vivo* study. To enhance the plasmid expression of Ca-P nanoparticle delivery system for an animal study, the ratio of plasmid to Ca-P nanoparticle solution was varied from 1, 2, 5, and 10 µg of scramble-GFP plasmid to 100 µL of Ca-P nanoparticle solution. The green color exhibits the GFP produced by the transfected cells.

จุฬาลงกรณ์มหาวิทยาลัย
CHULALONGKORN UNIVERSITY

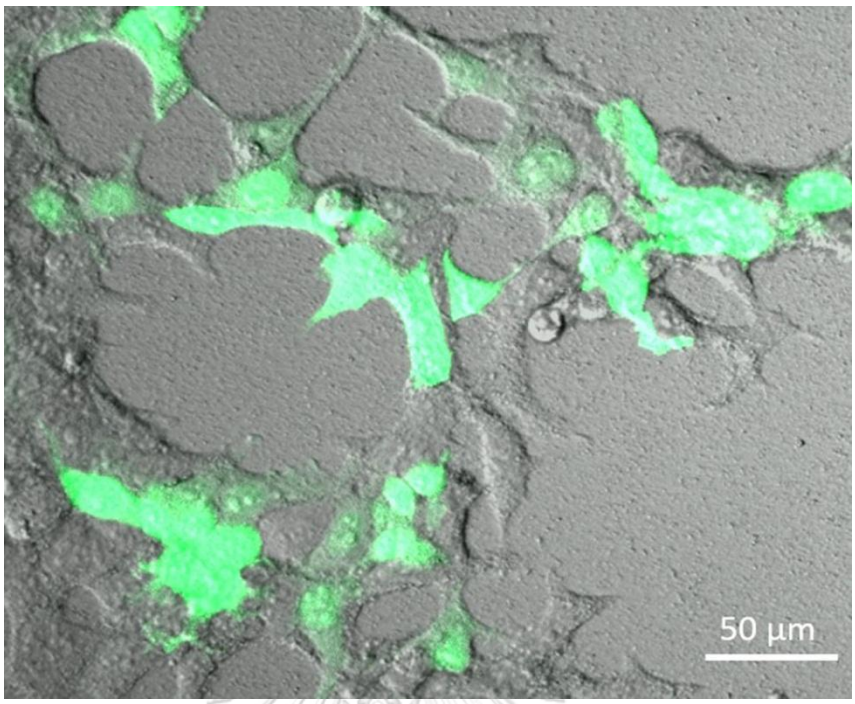

Figure 4-3: Box A with GFP-expressing HEK293 cells 48 hours after Ca-P nanoparticle transfection by confocal microscopy. To confirm Ca-P nanoparticle transfection efficiency, a total of $5x10^4$ cells were transfected with nanoparticle-coated Box A-GFP plasmid (5 µg plasmid/100 µl Ca-P nanoparticle solution). At 48 hours after transfection, the images were captured using a confocal microscope at 20X (Zeiss LSM 800, Carl Zeiss, USA). The green color displays the GFP produced by the transfected cells.

จุฬาลงกรณ์มหาวิทยาลัย
Chulalongkorn University

The FLAG expression *in vivo* study by the topical application and the systemic administration of the FLAG-containing plasmid/Ca-P nanoparticle complex.

Besides, I also investigated the transfection efficiency of the Ca-P nanoparticle through topical and systemic administration in an animal model. As mentioned in Chapter 4 (Materials and Methods), a fresh plasmid/Ca-P nanoparticle coating preparation was applied to two different animal models. First, a study of plasmid/Ca-P complex delivery by a topical application, an excisional wound model was generated in nondiabetic (normal), and diabetic rats, and the FLAG protein expression was observed in the rat skin sections. Second, a study of plasmid/Ca-P complex delivery by a systemic administration via an intraperitoneal injection, a rat model was utilized to explore the expression of the FLAG protein in several internal organs, including liver, muscle (gastrocnemius), kidney, adipose tissue, and spleen.

The plasmid-encapsulated Ca-P nanoparticle successfully delivered and expressed the FLAG protein in both murine normal and diabetic wound models. To transfect the pDNA/Ca-

P nanoparticle complex into rat wound cells, five µg of Box A of HMGB1-FLAG plasmid coating with 100 µl of Ca-P nanoparticle was topically applied to one excision wound, and the PC (pcDNA3.1-FLAG)/Ca-P nanoparticle complex was applied to the contralateral wound once daily for 14 days; the control wound was treated with a normal saline solution (NSS). At the end of the study, the rat wounds were collected and immediately fixed in 10% formaldehyde buffer to detect plasmid expression using rabbit anti-FLAG antibody. Positive anti-FLAG staining was found in various cell types, mainly mature fibroblasts, in the dermis

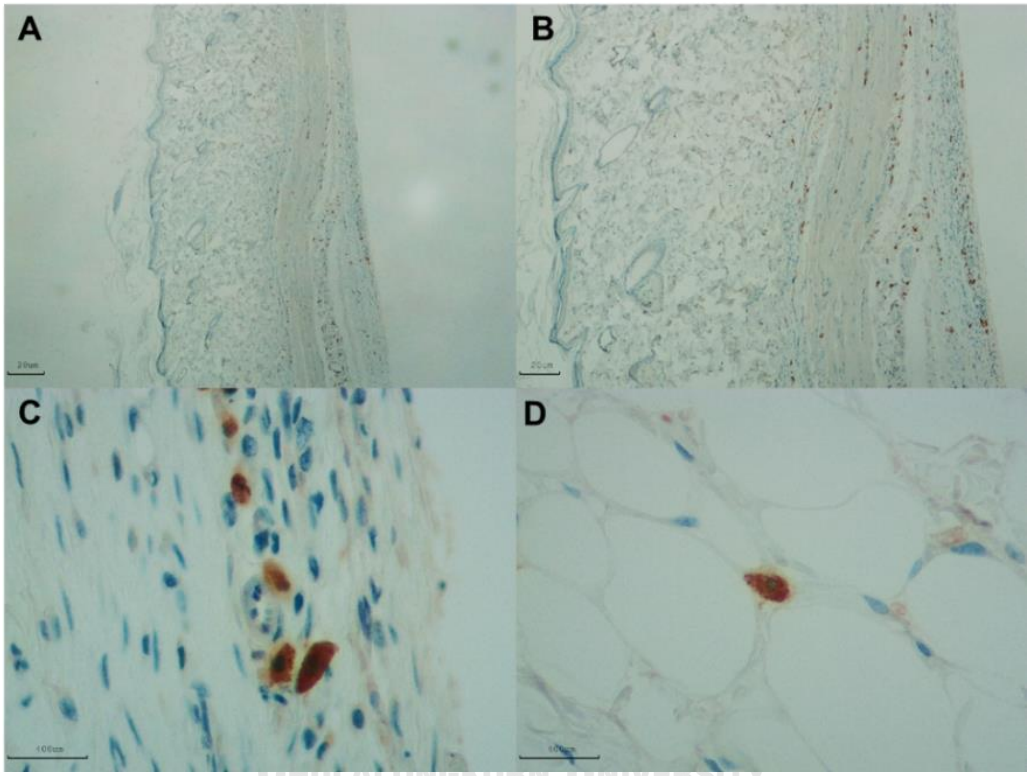

and *panniculus carnosus* (the deepest muscle layer of murine skin), when treated with the FLAG-containing plasmid/Ca-P complex into the normal (nondiabetic) rat wounds (**Figure 4-4** and **Figure 4-5**) and the diabetic rat wounds (**Figure 4-6,** lower panel) compared to NSS-treated wounds (negative control for anti-FLAG staining, **Figure 4-6**, upper panel). Furthermore, the expression of FLAG protein was also detected in adipocytes of the rat wounds (**Figure 4-4, D** and **Figure 4-5, C**) and endothelial cells (**Figure 4-5, B)**.

Figure 4-4 Expression of the FLAG protein by a FLAG-containing pDNA/Ca-P nanoparticle transfection in non-diabetic (normal) rat wounds. Wound sections were stained with an anti-FLAG antibody. Brown color represents the positive FLAG protein-expressing cells by immunohistochemical (IHC) staining (anti-FLAG antibody), including

mature fibroblasts as shown in **A**, **B**, and **C** (2X, 4X, and 40X magnifications, respectively). Adipocytes also displayed positive anti-FLAG staining (**D**, 40X magnification).

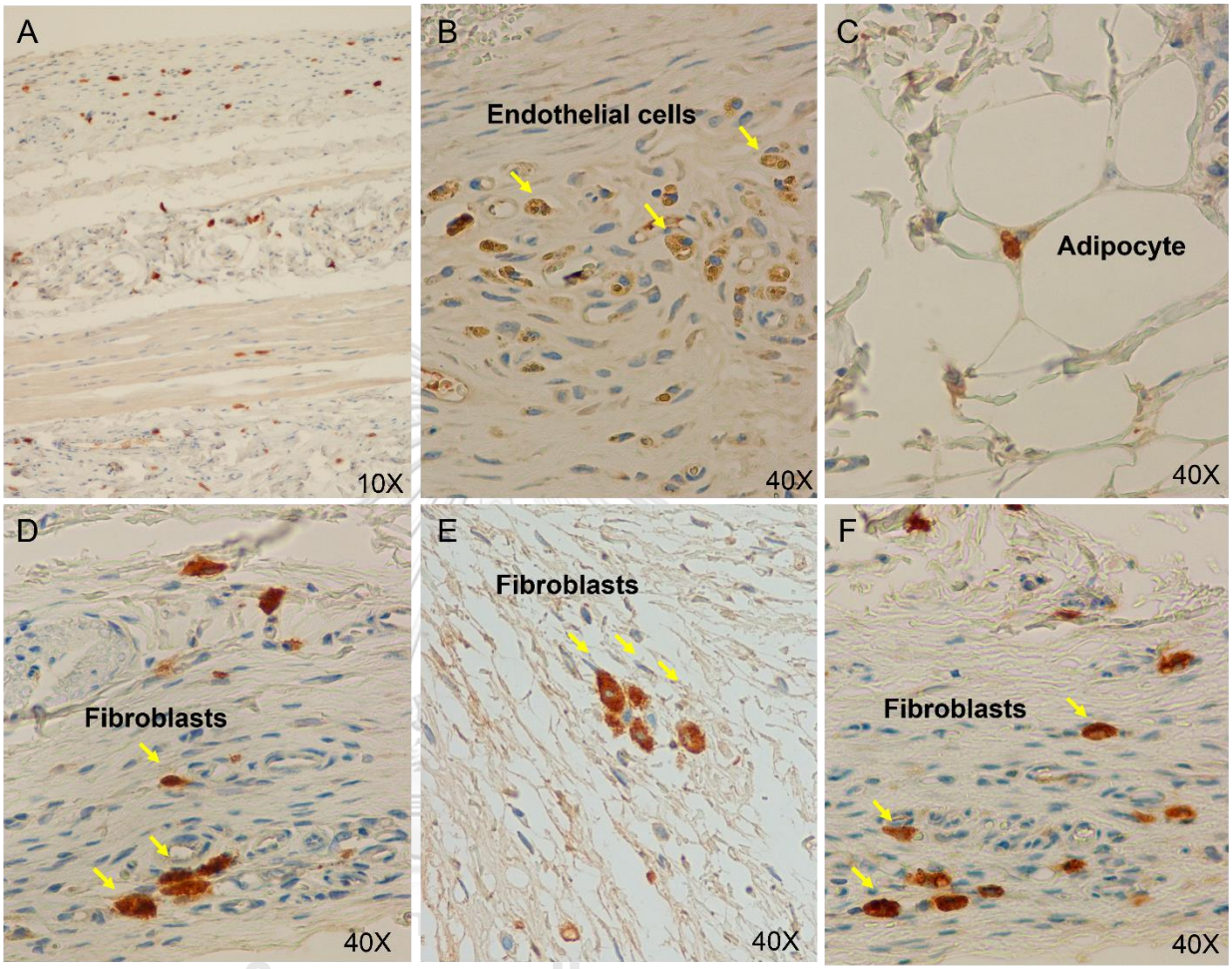

Chulalongkorn University

Figure 4-5 The FLAG-containing plasmid/Ca-P nanoparticle complex transfection by a topical application in normal rat wounds. At the end of the study (day 14), the rat wounds were collected and stained for FLAG protein expression. Positive anti-FLAG staining (brown color) was found in several skin layers (**A**), endothelial cells (**B**), adipocytes (**C**), and mature fibroblasts (**D** to **F**). Representative images of nondiabetic wounds were acquired at 400 magnifications.

Topical application of plasmid/Ca-P delivery study in streptozotocin (STZ)-induced diabetic rat wound model.

A single high dose of streptozotocin (65 mg/kg body weight) was administered to animals to induce type 1 diabetes, whereas the age-matched control rats were injected with

sodium citrate buffer (the STZ solvent) (Furman, 2015a). After one week of STZ induction, the fasting blood sugar (FBS) levels were examined in all rats. The appearance of body weight loss, which is a typically diabetic physiological effect after STZ administration, was also reported, as shown in **Table 1**. The STZ-induced diabetic rats showed significantly higher FBS (432.5 ± 17.7 mg/dL) levels than those of the control littermates (127.0 ± 8.6 mg/dL, ***P<0.001), as displayed in **Table 1**. The eight-mm excisional wounding was then performed on the dorsa of diabetic and control rats, followed by a silicone ring-splinting technique to imitate a healing process in humans and to avoid wound contraction, which normally occurs as a primary mechanism of wound healing in a murine model (Davidson et al., 2013). Fourteen days after wound treatment, the levels of FBS in the diabetic group (417.8 ± 11.2 mg/dL) were still significantly higher than those in the standard group (127.0 ± 8.6 mg/dL, ***P<0.001) (**Table 1)**.

Table 1. The body weight and fasting blood glucose level of nondiabetic and diabetic rats at the end of the study. After seven days of STZ induction, fasting blood glucose levels were measured (>250 mg/dL defined as a diabetic rat) and used as a diabetic group (N=6 each group). Citrate buffer was injected into a nondiabetic group (FBS<150 mg/dL) acting as a control group. After wounding, the diabetic wounds were treated daily with NSS, Nano-PC, or Nano-Box A compared to the nondiabetic (normal) wound.

Group	Non-DM	DM + NSS	DM + Nano-PC	DM + Nano-Box A
Bodyweight (g)	277.5 ± 3.4	192.8 ± 5.7***	190.2 ± 7.3***	195.2 ± 6.8***
Fasting blood glucose (mg/dL)	127.0 ± 8.6	432.5 ± 17.7***	407.6 ± 25.1***	417.8 ± 11.2***

จุฬาลงกรณ์มหาวิทยาลัย
CHULALONGKORN UNIVERSITY

Abbreviation: Non-DM, Nondiabetic group; DM, diabetic group; DM + NSS, diabetic wound treated with normal saline; DM + Nano-PC, diabetic wound treated with nanoparticle with plasmid control; DM + Nano-Box A, diabetic wound treated with nanoparticle with Box A plasmid. Data are presented as the means ± SEM. *** P < 0.001 significant difference compared with the non-DM group.

In addition, the systemic delivery of the plasmid/Ca-P nanoparticle complex was performed in a rat model through an intraperitoneal (i.p.) injection. The i.p. administration successfully expressed the FLAG protein in a rat model after the weekly i.p. injection of the

plasmid/Ca-P nanoparticle for consecutive 8 weeks. The rat organs were collected and dissected for anti-FLAG immunohistochemistry staining. Positive anti-FLAG staining (brown color) was appeared in many organs, including the spleen, muscle, liver, adipose tissue, and kidney (**Figure 4-7**), indicating a capability of Ca-P nanoparticle coating technique for a systemic gene transfer. The FLAG protein is dominantly expressed in spleen tissue when compared to the negative control anti-FLAG staining (**Figure 4-7: A**, upper panel). Additionally, the expression of FLAG protein was detected in Rt. gastrocnemius muscle (**Figure 4-7: A**, lower panel), liver, adipose tissue, and kidney (**Figure 4-8: B**). The results indicated that the novel formula of plasmid/Ca-P transfection (the formula 31:1 of Ca-P nanoparticle solution) efficiently delivered plasmids into the target cells in both cell culture and animal models through topical and systemic administration (an intraperitoneal route).

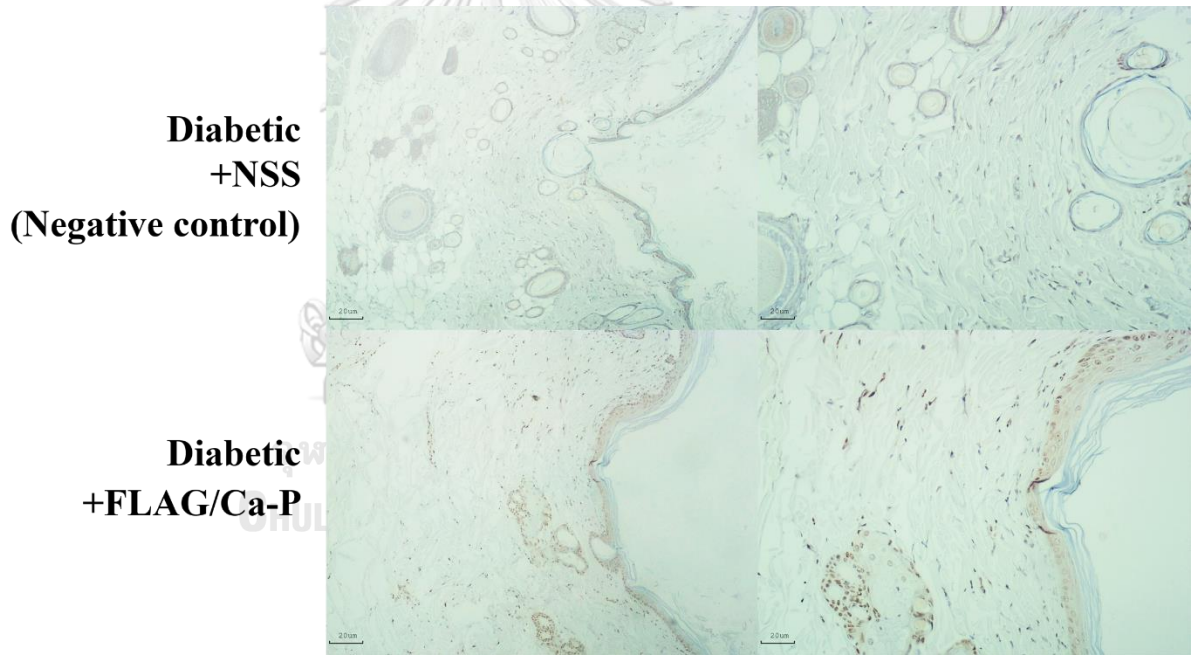

Figure 4-6. FLAG-expressing cells in diabetic wounds. FLAG-tagged plasmid control (pcDNA3.1)-encapsulated Ca-P nanoparticles (lower panel) were applied daily to excisional wounds in diabetic rats by topical treatment for 14 consecutive days, and the control wounds were treated with NSS (negative control, upper panel). At the end of the study, the wounds were dissected and stained for FLAG protein expression by IHC staining. Positive anti-FLAG staining (brown color, lower panel) was observed in many cell types in the epidermis, dermis, and *panniculus carnosus* muscle layer, including mainly mature fibroblasts and keratinocytes,

compared to the no transfection control (the NSS-treated wounds). Representative images of diabetic wounds were acquired at 4X (left panel) and 10X (right panel) magnifications.

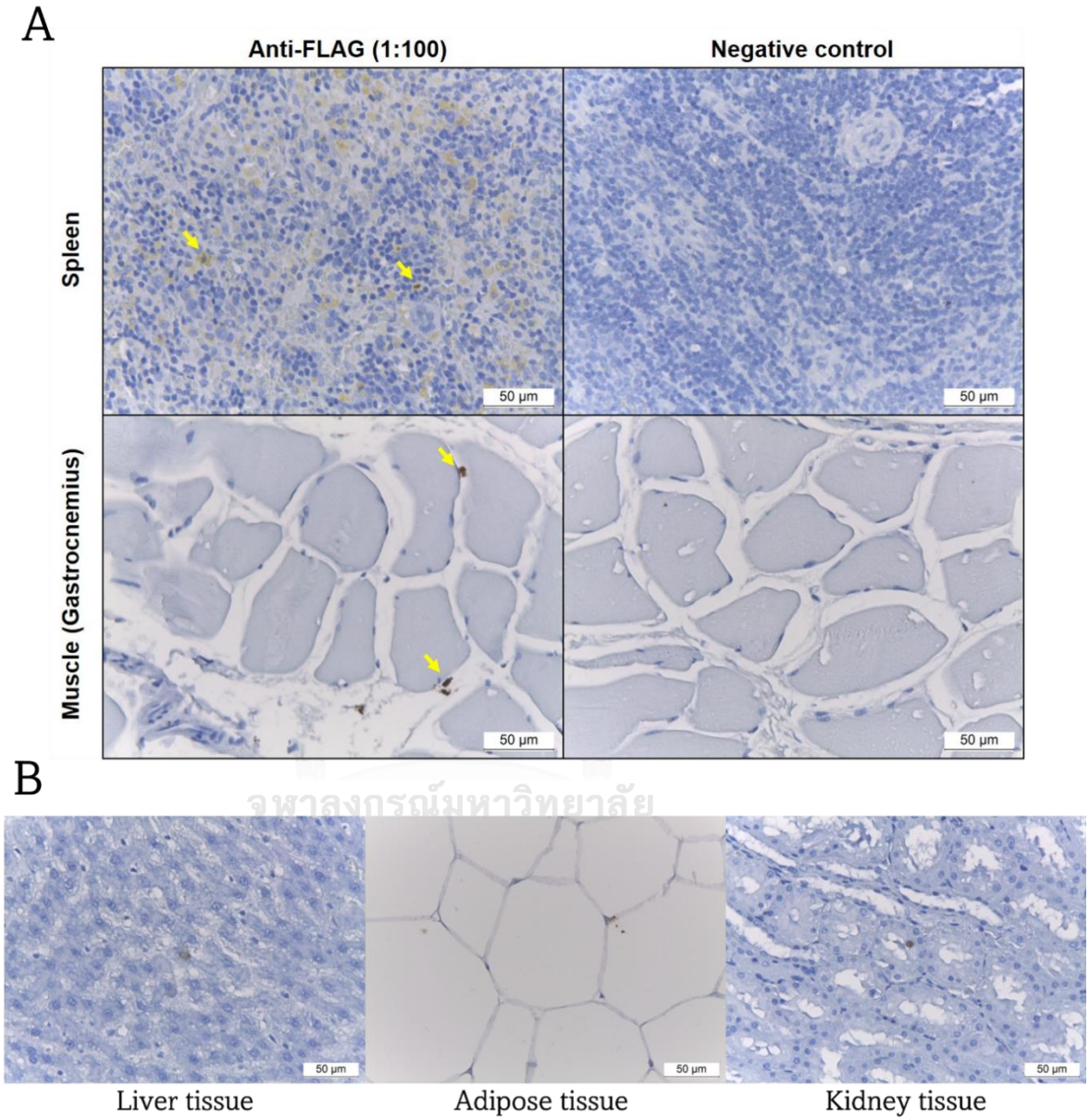

Figure 4-7: The FLAG expression in rat organs after 8-week of the FLAG-containing plasmid/Ca-P weekly injection. (A) Positive staining (brown color) of anti-FLAG antibody by IHC assay was observed spleen tissue (upper, left panel) and muscle (Rt. gastrocnemius, lower, left panel when compared to negative control staining (right panel). **(B)** The FLAG protein expression (brown color) was found in rat liver, adipose tissue, and kidney.

PART 2: Box A of HMGB1 treatment in two aging rat models

1. The reduction of phy-RIND-EDSBs or youth-associated genome-stabilizing DNA gaps (Youth-DNA-GAPs) found in aging rats.

Recently, our lab group reported youth-DNA-GAP reduction in aging human white blood cells by the measurement of Youth-DNA-GAP numbers in humans aged 36 to 81 years (n=80) (Yasom S, et al., 2021, under consideration). We found that the number of DNA gaps was negatively correlated with increasing age. Consistently, Youth-DNA-GAPs significantly decreased in the same individuals after four years. (Yasom S, et al., 2021, under consideration). We performed DNA-GAP PCR, which quantitates DNA gaps from interspersed repetitive sequences (IRSs) (Pornthanakasem, W. et al., 2008). In this study, I investigated the number of Youth-DNA-GAPs in two models of aging rats, consisting of D-galactose (D-gal)-induced aging rat and naturally aging rat.

For the aging rat models, two approaches were accessed, including D-galactose-induced aging model and the naturally aging model. Much evidence has demonstrated that D-gal-induced aging models exhibited similar aging-related marker characteristics as in naturally aging models. (Aydin S. et al., 2012, Cebe T. et al., 2014, Ji M. et al., 2017, Shwe T. et al., 2018) Consistent with the human results, I also found a reduction in Youth-DNA-GAPs in D-gal-induced aging rats and chronologically aging rats (**Figure 4-8, A**).

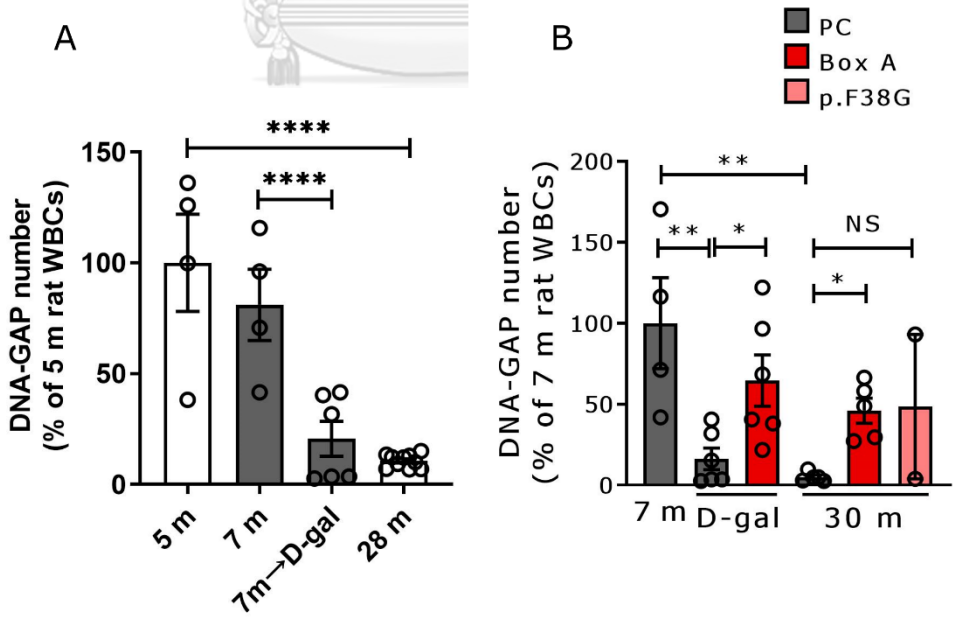

Figure 4-8: A decrease in the number of DNA gaps in aging rat WBCs and the restored DNA gap numbers in aging rats produced by Box A treatment. A lowering of DNA-GAP numbers during aging and D-gal-induction in rat WBCs **(A)**. The number of DNA-GAPs was

increased after Box A treatment for 8 weeks **(B)**. The DNA-GAP numbers of 5-month-old (5 m) rat WBCs (**A**) and PC-treated 7-month-old (7 m) rat WBCs **(B)** were normalized to 100%. Data represent means ± s.e.m.*P ≤ 0.05, **P ≤ 0.01, and ****P ≤ 0.0001 one-way ANOVA followed by post hoc analysis and not significance (NS) in 30 m p.F38G versus PC.

We summarize that Youth-DNA-GAPs are a ubiquitous alteration of DNA existing in a wide range of eukaryotic cells, including yeast, rodents, and humans. Additionally, the reduction of Youth-DNA-GAPs varies based on the aging degree and this decrease can result from chemical-induced or natural aging (**Figure 4-8, A**). The decrease in Youth-DNA-GAPs was related to aging regardless the caused. In rat studies, the reduction was observed both in naturally and D-gal-induced aging models. The formation of Youth-DNA-GAPs was significantly elevated in the aging rat DNA, both models, after Box A treatment (**Figure 4-8, A**). Similar to the previous findings that Youth-DNA-GAPs prevent pathological EDSBs (Kongruttanachok et al., 2010; Thongsroy et al., 2018). This suggested that the reduction of Youth-DNA-GAPs is rather associated with cellular senescence process than mechanism of action of the senescence induced compounds.

This study showed the inverse correlation between the gaps and the number of senescence cells. In addition, we found the similar decline in 30-month-old naturally and 7-month-old D-gal-induced aging rats. Hence, mammalian Youth-DNA-GAPs are a marker of degree of aging phenotypes. In human hypomethylation of IRS is also aged related (Bo-Htay et al., 2020; Bollati et al., 2009; Cardelli, 2018; Jintaridth & Mutirangura, 2010). Surprisingly, the decrease in the epigenetic marks are also correlated with severity of age associated NCD (Jintaridth et al., 2013; Thongsroy et al., 2017). Human Youth-DNA-GAPs are located in methylated DNA (Pornthanakasem et al., 2008), Therefore, it is possible that Youth-DNA-GAPs may be a biomarker of severity of age associated NCDs.

จุฬาลงกรณ์มหาวิทยาลัย
CHULALONGKORN UNIVERSITY

2. Box A of HMGB1 improved aging liver function parameters, decreased in aging and DNA damage marker γ-H2A.X, showed the improvement of cognitive functions in aging rat brain, and a reduction of visceral fat weight in aging rats.

Study in two aging rat models assisted validated the effectiveness of Box A in aging biomarker reversal. The D-gal rat model demonstrated larger liver sinusoidal space and more extensive liver fibrosis (**Figure 4-11** and **Figure 4-12**). Most of the other aging features, visceral fat size, liver function test, and number of positive SA-β-gal staining liver cells, other

senescence associate proteins, learning and memory, of our D-gal rat model were similar to those in naturally aged rats (**Figure 4-9** to **Figure 4-19**).

The findings indicate that Box A-treated groups had elevated Youth-DNA-GAPs (**Figure 4-8, B**) and effectively improved aging features in the aging rat liver (**Figure 4-13** to **Figure 4-17**). In both rat models of aging, we investigated Youth-DNA-GAPs, DDR, aging biomarkers (SA-β-gal, biochemical liver function tests, and senescence-associated proteins, **Figure 4-8** to **Figure 4-17**), and aging tissue/functional phenotypes, including the measurement of liver sinusoidal space (**Figure 4-11**), histopathologic staining of liver fibrosis (**Figure 4-12**), learning/memory behaviors (**Figure 4-18**), visceral fat weight (**Figure 4-19**), and islets of Langerhans (**Figure 4-20**). Box A reversed all markers to be closed to the youth littermates. We also evaluated the levels of serum AST, ALT, ALP, total protein, albumin, and globulin levels for liver function measurement. Both aging rat models had high levels of serum AST, ALT and ALP but total protein, albumin, and globulin levels of both aging groups were not different to the youth (**Figure 4-9** and **Figure 4-10**). Box A treatment reduced the levels of serum AST, ALT and ALP to be closed to the youth (**Figure 4-9** and **Figure 4-10**, **A-B**). Box A did not alter the total protein, albumin, and globulin levels, significantly (**Figure 4-10**, **C-E**). We found a marked decrease in the aging marker SA-β-gal of the Box A-treated rat liver sections in two aging models (**Figure 4-13** to **Figure 4-15**). Box A reduced the visceral fat in both aging models (**Figure 4-19**). Furthermore, the MWM test showed that Box A treatment exhibited significantly improved learning behaviour (latency time) at day 3 and 4 and the restored memory (probe test) in both D-gal and naturally aging models (**Figure 4-18**).

จุฬาลงกรณ์มหาวิทยาลัย
Chulalongkorn University

Box A treatment markedly decreased γH2A.X protein levels (**Figure 4-16** and **Figure 4-17**). The opposite DNA gaps and DSB response results suggested that Box A produced DNA gaps had a protective role against DNA damage at the organ level. Consistently, the accumulation of senescence-related protein $p16^{INK4A}$ and p21 significantly declined after Box A treatment (**Figure 4-16** and **Figure 4-17**). Finally, Box A improved aging brain functions by testing additional brain markers associated with inflammation and cognitive memory in the D-gal rats (data not shown).

A Box A mutant, (glycine-mutant Box A plasmid, pF38G) were tested for rejuvenating in aging rat model, and p.F38G was selected to treat naturally aging rats. The mutant Box A plasmid had no rejuvenation effects to statistically significant levels. It indicates that when Box A plasmid mutant (p.F38G) lost the capability in producing DNA gaps, it also lost the ability to rejuvenate aging rats (Figure 5-9 to Figure 5-20). Therefore, the rejuvenation effects of Box

A required its intact DNA gap production function. Our series of experiments supported that the aging marker reversal role of Box A was due to the DNA protection of the Box A-produced DNA gaps.

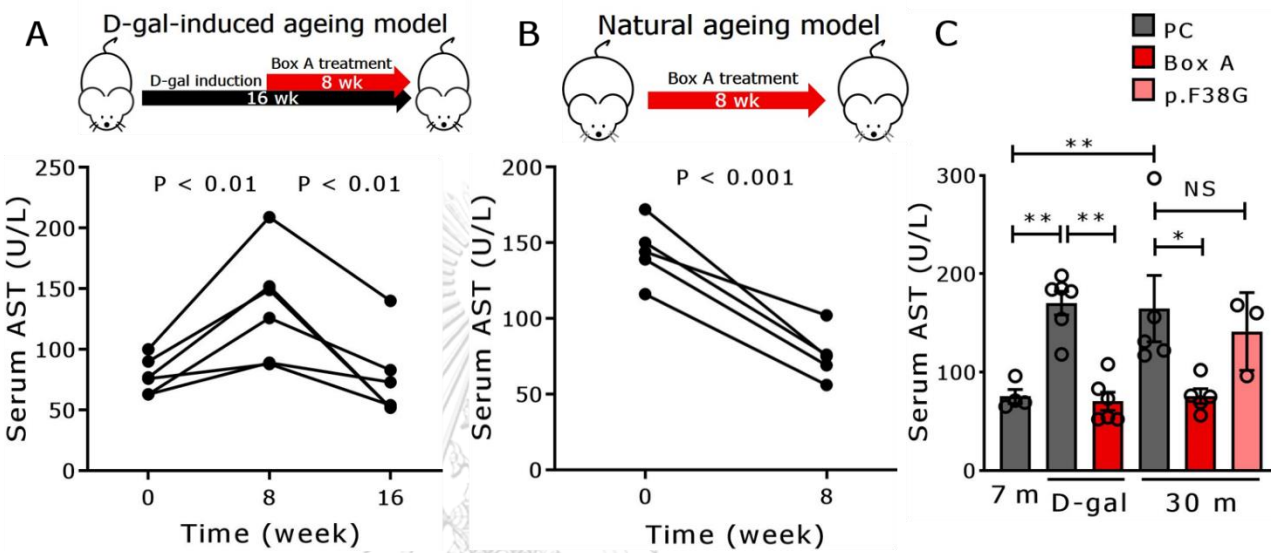

Figure 4-9 Serum aspartate aminotransferase (AST) levels of the D-gal and natural aging rat models. Schematic diagrams for D-gal-induced and natural ageing rats treated with Box A for 8 weeks **(A-B)**. **(A)** Serum AST levels of the D-gal ageing model (n=6) were determined before D-gal induction (baseline; rats were 3 months old), after 8 weeks of D-gal induction and after Box A treatment. For the natural ageing model **(B)**, the levels of serum AST were measured before (the age of 28 m) and after Box A treatment (n=6). **(C)** serum AST levels of 7 m, D-gal and 30 m treated with PC or Box A plasmids; n=4-6, and 30 m with p. F38G; n=3. Data represent means ± s.e.m.*P ≤ 0.05, **P ≤ 0.01 paired t-test **(A-B)**, one-way ANOVA followed by post hoc analysis **(C)** and not significance (NS) in 30 m p.F38G versus PC **(C).**

จุฬาลงกรณ์มหาวิทยาลัย
CHULALONGKORN UNIVERSITY

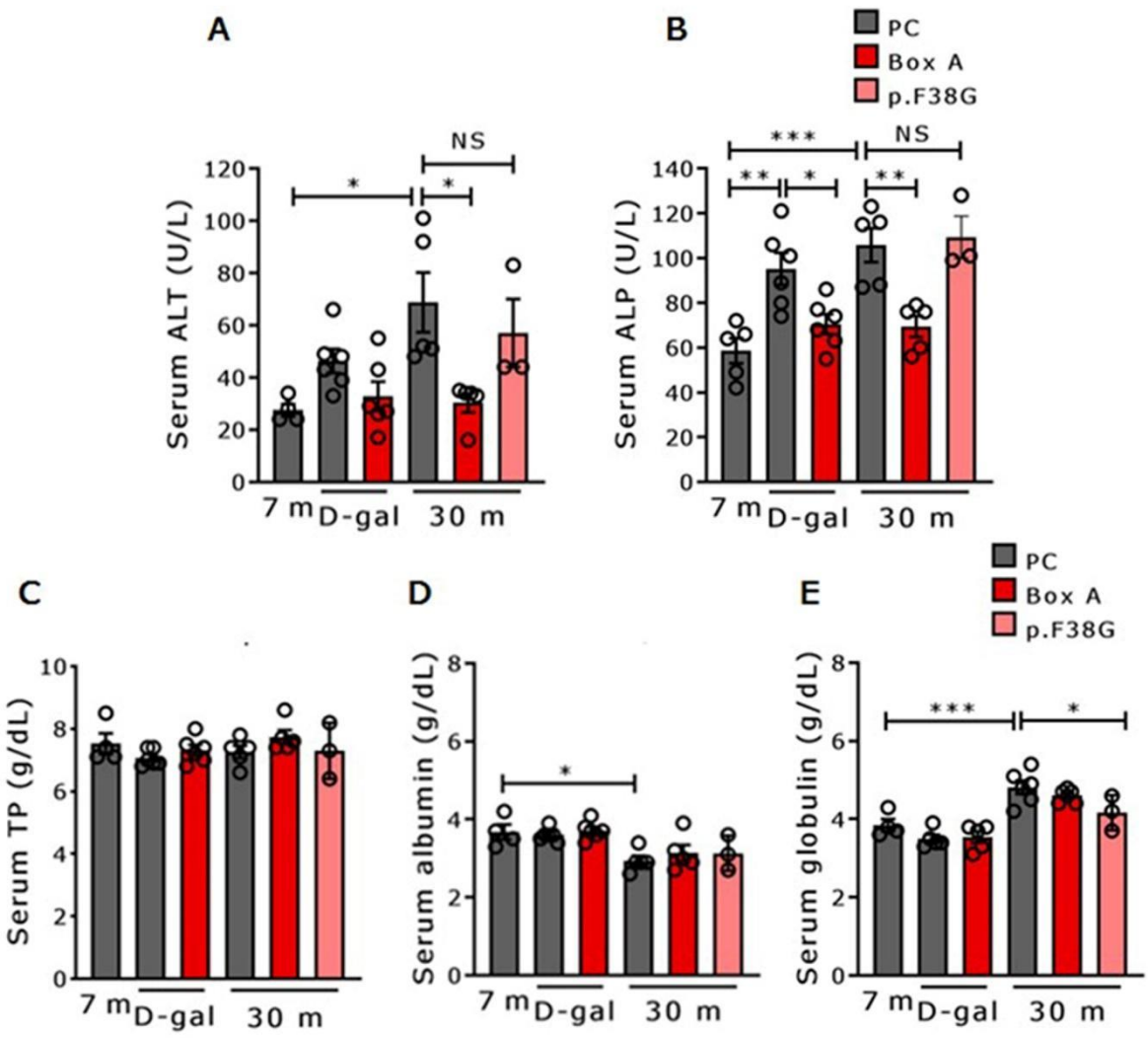

จุฬาลงกรณ์มหาวิทยาลัย
Chulalongkorn University

Figure 4-10: Improvements in serum liver function parameters by Box A treatment. The levels of (**A**) alanine aminotransferase (ALT), (**B**) alkaline phosphatase (ALP), (**C**) total protein (TP), (**D**) albumin, and (**E)** globulin in rat serum were also detected after 8 weeks of both D-gal treatment and natural aging studies (PC) and Box A, n=4-6; p.F38G, n=3). Box A treatment restored liver dysfunction in both aging rat models, shown by significant decreases in serum ALT and ALP levels (a-b). Levels of TP, albumin and globulin were not significantly different among all groups (c-e). Serum globulin levels were calculated from serum TP and serum albumin levels, as mentioned in the Methods. Data represent the means ± s.e.m., *P ≤ 0.05, **P ≤ 0.01 and ***P ≤ 0.001 one-way ANOVA followed by post hoc analysis.

.

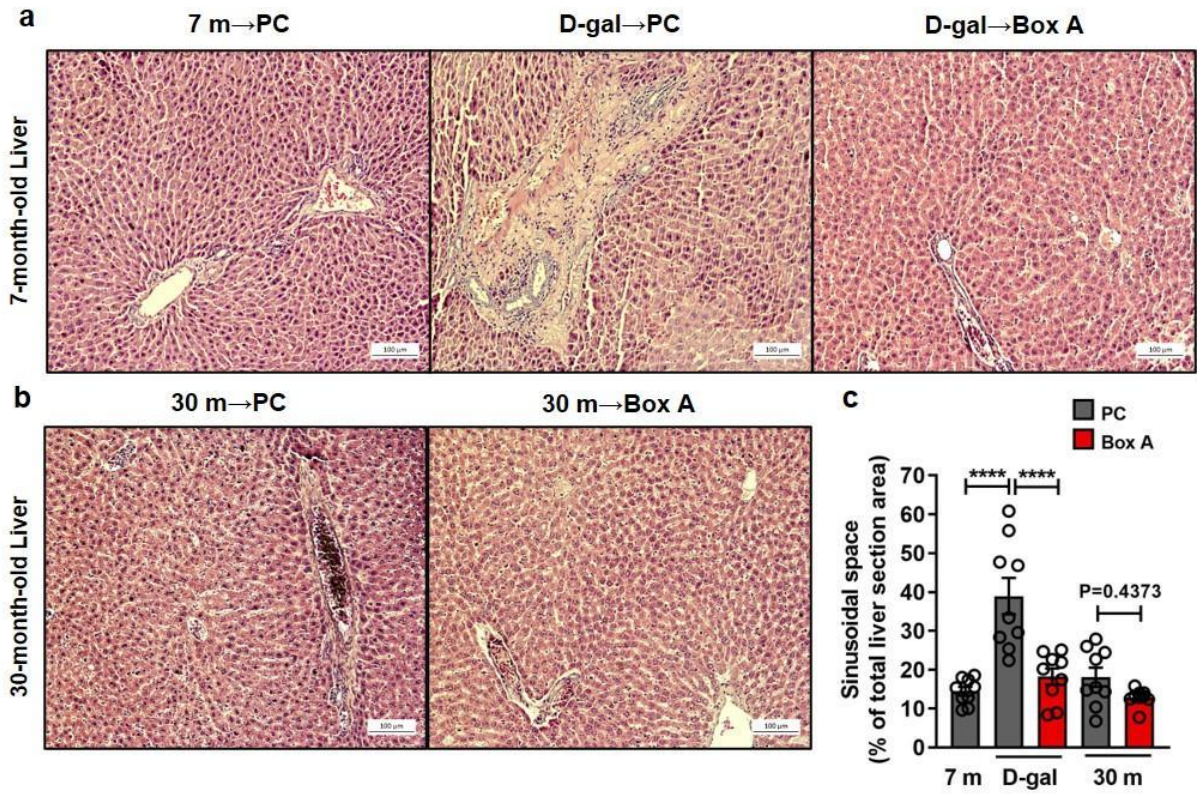

Figure 4-11: Reduction of D-gal-increased sinusoidal space under Box A treatment. Histopathological examination of rat liver tissue sections after 8 weeks of Box A treatment in D-gal and natural aging studies. (**a**) For the D-gal aging model, rat liver histopathological sections of PC-treated normal control (7 m→PC), PC-treated D-gal (D-gal→PC), and Box A-treated D-gal (D-gal→Box A) rats were examined using standard H&E staining (n=3 rats per group). (**b**) For the natural aging model, rat liver sections of PC- (30 m→PC)- or Box A- (30 m→Box A)-treated rats were also analyzed for anatomical structures after the treatment period (n=3 rats per group). A high degree of fibrosis was found in (A) D-gal→PC but not D-gal→Box A. The percentage of sinusoidal space per total area of the liver section was evaluated using ImageJ (**c**). D-gal rats displayed a significantly larger hepatic sinusoidal space than normal rats (7 m→PC). Box A-treated (D-gal→Box A) rats showed a lower percentage of the sinusoidal area than untreated D-gal rats. No significant difference in sinusoidal area among 7 m→PC, 30 m→PC. Data represent means ± s.e.m. ****P ≤ 0.0001 one-way ANOVA followed by post hoc analysis.

จุฬาลงกรณ์มหาวิทยาลัย
Chulalongkorn University

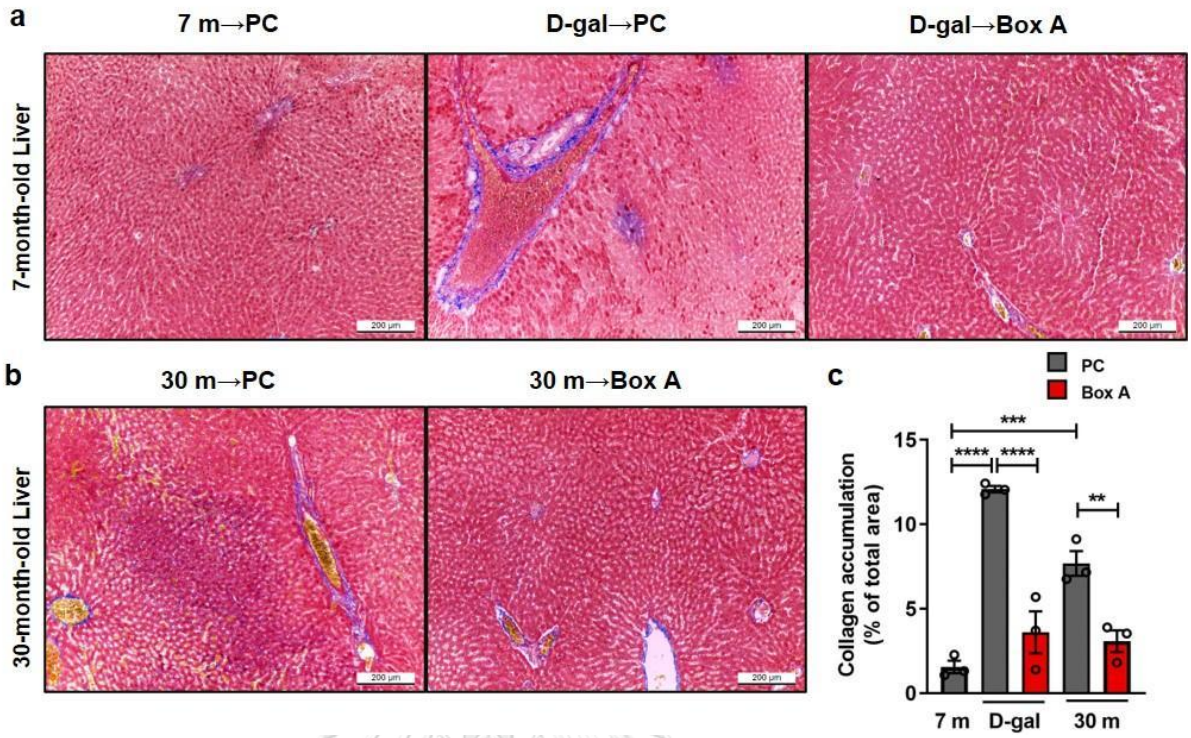

Figure 4-12: Liver fibrosis reduction by Box A treatment. Microscopic observation of liver sections stained with Masson's trichrome at 200x. Histopathology revealed that fibrosis in the liver was reduced after treating rats with Box A compared to D-gal and natural aging models. (**A**) Rat liver sections from PC-treated normal control (7 m→PC), PC-treated D-gal (D-gal→PC), Box A-treated D-gal (D-gal→Box A) (left to right panel) and (**B**) PC (30 m→PC) and Box A (30 m→Box A) exhibited accumulation of collagen (blue). (**C**) Quantification of collagen was performed by ImageJ. Both aging models showed significantly higher collagen accumulation levels in the liver compared to 7 m→PC. After Box A intervention, a significant reduction in collagen deposits was observed in the two aging models. Data represent means ± s.e.m. **P ≤ 0.01, ***P ≤ 0.001, and ****P ≤ 0.0001 one-way ANOVA followed by post hoc analysis.

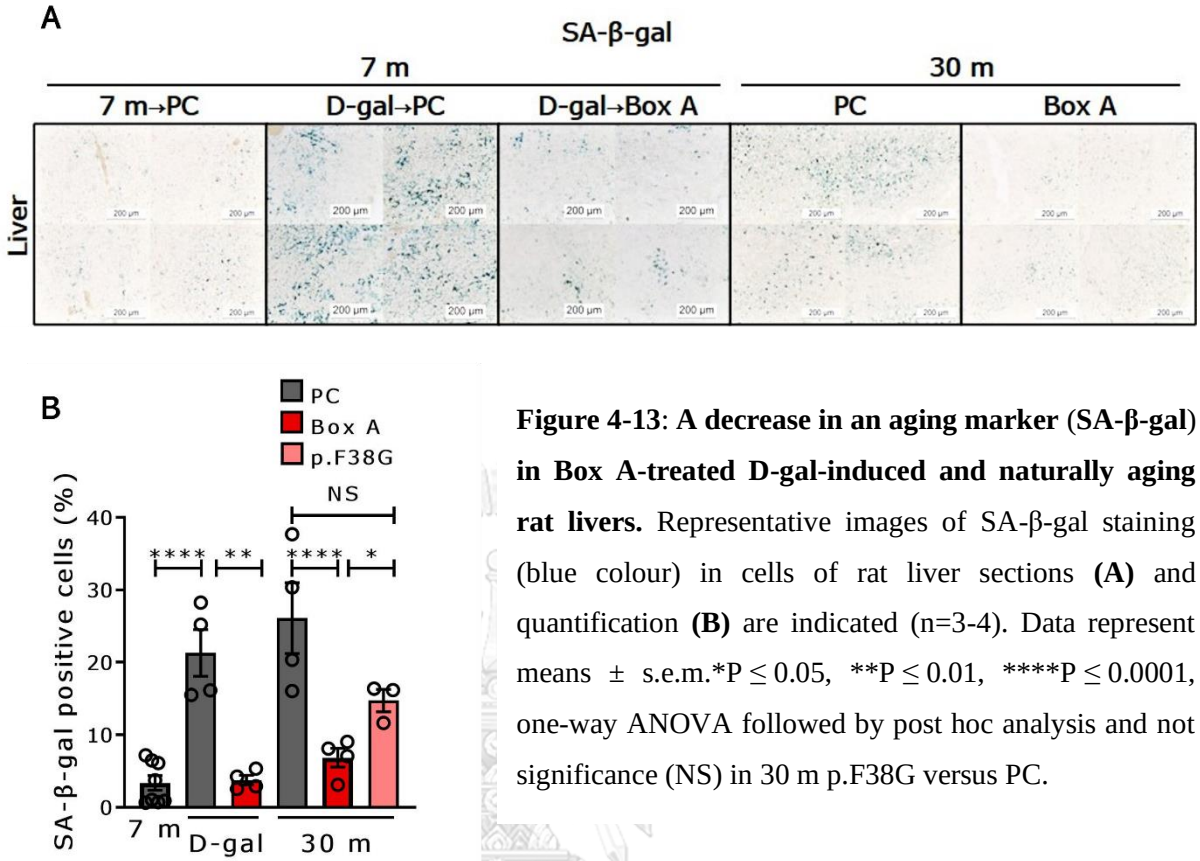

Figure 4-13: **A decrease in an aging marker** (**SA-β-gal**) **in Box A-treated D-gal-induced and naturally aging rat livers.** Representative images of SA-β-gal staining (blue colour) in cells of rat liver sections **(A)** and quantification **(B)** are indicated (n=3-4). Data represent means ± s.e.m.*P ≤ 0.05, **P ≤ 0.01, ****P ≤ 0.0001, one-way ANOVA followed by post hoc analysis and not significance (NS) in 30 m p.F38G versus PC.

จุฬาลงกรณ์มหาวิทยาลัย
Chulalongkorn University

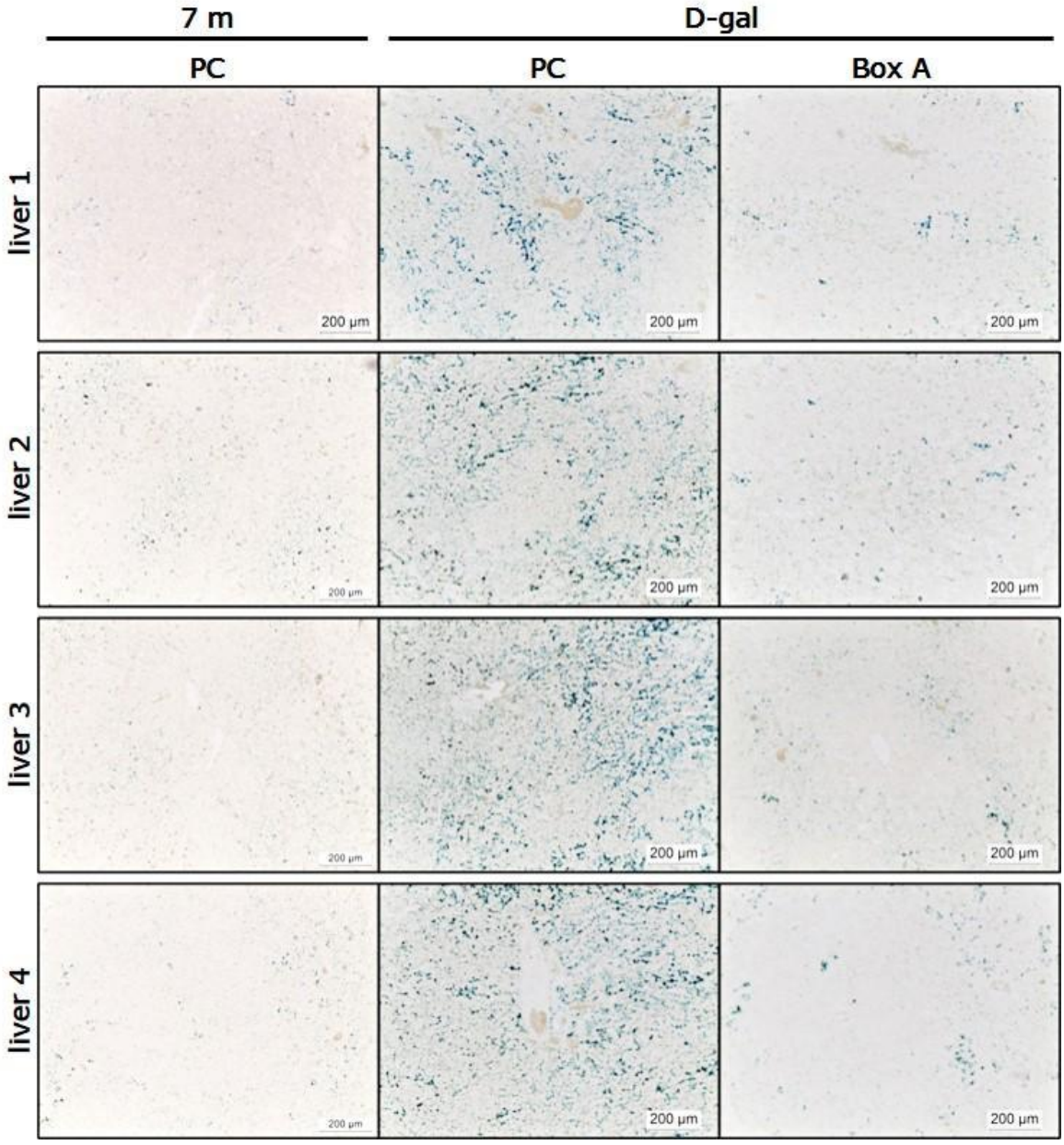

Figure 4-14: A lowering of an aging marker (SA-β-gal) in Box A-treated D-gal-induced aging rat livers. Rat liver sections were stained for SA-β-gal activity (blue) to investigate the effect of Box A treatment in D-gal rats compared to the age-matched PC-treated rats and normal groups (n=4 rats per group). The images were captured at 10x magnification.

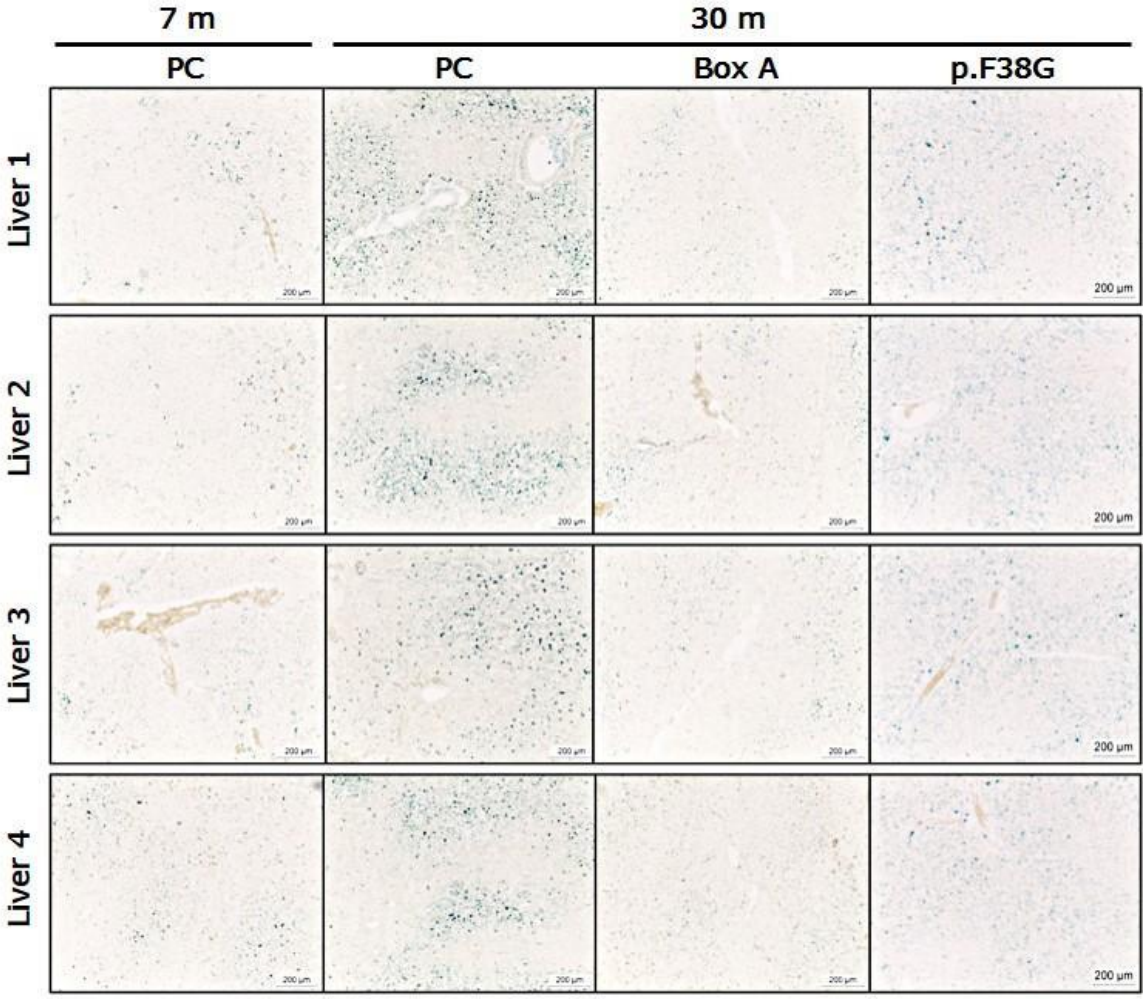

Figure 4-15: A reduction of an aging marker (SA-β-gal) in Box A-treated naturally aging rat livers. Rat liver sections were stained for SA-β-gal activity (blue color) to investigate the effect of Box A treatment in 30-month-old rats compared to the age-matched PC- or p.F38G-treated rats and 7-month-old normal groups (n=3-4 rats per group). The images were captured at 10x magnification.

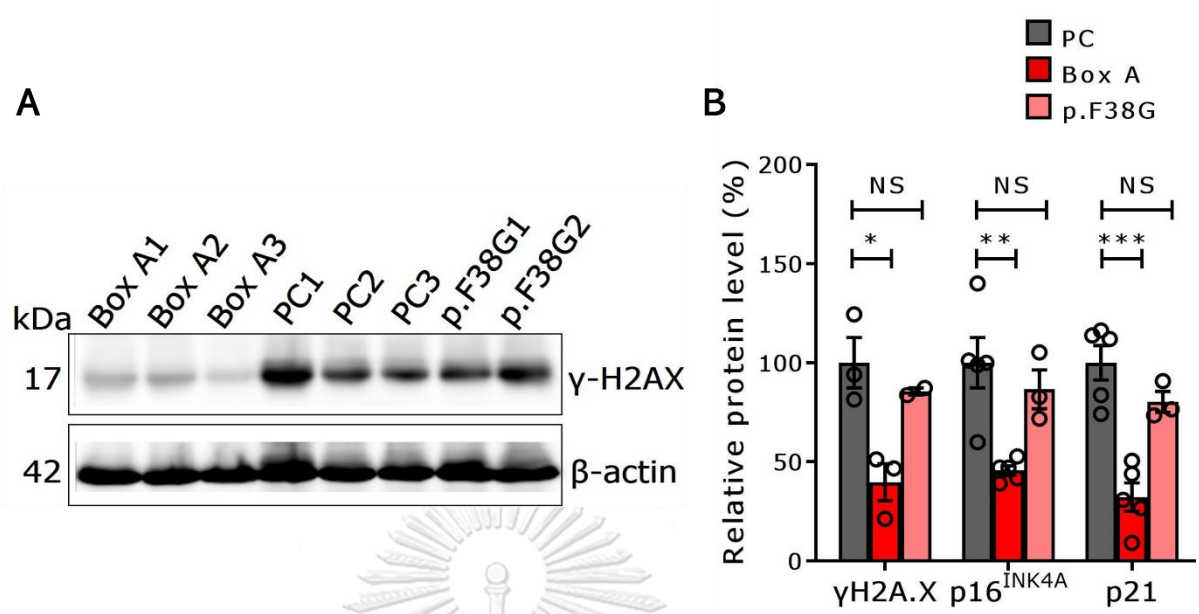

Figure 4-16: Aging and DNA damage marker protein reduction by Box A treatment in naturally ageing rat liver. (A) Immunoblotting levels of γH2A.X and β-actin proteins in 30 m rat livers (n=2-3) and (**B**) percentage of relative protein level of γH2A.X, $p16^{INK4A}$, and p21 (n=3-6). Data represent means ± s.e.m.*P ≤ 0.05, **P ≤ 0.01, ***P ≤ 0.001, one-way ANOVA followed by post hoc analysis and not significance (NS) in 30 m p.F38G versus PC.

จุฬาลงกรณ์มหาวิทยาลัย
Chulalongkorn University

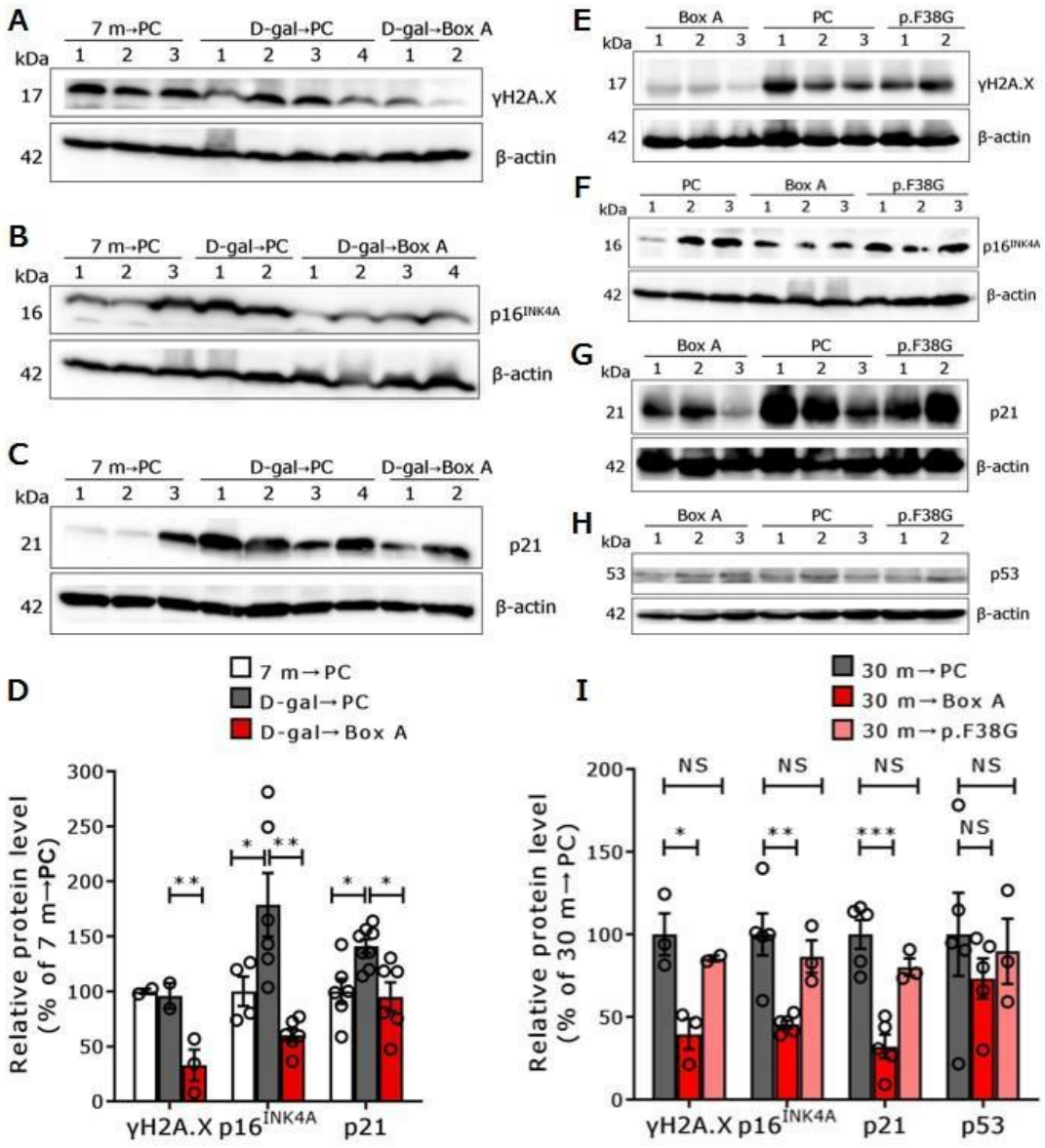

Figure 4-17: Aging marker protein reduction by Box A treatment in two ageing models. Not only γH2A.X but also the late-stage aging marker proteins $p16^{INK4A}$ and p21 were reduced in both aging rat models. (**A**, **B**, **C**) γH2A.X, $p16^{INK4A}$, and p21 protein levels in D-gal rat liver after Box A treatment compared to normal vehicle (7 m→PC) or D-gal vehicle (D-gal →PC) (n=2-6). (**E**, **F**, **G**, **H**) γH2A.X, $p16^{INK4A}$, p21, and p53 protein expression levels of 30 m rat liver after treatment, compared to age-matched vehicle or p.F38G mutant. β-Actin was re-probed and used as a loading control. The percentages of relative protein levels of D-gal (**D**) and natural (**I**) aging studies were evaluated. Each protein of PC-treated rats was normalized to 100%. Data represent means ± s.e.m. *P ≤ 0.05, **P ≤ 0.01 and ***P ≤ 0.001 one-way ANOVA followed by post hoc analysis.

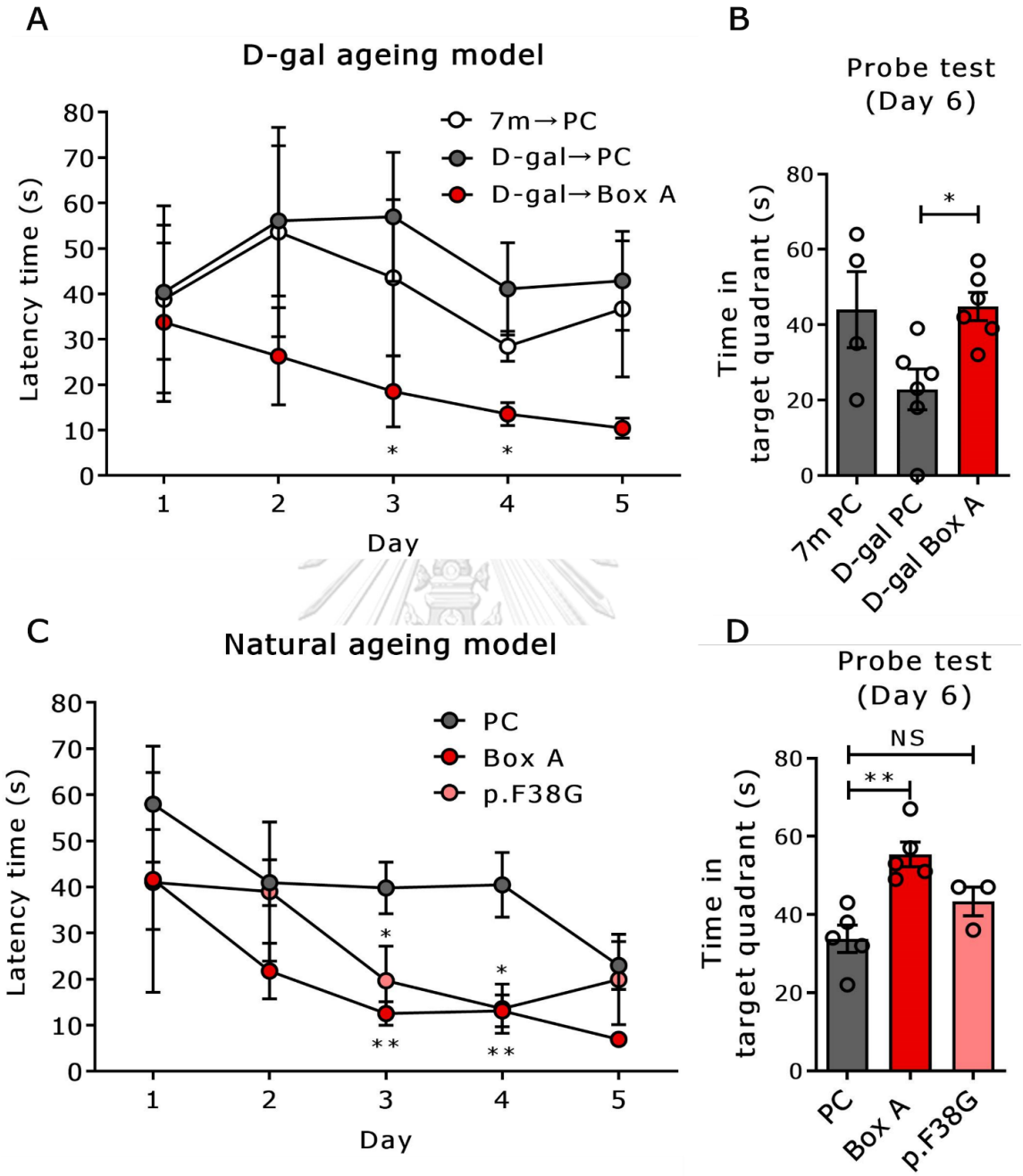

Figure 4-18: Morris water maze tests in D-gal-induced and natural ageing models were assessed. Including the acquisition training test **(A and C)** and the probe test **(B** and **D**; n=4-6, p.F38G; n=3**)**. Data represent means ± s.e.m.*P ≤ 0.05 and **P ≤ 0.01 one-way ANOVA followed by post hoc analysis and not significance (NS) in 30 m p.F38G versus PC.

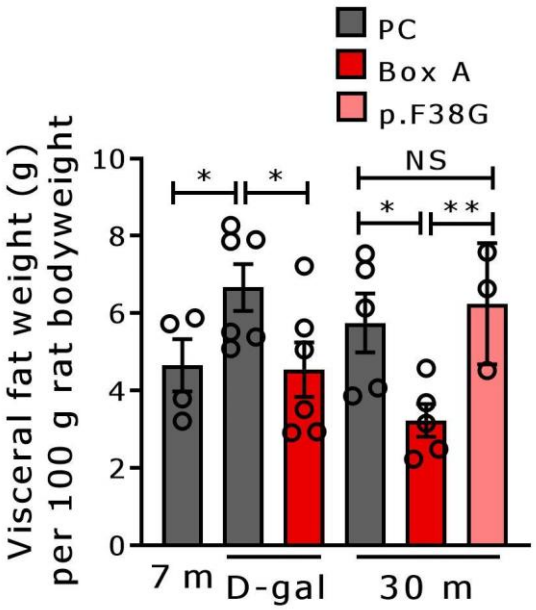

Figure 5-19: Visceral fat weight (g) per 100 g of body weight in D-gal-induced and naturally aging models (n=5-7, p.F38G; n=3). Data represent means ± s.e.m.*P ≤ 0.05 and **P ≤ 0.01 one-way ANOVA followed by post hoc analysis and not significance (NS) in 30 m p.F38G versus PC.

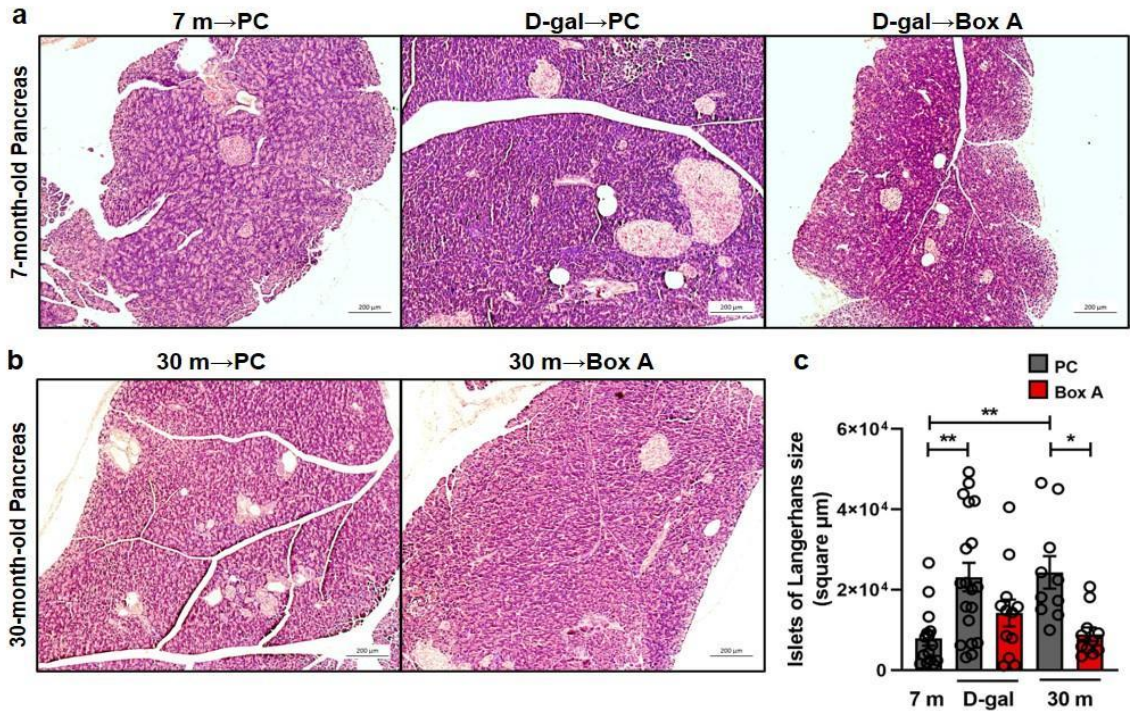

Figure 4-20: Islets of Langerhans sizes of natural aging rats reduced by Box A treatment. Histopathological examination of rat pancreas tissue sections after 8 weeks of Box A treatment

in D-gal and natural aging studies. (**A**) For the D-gal aging model, rat pancreatic histopathological sections of PC-treated normal control (7 m→PC), PC-treated D-gal (D-gal→PC), and Box A-treated D-gal (D-gal→Box A) rats were examined using standard H&E staining (n=3 rats per group). (**B**) For the natural aging model, rat pancreatic sections of PC- (30 m→PC)- or Box A- (30 m→Box A)-treated rats were also analyzed for anatomical structures after the treatment period (n=3 rats per group). (A) The sizes of the islets of Langerhans of D-gal→PC were larger than those of both 7 m→PC and D-gal→BoxA. (B) Fat infiltration was found in the majority of the islets of Langerhans of 30 m→PC. Islets of Langerhans size were measured using ImageJ (**C**). D-gal and naturally aging rats exhibited enlarged islets of Langerhans (average size). In contrast, Box A treatment in both aging models unveiled the restoration of islets of Langerhans size compared to normal rats (7 m→PC). Data represent means ± s.e.m. *$P \leq 0.05$ and **$P \leq 0.01$ one-way ANOVA followed by post hoc analysis.

PART 3: Box A of HMGB1 intervention in a micropig model

In addition, we also investigated Box A effects on a growth rate of baby porcine. Micropigs (12-15 kg) in group 1 and 2 were intraperitoneally injected with a single dose of Box A plasmid/Ca-P nanoparticle and Ca-P nanoparticle, respectively as described in the Materials and Methods. Animals in all groups were biweekly recorded the body weight and food intake during the study until 14 weeks after the administration. We found that the significant increases in porcine body weight of the Box A-treated pigs starting from week 4 until the end of the study (week 14) after the Box A injection, compared to no injection group (**Figure 5-21**, Box A-treated (blue line) vs no treated (grey line) group). Moreover, the significant elevation of porcine body weight also observed in the Box A-injected pigs from week 4 to week 12 when compared with the Ca-P nanoparticle-injected pigs (**Figure 4-21**, Box A-treated (blue line) vs Ca-P-treated (green line) group). Therefore, we conclude that using Box A of HMGB1 plasmid-coating Ca-P nanoparticles was not only safe in large animals, but also significantly enhanced a growth rate of the baby pigs during week 4 to week 12 of the intervention when compared to the Ca-P nanoparticle-injected control group.

จุฬาลงกรณ์มหาวิทยาลัย
CHULALONGKORN UNIVERSITY

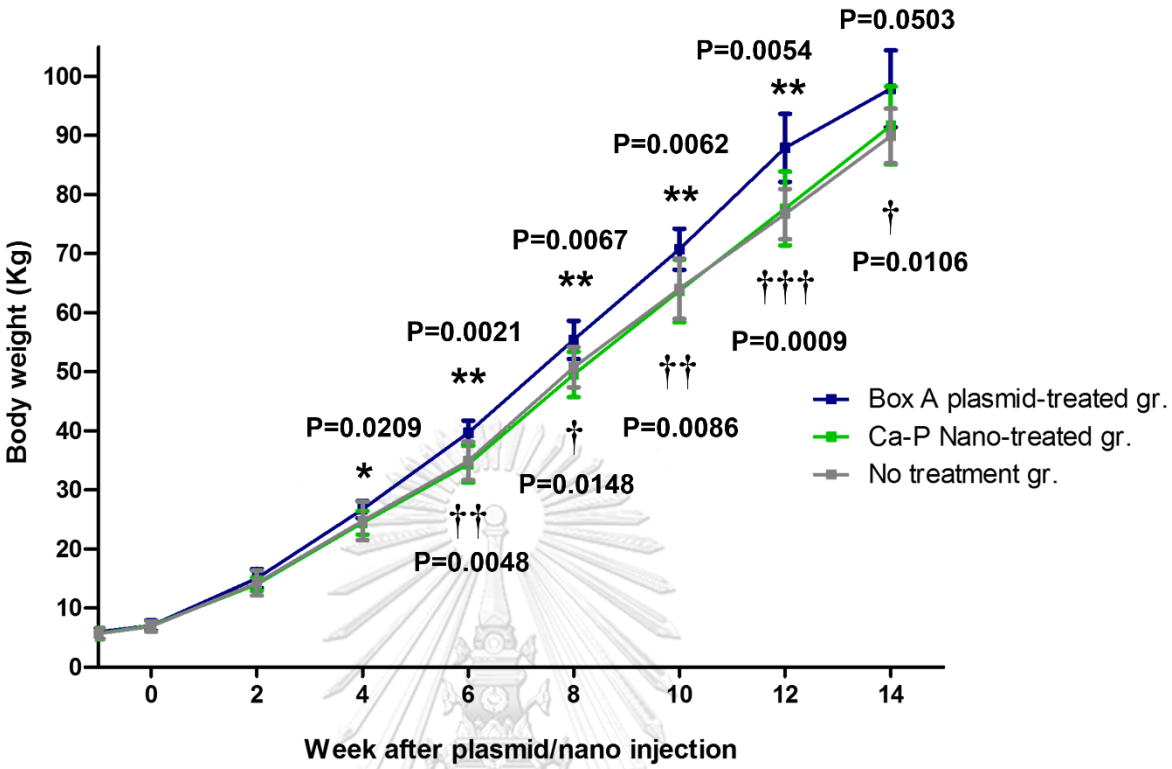

Figure 4-21: Box A treatment enhanced a growth rate of the baby porcine. A single dose of Box A intervention in the baby porcine showed the significantly increased porcine body weight (kg) during week 4 to week 12 of the study when compared to Ca-P nanoparticle-treated, or no treatment group. */ † $P < 0.05$, * */† † $P < 0.01$, † † † $P < 0.001$, */** indicated Box A-treated group vs Ca-P nanoparticle-treated group, †/††/† † † indicated Box A-treated group vs no treatment group.

จุฬาลงกรณ์มหาวิทยาลัย
Chulalongkorn University

PART 4: Box A of HMGB1 treatment in diabetic rat wound

Wound healing study in streptozotocin (STZ)-induced diabetic rat model.

Spontaneous accumulation of endogenous DNA damage was proposed to contribute to an impaired wound healing process in DM patients (Bolajoko et al., 2008; Bryan et al., 2012; Dunnill et al., 2017; Kido et al., 2017; Schafer & Werner, 2008; Wu et al., 2019). According to our findings, Box A of HMGB1 overexpression reduced endogenous DNA damage and the DDR and enhanced the cellular capacity of resistance to DNA-damaging agents, resulting in increased cell proliferation. To elucidate whether overexpressed Box A of HMGB1 repairs delayed wound healing in diabetic rats by limiting DNA damage and consequently the DDR,

the assessment of wound healing, including histopathological scores and the detection of γ-H2AX and 8-OHdG, was performed.

A single high dose of streptozotocin (65 mg/kg body weight) was administered to animals to induce type 1 diabetes, whereas the age-matched control rats were injected with sodium citrate buffer (the STZ solvent) (Furman, 2015b; King, 2012). After one week of STZ induction, the fasting blood sugar (FBS) levels were examined in all rats. The appearance of body weight loss, which is a typically diabetic physiological effect after STZ administration, was also reported, as shown in **Table 1**. The STZ-induced diabetic rats showed significantly higher FBS (432.5 ± 17.7 mg/dL) levels than those of the control littermates (127.0 ± 8.6 mg/dL, ***P<0.001), as displayed in **Table 1**. The eight-mm excisional wounding was then performed on the dorsa of diabetic and control rats, followed by a silicone ring-splinting technique to imitate a healing process in humans and to avoid wound contraction, which normally occurs as a primary mechanism of wound healing in a murine model (Davidson et al., 2013). Fourteen days after wound treatment, the levels of FBS in the diabetic group (417.8 ± 11.2 mg/dL) were still significantly higher than those in the standard group (127.0 ± 8.6 mg/dL, ***P<0.001) (**Table 1)**.

Box A of HMGB1 protein overexpression accelerates the wound healing process in diabetic rats.

To investigate the effect of Box A of HMGB1 plasmid/Ca-P treatment on diabetic wound closure, splinted 8-mm excisional wounds were topically treated with either Box A of the HMGB1 plasmid, the PC or NSS once per day for 14 days. A representative image of the diabetic wounds at days 0, 3, 5, 7, 10, and 14 after wounding exhibited a smaller area of the diabetic wounds after treatment with Box A of the HMGB1 plasmid compared to either the PC or NSS treatment (**Figure 4-22**). Overexpression of the Box A of HMGB1 protein contributed to a significant diabetic wound closure rate, starting from day 3 until day 10 after wounding, compared to the wound closure rate of plasmid control-treated and the NSS-treated diabetic wounds (**Figure 4-23**). Compared with the control-treated group, the treatment of Box A of HMGB1 plasmid revealed increased wound closure, especially during days 5 to 7, (***P<0.001). In contrast, no significant difference between the plasmid control-treated wounds and the NSS-treated wounds was observed at each time point (**Figure 4-23**). Additionally, the treatment of Box A of HMGB1 plasmid had no effects on wound closure in the nondiabetic (normal) rat group compared to that in the NSS-treated control group (**Figure 4-24**).

จุฬาลงกรณ์มหาวิทยาลัย
CHULALONGKORN UNIVERSITY

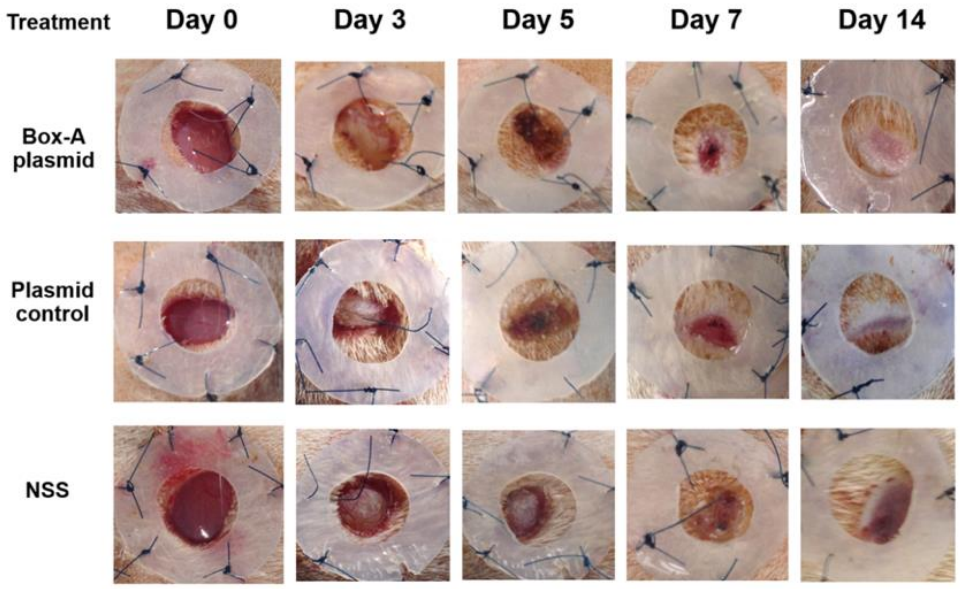

Figure 4-22: The appearance wound images of diabetic rats. The demonstration of splinted eight-millimeter excisional wounds at days 0, 3, 5, 7, 10, and 14 after daily treatment with Box A of HMGB1 plasmid/Ca-P (upper panel), plasmid control/Ca-P (middle panel), and NSS (untreated control, lower panel).

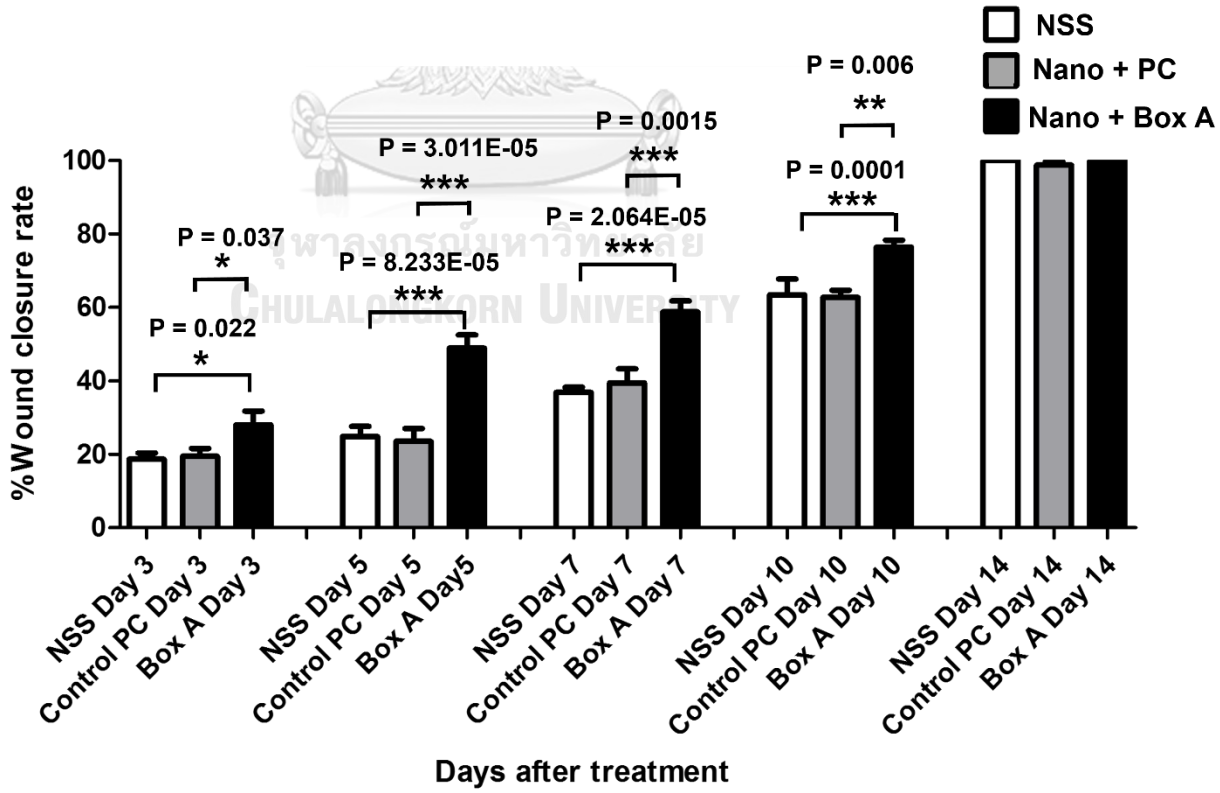

Figure 4-23: Effect of Box A of HMGB1 plasmid treatment on diabetic wound closure. The wound areas of each group were measured using the NIH ImageJ analyzing tool on days 3, 5, 7, 10, and 14 and were compared to those on day 0. The rate of diabetic wound closure was significantly enhanced in the Box A of HMGB1 plasmid-treated group (■) compared to the (plasmid control-treated (▩) or NSS-treated (□)) control group (*P<0.05, **P<0.01, and ***P<0.001, N=8 each group).

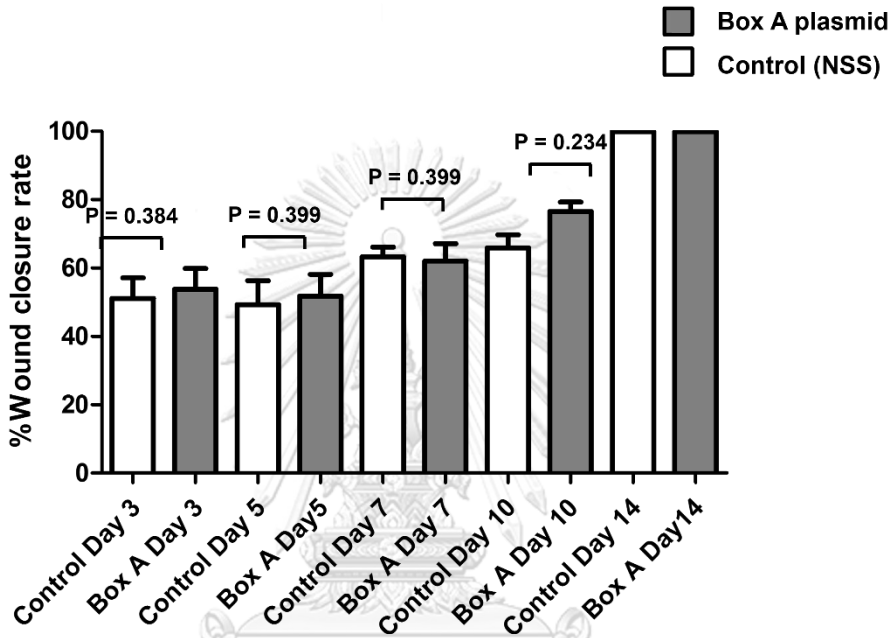

Figure 4-24: Box A of HMGB1 plasmid treatment in nondiabetic wounds. The nondiabetic (normal) wounds revealed no statistically significant difference in the closure rate between the Box A of HMGB1 plasmid-treated group (▩) and the NSS-treated (□) control group (N=4-6 each group).

The grading of histological sections (hematoxylin & eosin (H&E) staining) indicated a significantly improved average histological score with high numbers of mature fibroblasts and less inflammation (overall grading) at 14 days after Box A of HMGB1 treatment compared to either the PC-treated (††P<0.01) or NSS-treated wounds (*P<0.05), following the criteria in **Table 2**. In addition, the presence of fibroblasts was significantly elevated in Box A of HMGB1-treated wounds versus in PC-treated (†P<0.05) or NSS-treated wounds (*P<0.05). The formation of fibrosis was also significantly higher in the Box A of HMGB1-treated group than in the PC-treated group (†P<0.05). In contrast, there were no differences in new blood vessel formation and immune cell infiltration among the three treatment groups (**Table 2**). Box A of HMGB1 treatment resulted in significantly lower levels of 8-OHdG by IHC staining in

diabetic wound sections than the levels in either the PC-treated or NSS-treated sections. Fourteen days after treatment, wounds were excised, and IHC staining was performed with goat anti-8-OHdG antibody, followed by horseradish peroxidase (HRP) conjugated anti-goat secondary antibodies, respectively. A representative illustration exemplified anti-8-OHdG staining (**Figure 4-25**) in Box A of HMGB1-treated wound sections (**A** and **B**) compared to PC-treated (**C** and **D**) and NSS-treated wound sections (**E** and **F**). Grading of IHC staining by anti-γ-H2AX and anti-8-OHdG was also evaluated and summarized in **Table 2**.

Table 2 Histological parameters of diabetic wounds at day 14 after daily treatment with NSS (N=8), Nano-PC (N=8), and Nano-Box A (N=8). Histological scores were graded including overall grading (1=normal tissue, 2=plenty of mature fibroblast, 3=plenty of immature fibroblast, 4=mild inflammation, and 5=granulation tissue), fibroblast (0=absent, 1=immature, and 2=mature), fibrosis (0=absent and 1=present), new vessel formation and inflammatory infiltration (0=absent, 1= a few, 2= moderate, and 3= plenty).

Histological parameter	NSS-treated	PC-treated	Box A-treated
Overall grading	2.00 ± 0.00	2.80 ± 0.31	1.54 ± 0.14*/† †
Fibroblast	1.00 ± 0.00	1.00 ± 0.00	1.53 ± 0.14*/†
Fibrosis	0.20 ± 0.20	0.00 ± 0.00	0.46 ± 0.14†
New vessels	0.40 ± 0.24	1.00 ± 0.00	0.69 ± 0.13
Immune cell infiltration			
- Neutrophils	0.00 ± 0.00	0.20 ± 0.16	0.07 ± 0.07
- Lymphocytes	1.00 ± 0.00	1.00 ± 0.00	0.77 ± 0.12
- Macrophages	0.80 ± 0.58	0.80 ± 0.40	0.54 ± 0.18
- Plasma cells	1.00 ± 0.00	1.00 ± 0.00	0.76 ± 0.12
DNA damage marker			
- 8-OHdG	2.33 ± 0.21	2.17 ± 0.17	1.17 ± 0.17***/†††

จุฬาลงกรณ์มหาวิทยาลัย
Chulalongkorn University

- γH2A.X	2.50 ± 0.22	2.67 ± 0.21	1.50 ± 0.22**/††

Abbreviation: NSS-treated; normal saline solution-treated group, PC-treated; plasmid control-treated group, Box A-treated group; Box A of HMGB1 plasmid-treated group.

Data are presented as the mean ± SEM. *P<0.05, **P<0.01, and ***P<0.001 significant difference, in comparison with NSS-treated group, †P<0.05, ††P<0.01, and †††P<0.001 significant difference, in comparison with the PC-treated group.

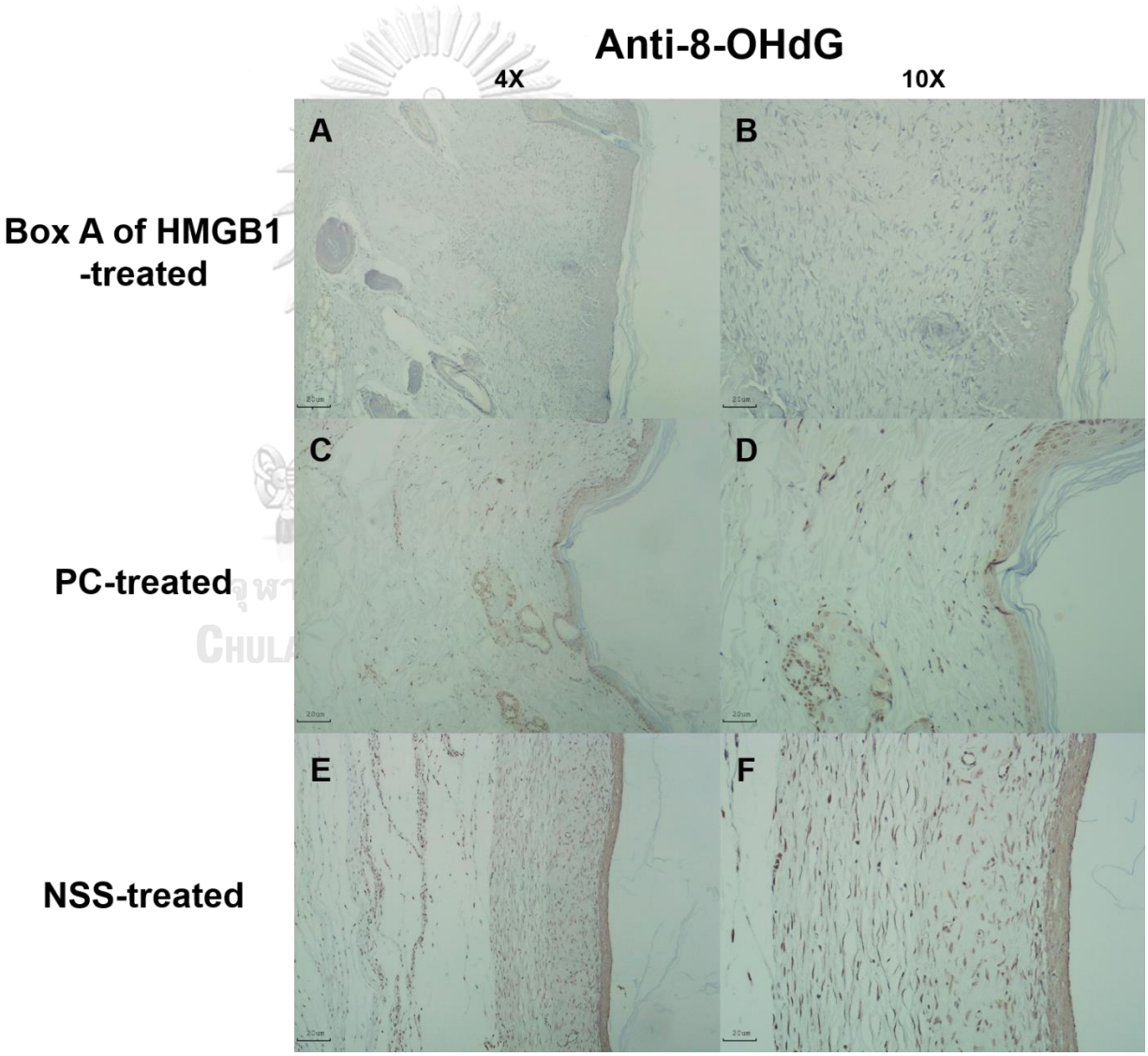

Figure 4-25: A representative illustration exemplified anti-8-OHdG staining after Box A treatment for 14 days. Box A of HMGB1-treated wound sections (**A** and **B**) compared to PC-treated (**C** and **D**) and NSS-treated wound sections (**E** and **F**).

PART 5: B1 siRNA treatment in diabetic rat wound

B1 siRNA topical treatment restores the B1 methylation level in diabetic wounds

Altered DNA methylation patterns found in certain gene promoters and intergenic regions are correlated with diabetes and age-related diseases. (Thongsroy et al., 2017) (Bansal & Pinney, 2017) (de Mello et al., 2014) Our group previously reported the association between hypomethylation of SINEs and Alu elements in prediabetic and diabetic patients. (Thongsroy et al., 2017) The use of STZ administration to generate a TIDM animal model is widely accepted for preclinical wound-healing studies. (King, 2012) (Furman, 2015a) In our study, the STZ-induced rats exhibited significantly higher levels of FBS 7 days after STZ injection (65 mg/kg rat body weight), and prolonged hyperglycemia was detected in diabetic rats compared to nondiabetic littermates at the end of the study (**Table 3**), and throughout the study (**Table 4)**. Five-time points of FBS detection were performed during the study and indicated as the red stars in the timeline. First, after 7-day acclimatization, FBS was measured to be the baseline of the blood glucose level before a diabetic induction. Second, the detection of FBS levels at 7-day of STZ injection was used for differentiation between nondiabetic and diabetic rats, as mentioned in the Materials and Methods. Third, the FBS levels were determined on the day of wounding (day eight after STZ injection, before starting the topical treatment (day 0)). Finally, to confirm the nondiabetic and diabetic conditions in rats, the FBS levels were observed in all groups on day 7 and day 14 (the fourth and the fifth times) after the treatment (**Table 4**).

จุฬาลงกรณ์มหาวิทยาลัย
CHULALONGKORN UNIVERSITY

We first explored whether a single dose of STZ induction in a TIDM rat model sufficiently induces hypomethylation of B1 elements. We demonstrated that STZ-induced diabetic rat DNA exhibited a significant decrease in B1 methylation levels at day 21 after STZ induction compared to normal (nondiabetic) wound DNA ($p = 0.0057$) (**Figure 4-26**). To investigate the capability of B1 siRNA to increase the level of B1 methylation, the B1 methylation status of diabetic rat wound DNA was measured between the B1 siRNA- and NSS-treated groups at 14 days after the intervention. B1 siRNA-treated wound DNA showed a significantly higher percentage of B1 methylation than the NSS-treated wound DNA ($p = 0.0002$) (**Figure 4-26**). Additionally, B1 siRNA treatment provided *de novo* DNA methylation into the rat genome in a specific manner (data not shown). Notably, B1 siRNA-treated nondiabetic rat wounds showed slightly enhanced levels of B1 methylation, but there was no significant difference from the NSS-treated control ($p = 0.080$) (data not shown). These findings

indicated that a single high dose of STZ induced T1DM with B1 hypomethylation in diabetic rat wounds and that topical B1 siRNA treatment successfully restored B1 methylation loss in diabetic wound DNA.

Table 3. The body weight and fasting blood glucose level of nondiabetic (normal) and diabetic rats at the end of the study. After 7 days of STZ induction, fasting blood glucose levels were measured (>250 mg/dL defined as a diabetic rat), and this group was designated as the diabetic group (n=5 each group). Citrate buffer was injected into the nondiabetic group (FBS<150 mg/dL), which was designated as the normal control group. After wounding, the diabetic wounds were treated daily with NSS or the B1 siRNA/Ca-P nanoparticle complex and were compared to the NSS nondiabetic wound.

Rat model	Nondiabetic	Diabetic	
		NSS treated	B1 siRNA treated
Body weight (g)	278.0 ± 4.1	193.6 ± 6.9***	191.6 ± 5.8***
Fasting blood glucose (mg/dL)	122.6 ± 8.6	424.4 ± 18.4***	410.8 ± 11.1***

Data are presented as means ± S.E.M. ***P < 0.001 significant difference compared with the nondiabetic group.

จุฬาลงกรณ์มหาวิทยาลัย
CHULALONGKORN UNIVERSITY

Table 4. The FBS level of nondiabetic and diabetic rats during the study. The nondiabetic group (FBS<150 mg/dL) was the normal control group. The rats with >250 mg/dL of FBS levels were defined as diabetic rats (n=5 each group). FBS; fasting blood sugar, NSS; normal saline solution, STZ; streptozotocin.

Time points of fasting blood glucose measurement

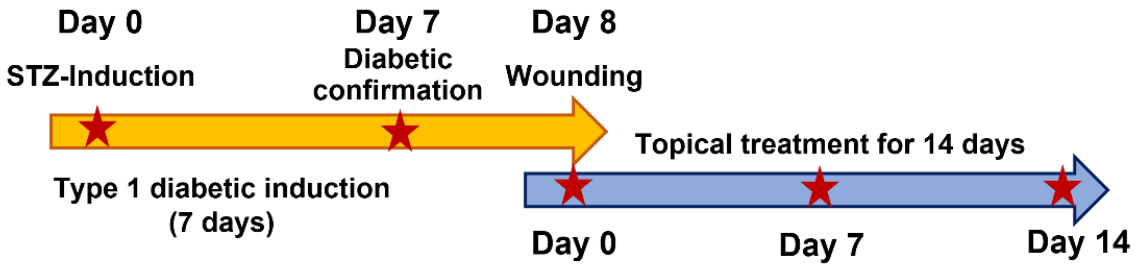

Fasting blood glucose (mg/dL)	Nondiabetic	Diabetic	
		NSS-treated	B1 siRNA-treated
1. Day 0 (baseline)	113.6 ± 4.03	119.2 ± 4.02	117.4 ± 4.73
2. Day 7 after STZ induction	120.4 ± 3.97	382.6 ± 18.88***	387.6 ± 14.64***
3. Day 0 (the day of wounding)	127.0 ± 5.58	448.4 ± 17.79***	450.8 ± 17.94***
4. Day 7 after treatment	128.6 ± 8.26	446.2 ± 25.67***	423.8 ± 11.14***
5. Day 14 after treatment (the end of study)	122.6 ± 8.6	424.4 ± 18.4***	410.8 ± 11.1***

Data are presented as means ± S.E.M. *** $P < 0.001$ significant difference compared with the nondiabetic group.

Increased B1 methylation levels accelerate wound healing with improved histopathological scores and lower DNA damage in diabetic rats

Diabetic patients have suffered from delayed wound healing for decades in both developed and developing countries. (Riedel et al., 2020) (Öhnstedt et al., 2019) (Thewjitcharoen et al., 2020) (Kosachunhanun et al., 2012) One of the major contributors that causes impaired tissue repair in diabetic wounds is oxidative stress-induced DNA damage, which interrupts the proliferative and inflammatory phases of wound healing. (Patel et al., 2019) (Rogulj et al., 2017) We hypothesized that the restoration of B1 methylation levels in DNA from diabetic wounds improves the wound-healing process. We investigated the closure of diabetic wounds and reported the percentage of wound closure. Representative images of the wounds in diabetic rats at days 0-14 after wounding are shown in Figure 4A. The wound closure rate demonstrated a higher degree of closure in B1 siRNA-treated wounds than in NSS-treated wounds (**Figure 4-27, A**). We found that the healing rate of B1 siRNA-treated wounds at days 5, 7, and 10 was significantly higher than that of the NSS-treated wounds ($p = 0.0088$, $p = 0.0063$, and $p = 0.0089$, respectively) (**Figure 4-27, B**). We confirmed that the higher rate of wound closure in B1 siRNA-treated wounds positively correlated with the anatomical appearance of wound

sections by scoring histological parameters (**Table 5**), and representative images of H&E staining are shown in **Figure 4-28**. Treatment with B1 siRNA resulted in the improvement of overall scores that were graded from a composition of mature and immature fibroblasts, an appearance of normal and granulation tissue, and inflammation by demonstrating a significantly lower degree of overall grading than the control-treated diabetic wounds ($p = 0.0037$) (**Table 5**). In addition, a significant increase in the fibroblast and fibrosis density grades as well as new blood vessel formation was observed in wounds treated with B1 siRNA compared to the control treatment ($p = 0.0247$, $p = 0.0462$, and $p = 0.0247$, respectively). We also investigated the endogenous DNA damage markers, 8-OHdG and γH2A.X, by IHC staining. The IHC staining of 8-OHdG and γH2A.X revealed a significant decrease in the endogenous DNA damage in diabetic wounds treated with B1 siRNA compared to NSS-treated diabetic wounds ($p = 0.0006$ and $p = 0.0051$, respectively) (**Table 5**). The representative images of 8-OHdG and γH2A.X IHC staining are shown in **Figure 4-29** and **Figure 4-30**, respectively. These findings revealed that treatment with B1 siRNA resulted in the restoration of B1 methylation in diabetic wounds, accelerated wound healing by improving histological parameters (mainly mature fibroblast proliferation), and reduced the DNA damage (as indicated by 8-OHdG and γH2A.X).

Table 5. Histological parameters of diabetic wounds at day 14 after daily treatment with NSS (n=6) and B1 siRNA (n=6). Histological scores were graded, including overall grading (1=normal tissue, 2=many mature fibroblasts, 3=many immature fibroblasts, 4=mild inflammation, and 5=granulation tissue), fibroblasts (0=absent, 1=immature, and 2=mature), fibrosis (0=absent and 1=present), new vessel formation (0=absent, 1= few, 2= moderate, and 3= many), inflammatory infiltration (0=absent, 1= few, 2= moderate, and 3= many), and DNA damage (8-OHdG and γH2A.X) (0=absent, 1= a few, 2= moderate, and 3= many).

Histological parameter	NSS-treated	B1 siRNA-treated
Overall grading	2.33 ± 0.21	1.33 ± 0.21**
Fibroblast	0.67 ± 0.21	1.33 ± 0.21*
Fibrosis	0.83 ± 0.17	1.33 ± 0.21*
New vessels	0.33± 0.21	1.17 ± 0.31*
Immune cell infiltration		

- Neutrophils	0.17 ± 0.17	0.00 ± 0.00
- Lymphocytes	1.00 ± 0.00	0.83 ± 0.17
- Macrophages	1.17 ± 0.40	0.00 ± 0.17**
- Plasma cells	1.00 ± 0.17	0.83 ± 0.21
DNA damage marker		
- 8-OHdG	2.67 ± 0.21	1.33 ± 0.21***
- γH2A.X	2.50 ± 0.22	1.50 ± 0.22**

Abbreviation: NSS-treated; normal saline solution-treated group.

Data are presented as the mean ± SEM. *P<0.05, **P<0.01, and ***P<0.001 indicate significant differences compared to the NSS-treated group.

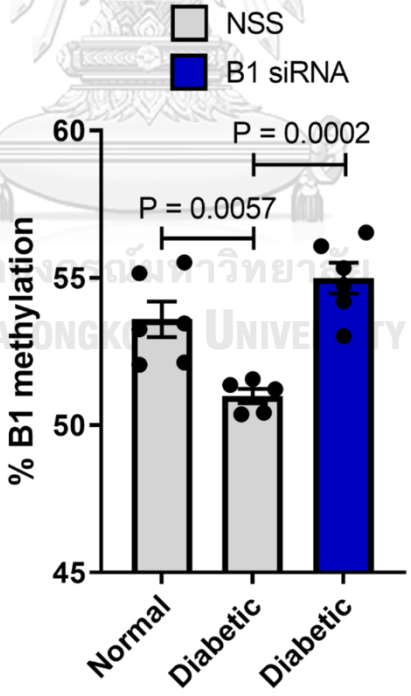

Figure 4-26. B1 siRNA treatment increases B1 methylation levels in diabetic rat wound DNA. Twenty-one days after STZ induction, rat wound DNA was extracted and modified by the bisulfite method followed by the B1-COBRA technique as described in the Materials and Methods. Diabetic wound DNA showed a significantly decreased B1 methylation level

compared to nondiabetic wound DNA. After 14 days of B1 siRNA daily treatment, the B1 methylation levels in B1 siRNA-treated DNA were significantly higher than those in NSS-treated DNA. Data represent the means ± S.E.M. **P ≤ 0.01 and ***P ≤ 0.001 according to one-way ANOVA followed by post hoc analysis (n=5-6 per group).

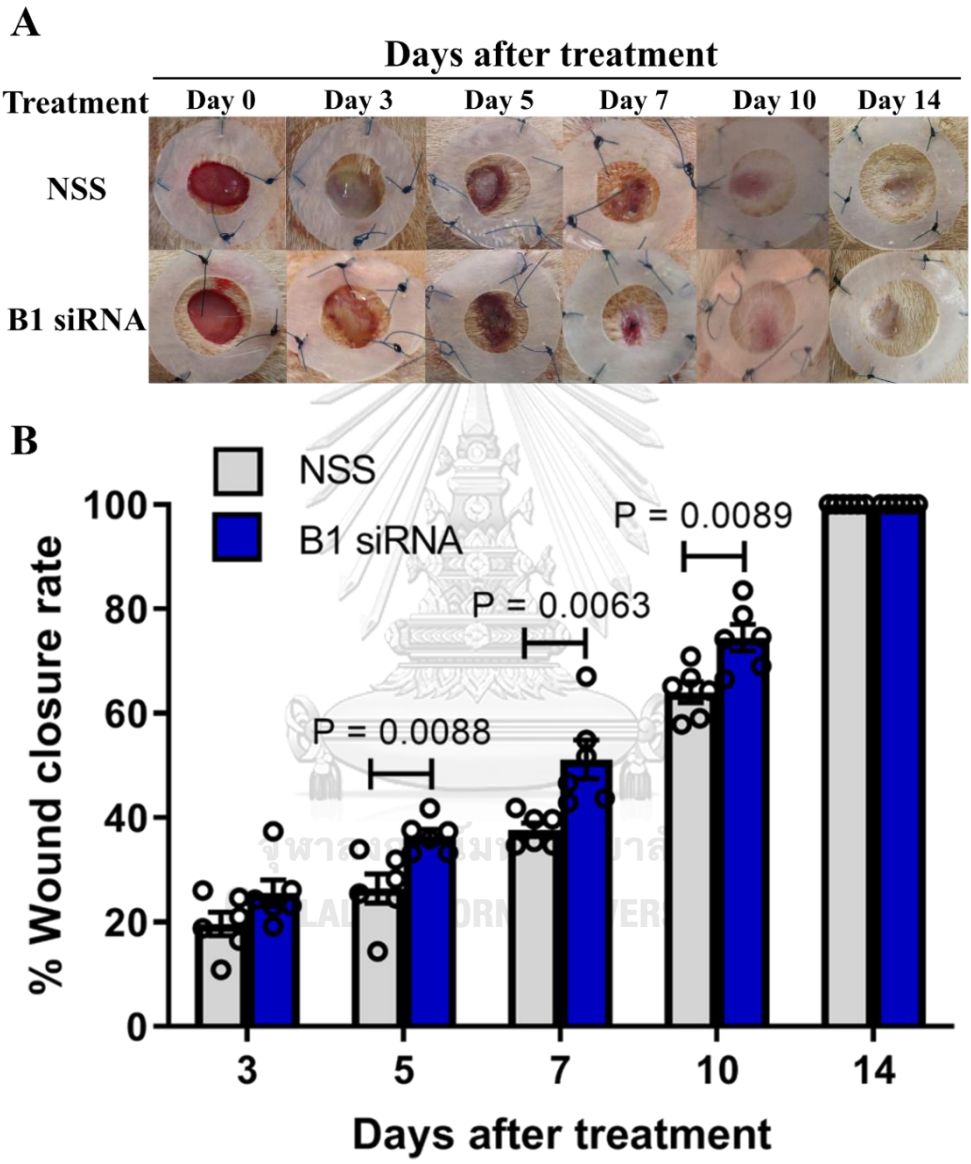

Figure 4-27. Diabetic wound healing is accelerated by B1 siRNA treatment. (A) Images of diabetic rat wounds. Splinted 8-mm excisional wounds at 0, 3, 5, 7, 10, and 14 days after daily treatment with NSS (control, upper panel) or B1 siRNA/Ca-P (lower panel). **(B) The percentage of wound closure rate after B1 siRNA treatment.** The wound areas were measured each day after B1 siRNA (blue bar) or NSS (gray bar) treatment, and the wound

closure rate was calculated by comparison with the wound area on day 0 using the formula mentioned in the Materials and Methods. A significantly improved wound healing rate was observed at 5, 7, and 10 days after treatment. Data represent the means ± S.E.M. **P ≤ 0.01 according to one-way ANOVA followed by post hoc analysis (n=5-6 per group).

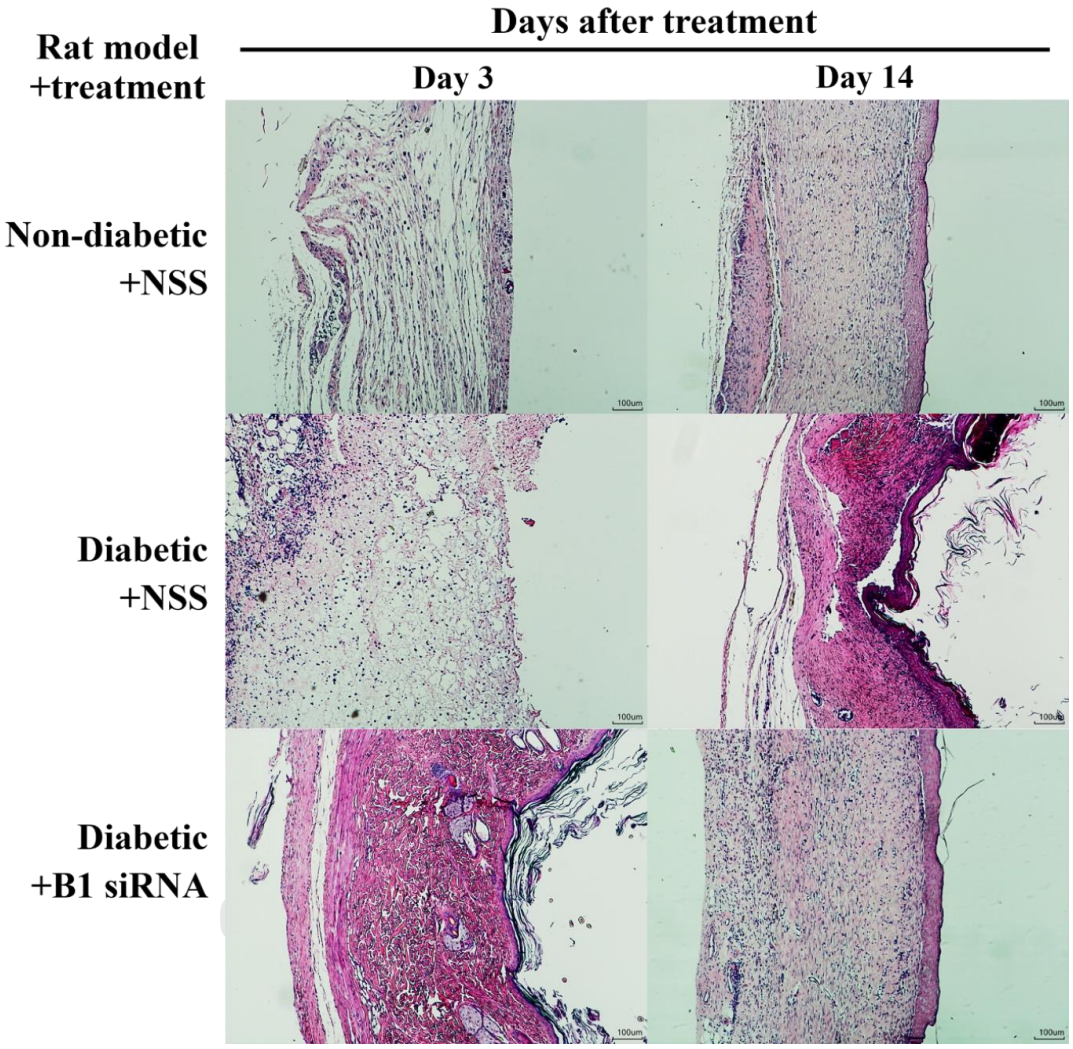

Figure 4-28. Histopathological parameters are improved, and fibroblast proliferation is increased in diabetic wounds after B1 siRNA treatment. H&E staining of wound sections was investigated in a rat model of nondiabetic +NSS (normal control, upper panel), diabetic +NSS (negative control, middle panel), and diabetic +B1 siRNA (treatment, lower panel) at 3 days after treatment and at the end of the study (14 days). B1 siRNA-treated diabetic wounds exhibited enhanced fibroblast proliferation and maturation as well as reduced immune cell infiltration after a treatment period compared to NSS-treated wounds. B1 siRNA treatment demonstrated complete wound closure and similar anatomical appearance of the wounds to nondiabetic (normal) wounds.

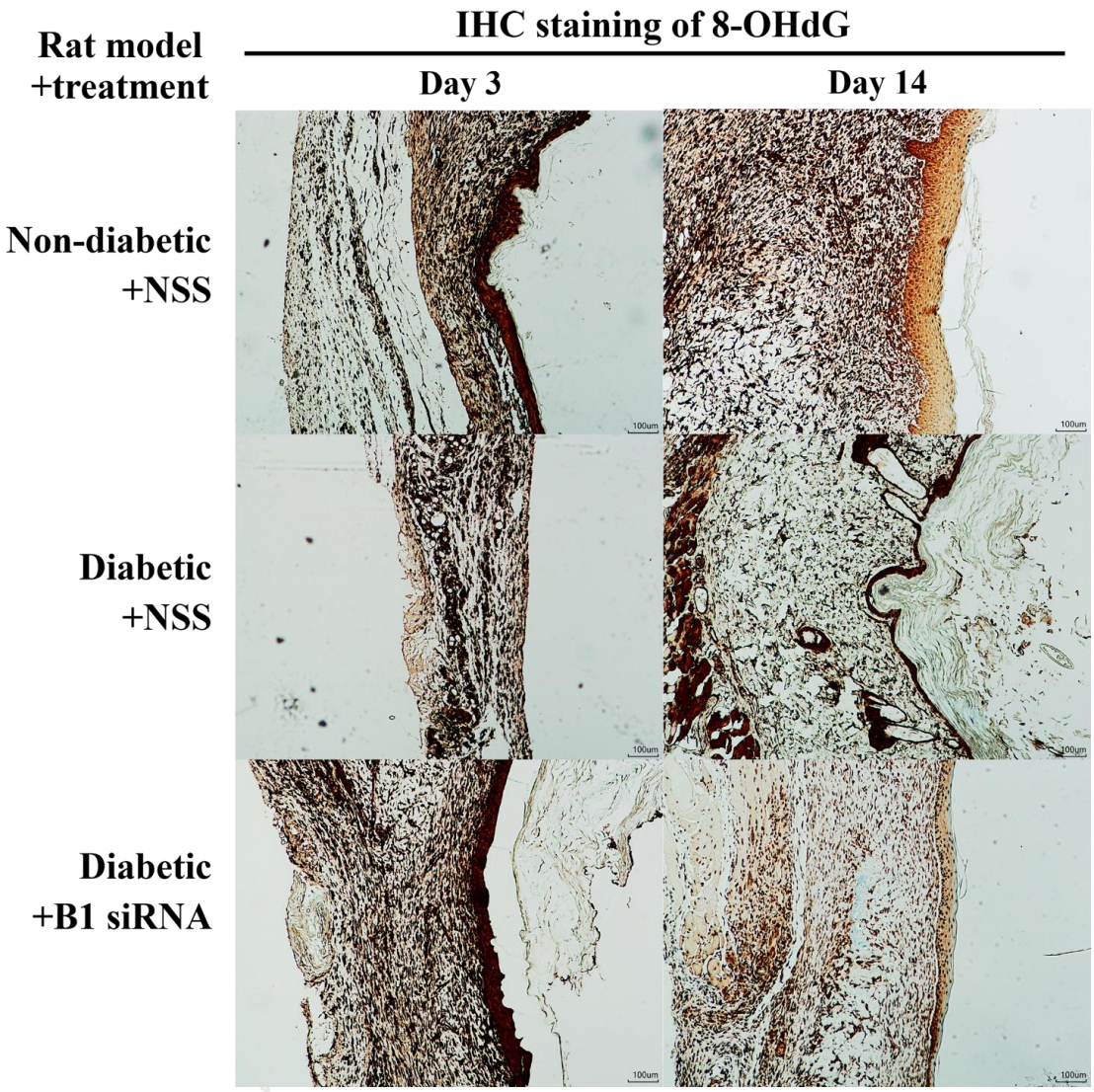

Figure 4-29. Immunohistochemistry (IHC) staining of the 8-OHdG DNA damage marker. B1 siRNA transfection showed a decrease in 8-OHdG endogenous DNA damage (brown color) in wound areas of diabetic rats at the end of the study (day 14 after treatment, lower panel) compared to NSS-treated diabetic rats (middle panel).

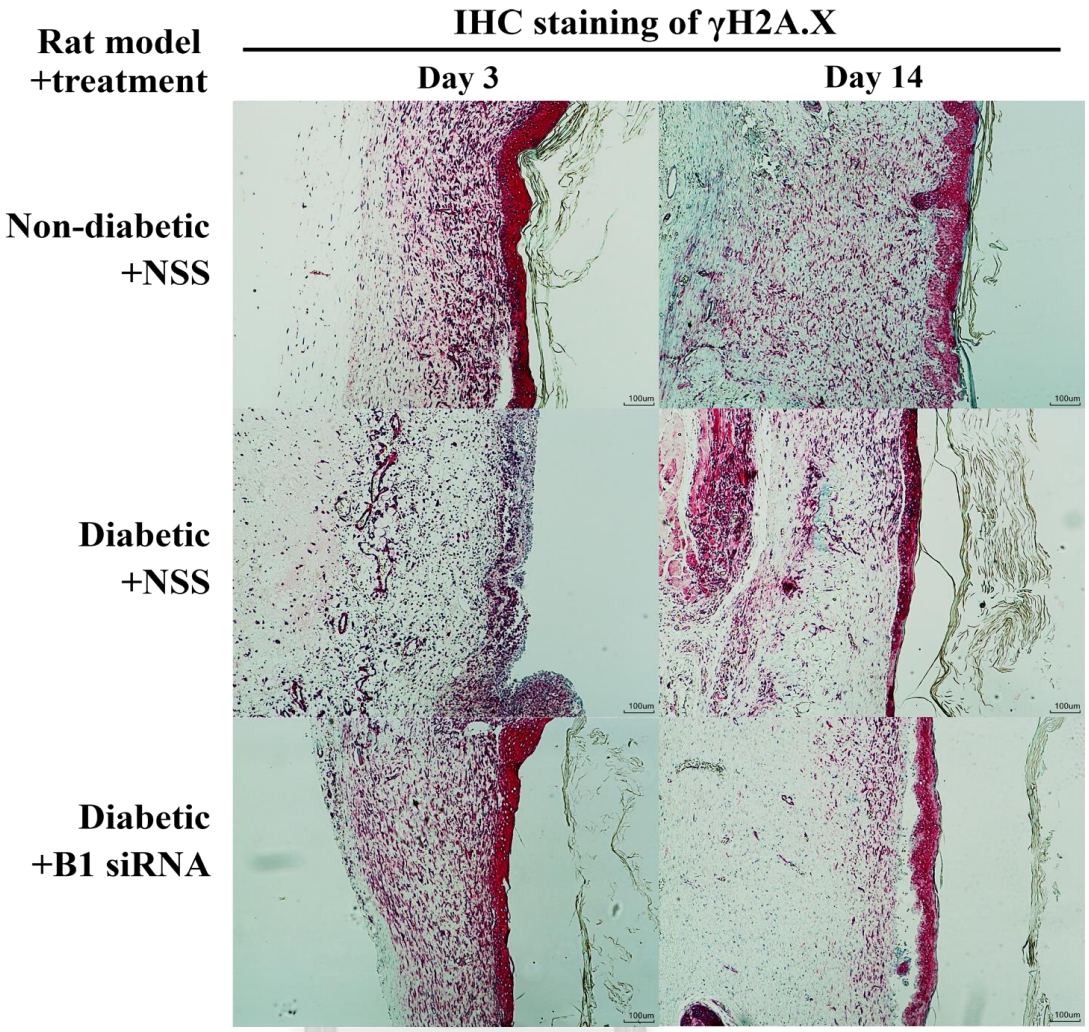

Figure 4-30. IHC staining of γH2A.X DNA damage marker. Treatment of B1 siRNA reduced levels of the γH2A.X DNA damage marker (brown color) in wound areas of diabetic rats at the end of the study (day 14, lower panel) compared to NSS-treated diabetic rats (day 14, middle panel).

จุฬาลงกรณ์มหาวิทยาลัย
CHULALONGKORN UNIVERSITY

Discussion

The genome stabilization function of HMGB1 is mediated by Youth-DNA-GAPs. Here, we showed that Box A of HMGB1 not only increased Youth-DNA-GAPs but also reduced endogenous DNA damage in the animal models. This study reported that Phy-RIND-EDSB or Youth-DNA-GAP is a type of epigenetic mark in mammals that decreases in both D-galactose-induced and naturally aging rats. In addition, we provided the evidence that treatment with Box A of HMGB1 in two aging rat models by showing the improvement of organ functions and age-related parameters in several organs, including liver, visceral fat, brain, and pancreas. Box A of HMGB1 was implicated in a diabetic wound treatment, resulting in a reduction of endogenous DNA damage 8-OHdG and γ-H2A.X, correlating with the previous study in the cell lines (Settayanon S, et al, unpublished data), and consequently led to the acceleration of wound healing in diabetic rats.

Cellular senescence and DNA damage are linked to a large number of noncommunicable diseases and clinical conditions, for example diabetes mellitus (DM), DNA damage due to environmental stimuli, and hereditary DNA repair defects (Palmer et al., 2019; Palmer et al., 2015). Because of the correlation with DNA damage and cellular senescence, the depletion of HMGB1, DNA binding protein, leading to Youth-DNA-GAP reduction may play a crucial role in the process of pathogenesis processes in age-associated diseases. Epigenetic changes in WBCs have been observed in NCDs associated with aging. For instance, genome-wide hypomethylation has been observed in WBCs of age-associated noncommunicable diseases in osteoporosis and DM (Jintaridth et al., 2013) (Thongsroy et al., 2017). The degree of genome-wide methylation is negatively correlated with the severity of these diseases (Jintaridth et al., 2013) (Thongsroy et al., 2017).

จุฬาลงกรณ์มหาวิทยาลัย
Chulalongkorn University

In this study, Box A treatment of aging rats showed a decrease in senescent cells and liver fibrosis. This suggests good potential for Box A of HMGB1 to assist the improvement of impaired liver and cognitive functions in the aging rat models. The aggregation of senescent cells has been reported in various organs of liver disease and cirrhosis (Papatheodoridi et al., 2020). The other common pathological lesions of age-related disorders consist of the fat cell deposition, the accumulation of abnormal macromolecules, for examples, fatty liver and increased visceral fat. Therefore, increased senescent cells in internal organs cause cellular dysfunction and loss of organ functions. Box A can rejuvenate aged cells by reversing the morphology and limiting the signaling proteins of senescence cells and restoring aging cells to the normal function. Therefore, Youth-DNA-GAP reduction in WBCs may affect the

deterioration of the target organs. Box A treatment may be an essential research tool to determine whether immune senescence is involved in disease or condition pathogenesis in the elderly.

Here, we also reported that STZ-induced type I diabetic wounds showing B1 hypomethylation and increased DNA damage could be reprogrammed by transfecting B1 siRNA/Ca-P, which improved genome instability and impaired healing. First, our study demonstrated that the type I diabetic rat model induced by a single high dose of STZ injection showed B1 hypomethylation and a high rate of DNA damage, typically characterized as genome instability features. Second, we demonstrated that B1 siRNA caused specific methylation at CpGs in repetitive B1 elements, resulting in a restoration of B1 methylation status, subsequently reducing DNA lesions and strengthening the genome through topical administration in a diabetic rat wound. Finally, the increased B1 methylation contributed to the acceleration of wound healing by decreasing immune cell infiltration and improving histopathologic scores. These findings suggested that abnormalities in epigenetic modifications, particularly DNA hypomethylation, in diabetes can be modulated, providing a promising epigenetic reprogramming technique to be used in preclinical studies for diabetic wound treatment.

Previous studies in mammalian cells and plants have elucidated the mechanism of *de novo* DNA methylation through the action of B1 siRNA, which is called RNA-directed DNA methylation (RdDM). (Chalertpet et al., 2019) (Zhang & Zhu, 2011) B1 siRNA transfection increases *de novo* DNA methylation levels that are targeted at interspersed or transposable B1 elements in the rat genome in a specific manner, which is mediated by B1 siRNAs, argonaute 4 (AGO4), and various accessory proteins. (Chalertpet et al., 2019) Notably, we observed that B1 siRNA transfection slightly increased the B1 methylation levels after B1 siRNA treatment in normal wounds, but there was no significant difference ($p = 0.080$) between the B1 siRNA treatment and control treatment. B1 elements in normal conditions (not under pathologic conditions) did not present B1 hypomethylation as found in the diabetic rat model. Therefore, a significant difference in B1 methylation levels after B1 siRNA treatment was observed only in diabetic rats when compared to untreated control wounds.

Even though the molecular mechanism whereby B1 (Alu) methylation decreases DNA damage and provides genome strength remains unclear, we proposed several possible mechanisms. First, compelling studies have reported the correlation between methylation in interspersed elements and heterochromatin formation, an epigenetic remark for maintaining

จุฬาลงกรณ์มหาวิทยาลัย
Chulalongkorn University

genome stability. (Baylin et al., 2001) Heterochromatin, the condensed fraction of the genome, may protect DNA against exposure to DNA-damaging agents (Grewal & Jia, 2007), and heterochromatin defects found in an age-associated phenomenon occur prior to accumulative DNA damage. (Pegoraro et al., 2009) Therefore, the present study indicated that increased IRS methylation that directly strengthens the genome may result in DNA lesion reduction and subsequently promote cell proliferation in diabetic wounds. Second, we previously reported that the hypermethylated genome retains replication-independent endogenous DNA double-strand breaks (RIND-EDSBs) (Pornthanakasem et al., 2008), which are redefined as youth-associated genomic-stabilizing DNA gaps (Youth-DNA-GAPs) depending on their role. (Mutirangura, 2019) The present study suggested that Youth-DNA GAPs may act as epigenetic regulators in reducing DNA lesion accumulation to release DNA tension in the same manner as a gap between two railway lines. (Kongruttanachok et al., 2010; Pongpanich et al., 2014; Thongsroy et al., 2013) Finally, increased IRS methylation may improve wound healing by indirectly reducing oxidative stress or the inflammatory response in diabetic wound beds through other mechanisms, consequently reducing DNA damage. While B1 (Alu) siRNA methylated approximately 5% of B1 (Alu) loci, genomic stabilization spanned the whole genome. Therefore, the RIND-EDSB hypothesis is the most likely possible mechanism. Thus, our results showed that B1 hypermethylation in the rat genome accelerated the closure rate of diabetic wounds to a greater extent than that in the untreated group. Correspondingly, our finding agreed with a previous study that transfected Alu siRNA into human cells, leading to *de novo* Alu methylation, resulting in increased DNA damage resistance and enhanced cell proliferation. (Patchsung et al., 2018) Similarly, the positive correlation between Alu hypermethylation and catch-up growth in young individuals has been previously reported. (Rerkasem et al., 2015) These findings suggest that B1 (or Alu) methylation may be reprogrammed, affecting genome integrity by reducing the accumulation of DNA lesions under some stress conditions.

High blood glucose causes excessive oxidative stress and leads to accumulated DNA damage in diabetic wounds. (Newsholme et al., 2016) A major contributor to delayed wound repair in diabetes is a high rate of accumulated DNA damage, which induces cell proliferation defects and coincides with prolonged inflammation associated with carcinogenesis in multiple types of cancer, resulting from a higher mutation rate in genomic DNA. (Lee & Chan, 2015) Genome-wide hypomethylation can be specifically reprogrammed by siRNA, indicating a beneficial role of siRNA intervention. Using B1 siRNA topical treatment resulted in DNA damage diminution by specifically methylating B1 elements and enhancing the growth of cells

จุฬาลงกรณ์มหาวิทยาลัย
Chulalongkorn University

in wound beds, mainly fibroblasts, which eventually accelerated wound healing in diabetes. Our findings may prompt the use of B1 (or Alu) siRNA transfection for therapeutic purposes, at least for local treatment, in DNA damage-derived disorders in a preclinical study. Taken together, B1 (or Alu) siRNA intervention may be advantageous to reprogram genome-wide hypomethylation in diabetes and other age-related diseases.

The present study used a calcium-phosphate nanoparticle, which is an inorganic, nonviral vector gene delivery system. We transfected B1 siRNA/Ca-P into target cells by topical administration and demonstrated successful and unharmful transfection *in vivo*. Due to the pre-existence of their composition in cells or tissues, Ca-P nanoparticles encapsulating the genetic material possess biocompatibility, biodegradation, low immunogenic, and low toxicity properties in the transfected cells. (Yin et al., 2014) (Ramamoorth & Narvekar, 2015) In addition, we provided an accessible technique for Ca-P nanoparticle coating and preparation with a simple material requirement. Thus, the present study supported that Ca-P nanoparticles are a biologically safe, suitable, and effective gene transfer tool for *in vivo* siRNA transfection treatment.

Although wound treatment complications were not observed, systemic B1 (or Alu) siRNA intervention was precautionary. In addition to DNA methylation, B1 (or Alu) siRNA may be incorporated into the RNA-induced silencing complex (RISC) to regulate mRNA degradation or interfere with protein synthesis. Therefore, B1 (or Alu) siRNA may interfere with the physiological function of some cells. Moreover, B1 and Alu genome distributions are different. Additionally, the present preclinical study consisted of diabetic wound treatment in a rat model; however, the beneficial roles and adverse effects using Alu siRNA, targeting Alu elements in the human genome, by a topical treatment in wound healing with normal or diabetic conditions need to be confirmed in a clinical study.

จุฬาลงกรณ์มหาวิทยาลัย
Chulalongkorn University

CHAPTER V
CONCLUSION

This study unveiled a novel finding of how DNA ages and developed an innovative approach to aging rejuvenation or alleviation. Whereas DNA damage can result in health deterioration in the elderly, our understanding of its etiological mechanisms and technology to handle this phenomenon is limited. Here, we proved that the number of Youth-DNA-GAPs is a biomarker for youthful DNA. Box A of HMGB1, a molecular scissor producing Youth-DNA-GAPs, is a technology to increase DNA durability and alleviate aging molecular and physical phenotypes to be close to those of youths. Therefore, Box A is a novel genomic stabilizing medicine that can be a realistic hope for a decline of many organismal aging features and may be an intervention that revolutionizes our aging society.

Furthermore, Box A of HMGB1 treatment in an early life of a mammalian model, baby porcine, provides the important evidence of safety use in large animals, and also demonstrates an effect of growth acceleration in baby pigs. Hence, this additional study may show the possibility of future implications in clinical phases.

In addition, the STZ-induced type I diabetic rat model is an appropriate and adequate diabetic animal model for the study of B1 hypomethylation and its consequences. The present study suggested that the STZ-induced rat model shows genome-wide hypomethylation, imitating the diabetic microenvironment milieu by generating and maintaining prolonged hyperglycemia and DNA damage (as shown in **A Summary Figure 1**). Box A of HMGB1 and B1 siRNA intervention in diabetic wounds limits DNA damage and restores B1 hypomethylation (for the B1 siRNA approach), directly accelerating wound repair. Box A of HMGB1 treatment and B1 hypermethylation by *de novo* DNA methylation result in depletion of DNA damage and ultimately accelerates diabetic wound healing, providing a promising outcome in translational medicine. Hence, these findings underpin the importance of epigenetic reprogramming as a potential therapeutic target for diabetes and its complications.

จุฬาลงกรณ์มหาวิทยาลัย
Chulalongkorn University

A summary figure for B1 siRNA intervention in a model of diabetic rat wound.

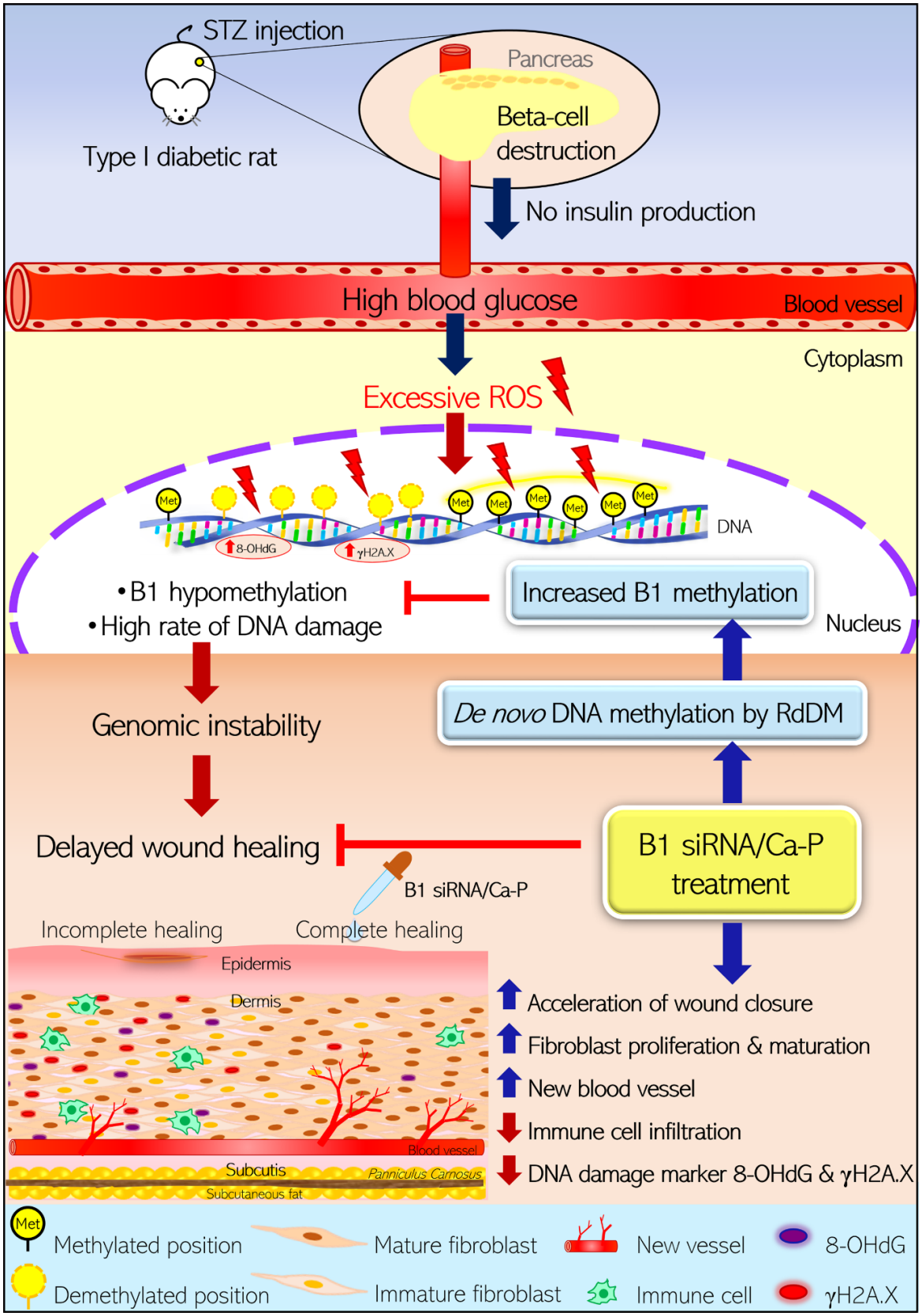

A Summary Figure 1. Reprogramming B1 methylation by B1 siRNA transfection restores delayed wound healing in diabetic wounds by limiting DNA damage. STZ-induced type I diabetic rats exhibited high blood glucose due to direct pancreatic β-cell destruction, resulting in no insulin production. Excessive ROS-derived high blood glucose caused oxidative damage of DNA as indicated by 8-OHdG and γH2A.X. STZ-induced diabetic wounds also demonstrated B1 hypomethylation, correlating with a high rate of DNA damage. The accumulation of DNA damage and B1 hypomethylation led to genomic instability and eventually delayed the wound closure rate in diabetic rats. Incomplete healing of wounds resulted in reduced fibroblast maturation and proliferation as well as new blood vessel formation and high immune cell infiltration, which were related to increased DNA damage (8-OHdG and γH2A.X) in the wound bed. In contrast, diabetic wounds treated with B1 siRNA/Ca-P showed an accelerated wound healing rate, correlating with higher fibroblast proliferation and new vessel formation in the wound area compared to diabetic control wounds. In addition, B1 siRNA/Ca-P treatment diminished immune cell infiltration and DNA damage markers, contributing to complete wound healing in diabetic microenvironments. B1 siRNA enhanced *de novo* DNA methylation in B1 elements and restored B1 hypomethylation via the RdDM mechanism. (STZ; streptozotocin, ROS; reactive oxygen species, RdDM; RNA-directed DNA methylation).

จุฬาลงกรณ์มหาวิทยาลัย
Chulalongkorn University

REFERENCES

1. Pal S and Tyler JK. Epigenetics and aging. Sci Adv. 2016;2(7):e1600584.
2. Finkel T, Serrano M, Blasco MA. The common biology of cancer and ageing. Nature. 2007;448 :767–74.
3. Wilson AS, Power BE, Molloy PL. DNA hypomethylation and human diseases. Biochim Biophys Acta 2007;1775 :138–162.
4. Jung M and Pfeifer GP. Aging and DNA methylation. BMC Biology. 2015;13(7). doi:10.1186/s12915-015-0118-4
5. Moore LD, Le T and Fan G. DNA Methylation and Its Basic Function. Neuropsychopharmacol Reviews. 2013;38 :23–38; doi:10.1038/npp.2012.112.
6. Heyna H, Lib N, Ferreiraa HJ, Morana S, Pisanoe DG, Gomeza A, Dieza J, Sanchez-Muta JV, Setiena F, Carmonaa FJ, Pucaf AA, Sayolsa S, Pujanah MA, Serra-Musachh J, Iglesias-Platasi I,Formigaj F, Fernandezk AF, Fragak MF, Heathm SC, Valenciae A, Gutm IG, Wangn J,and Esteller M. Distinct DNA methylomes of newborns and centenarians. Proc Natl Acad Sci U S A. 2012;109(26): 10522–10527.
7. Mustafina OE. The possible roles of human Alu elements in aging. 2013;4(96). doi: 10.3389/fgene.2013.00096.
8. Kramerov DA and Vassetzky NS. Short Retrosposons in Eukaryotic Genomes. Intern Rev Cytol. 2005;247 :165-221; doi: 10.1016/S0074-7696(05)47004-7.
9. Jintaridth P and Mutirangura A. Distinctive patterns of age-dependent hypomethylation in interspersed repetitive sequences. Physiol Genomics. 2010;41: 194–200.
10. Jintaridth P, Tungtrongchitr R, Preutthipan S, Mutirangura A. Hypomethylation of Alu Elements in Post-Menopausal Women with Osteoporosis. PLoS ONE. 2013;8(8): e70386. doi: 10.1371/journal.pone.0070386.
11. Kirkman MS, Vanessa Jones Briscoe VJ, Clark N, Florez H, Haas LB, Halter JB, Huang ES, Korytkowski MT, Munshi MN, Odegard PS, Pratley RE and Swift CS. Diabetes in Older Adults. Diabetic Care. 2012;35: 2650-2664.
12. Rönn T and Ling C. DNA methylation as a diagnostic and therapeutic target in the battle against Type 2 diabetes. Epigenomics. 2015;7(3) :451–460.
13. Thongsroy J, Patchsung M and Mutirangura A. The association between Alu hypomethylation and severity of type 2 Diabetes Mellitus. Clin Epigen. 2017;9 :93.
14. Lopez-Otin C, Blasco MA, Partridge L, Serrano M and Kroemer G. The Hallmarks of Aging. Cell. 2013;153 :1194-1216.

จุฬาลงกรณ์มหาวิทยาลัย
CHULALONGKORN UNIVERSITY

15. Tubbs A and Nussenzweig A. Endogenous DNA Damage as a Source of Genomic Instability in Cancer. Cell. 2017;168 :644-656.
16. Cheng KC, Cahill DS, Kasai H, Nishimura S and Loeb LA. 8-Hydroxyguanine, an abundant form of oxidative DNA damage, causes G→T and C→A substitutions. J Biol Chem. 1992;267(1) :166–72.
17. Patchsung M, Settayanon S, Pongpanich M, Mutirangura D, Jintarith P and Mutirangura A. Alu siRNA to increase Alu element methylation and prevent DNA damage. Epigenomics. 2018;10(2) :175–185.
18. Rerkasem K, Rattanatanyong P, Rerkasem A, Wongthanee A, Rungruengthanakit K, Ampica Mangklabruks A, Mutirangura A. Higher Alu Methylation Levels in Catch-Up Growth in Twenty-Year-Old Offsprings. PLoS ONE. 2015;10(3): e0120032. doi: 10.1371/journal.pone.0120032.
19. Kang R, Chen R, Zhang Q, Hou W, Wu S, Cao L, Huang J, Yu Y, Fan XG, Yan Z, Sun X, Wang H, Wang Q, Tsung A, Billiar TR, Zeh HJ, Lotze MT and Tang D. HMGB1 in health and disease. Mol Aspects Med. 2014;40 :1-116. doi: 10.1016/j.mam.2014.05.001.
20. Ugrinova I and Pasheva E. HMGB1 Protein: A Therapeutic Target Inside and Outside the Cell. Advances in Protein Chemistry and Structural Biology. 2016;107. doi: 10.1016/bs.apcsb.2016.10.001
21. Hwang JS, Choi HS, Ham SA, Yoo T, Lee WJ, Paek KS and Seo HG. Deacetylation-mediated interaction of SIRT1-HMGB1 improves survival in a mouse model of endotoxemia. Sci Rep. 2015;5: 15971. doi: 10.1038/srep15971.
22. Mitsouras K, Wong B, Arayata C, Johnson RC, and Carey M. The DNA Architectural Protein HMGB1 Displays Two Distinct Modes of Action That Promote Enhanceosome Assembly. Mol Cell Biol. 2002;22(12) :4390–4401. doi: 10.1128/MCB.22.12.4390–4401.2002.
23. Štros M. HMGB proteins: Interactions with DNA and chromatin. Biochimica et Biophysica Acta. 2010;1799 :101–113.
24. Yang H, Wang H, Chavan SS, and Andersson U. High Mobility Group Box Protein 1 (HMGB1): The Prototypical Endogenous Danger Molecule. Mol Med. 2015; 21(Suppl 1): S6–S12
25. Giavara S, Kosmidou E, Hande MP, Bianchi ME, Morgan A, Fagagna F and Jackson SP. Yeast Nhp6A/B and Mammalian Hmgb1 Facilitate the Maintenance of Genome Stability. Curr Biol. 2005;15 :68–72. doi: I 10.1016/j.cub.2004.12.065.

จุฬาลงกรณ์มหาวิทยาลัย
Chulalongkorn University

26. Pongpanich M, Patchsung M, Thongsroy J and Mutirangura A. Characteristics of replication-independent endogenous double-strand breaks in Saccharomyces cerevisiae. BMC Genomics. 2014;15(750) :1-12.
27. Pornthanakasem W, Kongruttanachok N, Phuangphairoj C, Suyarnsestakorn C, Sanghangthum T, Oonsiri S, Ponyeam W, Thanasupawat T, Matangkasombut O and Mutirangura A. LINE-1 methylation status of endogenous DNA double-strand breaks. Nucleic Acids Research. 2008;36(11) :3667-3675.
28. Thongsroy J, Patchsung M, Pongpanich M, Settayanon S, and Mutirangura A. Reduction in replication-independent endogenous DNA double-strand breaks promotes genomic instability during chronological aging in yeast. FASEB J. 2018; fj201800218RR. doi: 10.1096/fj.201800218RR.
29. Zhu ZY, Zhu GH. Establishment and measurement of D-galactose induced aging model. Fudan University Journal of Medical Sciences. 2007;34(4) :617–9.
30. Ho SC, Liu JH and Wu RY. Establishment of the mimetic aging effect in mice caused by D-galactose. Biogerontology. 2003;4 :15–18.
31. Zhou YY, Ji XF, Fu JP, Zhu XJ, Li RH, Mu CK, Wang CL and Song WW. Gene Transcriptional and Metabolic Profile Changes in Mimetic Aging Mice Induced by D-Galactose. PLoS One. 2015;10(7) :e0132088. doi: 10.1371/journal.pone.0132088. eCollection 2015.
32. Shwe T, Pratchayasakul W, Nipon Chattipakorn N and Chattipakorn SC. Role of D-galactose-induced brain aging and its potential used for therapeutic interventions. Experimental Gerontology. 2018;101 :13-36.
33. Lombard DB, Chua KF, Mostoslavsky R, Franco S, Gostissa M and Alt FW. DNA Repair, Genome Stability, and Aging. Cell. 2005;120 :497–512. doi: 10.1016/j.cell.2005.01.028.
34. Huang CC, Chiang WD, Huang WC, Huang CY, Hsu MC, and Lin WT. Hepatoprotective Effects of Swimming Exercise against D-Galactose-Induced Senescence Rat Model. Evidence-Based Comp and Alt Med. 2013;275431 :1-9. doi: org/10.1155/2013/275431.
35. Sadigh-Eteghad S, Majdi A, McCann SK, Mahmoudi J, Vafaee MS, Macleo MR. D-galactose-induced brain ageing model: A systematic review and meta-analysis on cognitive outcomes and oxidative stress indices
36. Ji M, Su X, Liu J, Zhao Y, Li Z, Xu X, Li H and Nashun B. Comparison of naturally aging and D-galactose induced aging model in beagle dogs. Exp Ther Med. 2017;14(6):5881-5888. doi: 10.3892/etm.2017.5327.

จุฬาลงกรณ์มหาวิทยาลัย
CHULALONGKORN UNIVERSITY

37. Zhen YZ, Lin JY, Li JK, Zhang GL, Zhao YF, Wang MM, Wei JB, Wei J and Hu G. Effects of rhein lysinate on D-galactose-induced aging mice. Exp Ther Med. 2016;11 :303-308.
38. Heidari S, Mehri S and Hosseinzadeh H. Memory enhancement and protective effects of crocin against D-galactose aging model in the hippocampus of Wistar rats. Iran J Basic Med Sci. 2017;20 :1250-1259. doi: 10.22038/IJBMS.2017.9541.
39. Zhang Q, Li X, Cui X and Zuo P. D-Galactose injured neurogenesis in the hippocampus of adult mice. Neurol Res. 2005;27 :552-556.
40. Cebe T, Yanar K, Atukeren P, Ozan T, Kuruç AI, Kunbaz A, Sitar ME, Mengi M, Aydın MS, Eşrefoğlu M, Aydın S and Cakatay U. A comprehensive study of myocardial redox homeostasis in naturally and mimetically aged rats. Age. 2014;36 :9728.
41. Liu J, Wang J, Chen X, Guo C, Guo Yand Wang H. Ginkgo biloba extract EGB761 protects against aging-associated diastolic dysfunction in cardiomyocytes of D-galactose-induced aging rat. Oxid Med Cell Longev. 2012;2012 :418748.
42. Childs BG, Durik M, Baker DJ and van Deursen JM. Cellular senescence in aging and age-related disease: from mechanisms to therapy. Nat Med. 2015;21(12) :1424-1435. doi: 10.1038/nm.4000.
43. Baker DJ, Jeganathan KB, Cameron JD, Thompson M, Juneja S, Kopecka A, Kumar R, Jenkins RB, de Groen PC, Roche P and van Deursen JM. BubR1 insufficiency causes early onset of aging-associated phenotypes and infertility in mice. Nat Genet. 2004;36(7) :744-9.
44. Vanyushin BF, Nemirovsky LE, Klimenko VV, Vasiliev VK and Belozersky AN. The 5-methylcytosine in DNA of rats. Tissue and age specificity and the changes induced by hydrocortisone and other agents. Gerontol. 1973;19(3):138-152.
45. Testa R and Ceriello A. Pathogenic loop between diabetes and cell senescence. Diabetes Care. 2007;30(17).
46. Global Report on Diabetes WHO 2016.
47. Giurini JM and Lyons TE. Diabetic foot complications: diagnosis and management. Int J Low Extrem Wounds. 2005;4 :171-182.
48. Jeffcoate WJ, Price P and Harding KG. Wound healing and treatments for people with diabetic foot ulcers. Diabetes/Metab Res Rev 2004;20: S78-S89.
49. Allyson K. Palmer, Tamara Tchkonia, Nathan K. Lebrasseur, Eduardo N. Chini, Ming Xu, and James L. Kirkland. Cellular Senescence in Type 2 Diabetes: A Therapeutic Opportunity. Diabetes. 2015;64(7) :2289-2298.

จุฬาลงกรณ์มหาวิทยาลัย
CHULALONGKORN UNIVERSITY

50. Huang JS, Wang YH, Ling TY, Chuang SS, Johnson FE & Huang SS. Synthetic TGF-ß antagonist accelerates wound healing and reduces scarring. FASEB J 2002; 16:1269-1270.
51. Keswani SG, Katz AB, Lim F-L, Zoltick P, Radu A, Alaee D, Herlyn M & Crombleholme TM. Adenoviral mediated gene transfer of PDGF-ß enhances wound healing in type 1 and type 11 diabetic wounds. Wound Repair Regen. 2004;12 :497-504.
52. Aileen JK. The use of animal models in diabetes research. Br J Pharm. 2012;166 :877–894.
53. Deeds MC, Anderson JM, Armstrong AS, Gastineau DA, Hiddinga HJ, Jahangir A, Eberhardt NL and Kudva YC. Single Dose Streptozotocin Induced Diabetes: Considerations for Study Design in Islet Transplantation Models. Lab Anim. 2011;45(3) :131–140. doi:10.1258/la.2010.010090.
54. Thiruvoth FM, Mohapatra DP, Kumar D, Chittoria SRK and Nandhagopa V. Current concepts in the physiology of adult wound healing. Plast Aesthet Res. 2015;2 :250-256.
55. McLennan S, Yue DK and Twigg SM. Molecular aspects of wound healing in diabetes. Prim Intention. 2006; 14(1): 8-13.
56. Brem H and Tomic-Canic M. Cellular and molecular basis of wound healing in diabetes. J Clin Invest. 2007;117 :1219–1222. doi:10.1172/JCI32169.
57. Sambrook JF and Russell DW, Molecular Cloning: A Laboratory Manual, The third edition, Vols 1,2 and 3, Cold Spring Harbor Laboratory Press, 2001.
58. Tunapong W, Apaijai N, Yasom S, Tanajak P, Wanchai K,Chunchai T, Kerdphoo S, Eaimworawuthikul S, Thiennimitr P, Pongchaidecha A, Lungkaphin A, Pratchayasakul W, Chattipakorn SC and Chattipakorn N. Chronic treatment with prebiotics, probiotics and synbiotics attenuated cardiac dysfunction by improving cardiac mitochondrial dysfunction in male obese insulin-resistant rats. Eur J Nutr. 2017: 1-14. doi: 10.1007/s00394-017-1482-3.
59. Chattipakorn N, Incharoen T, Kanlop N and Chattipakorn SC. Heart rate variability in myocardial infarction and heart failure. Int J Cardiol. 2007;120(3) :289–296.
60. Apaijai N, Pintana H, Chattipakorn SC and Chattipakorn N. Effects of vildagliptin versus sitagliptin, on cardiac function, heart rate variability and mitochondrial function in obese insulin-resistant rats. Br J Pharmacol. 2013;169(5) :1048–1057.
61. Samniang B, Shinlapawittayatorn K, Chunchai T, Pongkan W, Kumfu S, Chattipakorn SC, KenKnight BH and Chattipakorn N. Vagus Nerve Stimulation Improves Cardiac

จุฬาลงกรณ์มหาวิทยาลัย
CHULALONGKORN UNIVERSITY

Function by Preventing Mitochondrial Dysfunction in Obese-Insulin Resistant Rats. Sci Rep. 2016;6 :19749.

62. Pintana H, Apaijai N, Chattipakorn N and Chattipakorn SC. DPP-4 inhibitors improve cognition and brain mitochondrial function of insulin resistant rats. J Endocrinol. 2013;218(1) :1–11.
63. Vorhees CV and Williams MT. Morris water maze: procedures for assessing spatial and related forms of learning and memory. Nat Protoc. 2006;1(2) :848–58.
64. Stanford SC. The open field test: reinventing the wheel. J Psychopharmacol. 2007;21(2) :134–5.
65. Denenberg VH. Open-field behavior in the rat: what does it mean? Ann N Y Acad Sci. 1969;159(3) :852–9.
66. Chunchai T, Thunapong W, Yasom S, Wanchai K, Eaimworawuthikul S, Metzler G, Lungkaphin A, Pongchaidecha A, Sirilun S, Chaiyasut C, Pratchayasakul W, Thiennimitr P, Chattipakorn N and Chattipakorn SC. Decreased microglial activation through gut-brain axis by prebiotics, probiotics, or synbiotics effectively restored cognitive function in obese-insulin resistant rats. J Neuroinflam 2018;15 :11.
67. Baker DJ, Wijshake T, Tchkonia T, LeBrasseur NK, Childs BG, van de Sluis B, Kirkland JL and van Deursen JM. Clearance of p16Ink4a-positive senescent cells delays ageing-associated disorders. Nature. 2011;479(7372) :232-6. doi: 10.1038/nature10600.
68. Yao Z, Huang Y, Luo G, Wu J and Weifeng H. A biological membrane-based novel excisional wound-splinting model in mice. Burns & Trauma 2014;2 :20040196.
69. Kuo LJ and Yang LX. Gamma-H2AX - a novel biomarker for DNA double-strand breaks. In Vivo. 2008;22 :305-310.
70. Kosar M, Bartkova J, Hubackova S, Hodny Z, Lukas J and Bartek J. Senescence-associated heterochromatin foci are dispensable for cellular senescence, occur in a cell type- and insult-dependent manner and follow expression of p16(ink4a). Cell Cycle. 2011;10(3):457-68.
71. Chalitchagorn K, Shuangshoti S, Hourpai N, Kongruttanachok N, Tangkijvanich P, Thong-ngam D, Voravud N, Sriuranpong V, Mutirangura A. Distinctive pattern of LINE-1 methylation level in normal tissues and the association with carcinogenesis. Oncogene. 2004;23(54): 8841-6.
72. Song C, Peng W, Yin S, Zhao J, Fu B, Zhang J, Mao T, Wu H and Zhang Y. Melatonin improves age-induced fertility decline and attenuates ovarian mitochondrial oxidative stress in mice. Sci Rep. 2016;6 :35165. doi:10.1038/srep35165.

จุฬาลงกรณ์มหาวิทยาลัย
Chulalongkorn University

73. Zaika E, Wei J, Yin D, Andl C, Moll U, El-Rifai W and Zaika AI. p73 protein regulates DNA damage repair. FASEB J. 2011;25: 4406-4414.
74. Qiao YF, Guo W, Li L, Shao S, Qiao X, Shao J, Zhang Q, Li R and Wang L. Melatonin attenuates hypertension-induced renal injury partially through inhibiting oxidative stress in rats. Mol Med Rep. 2016 doi: 10.3892/mmr.2015.4495.
75. Aydin, S. *et al.* Comparison of oxidative stress biomarkers in renal tissues of D-galactose induced, naturally aged and young rats. *Biogerontology* **13**, 251-260, doi:10.1007/s10522-011-9370-3 (2012).
76. Algire, C., Moiseeva, O., Deschênes-Simard, X., Amrein, L., Petruccelli, L., Birman, E., Viollet, B., Ferbeyre, G., & Pollak, M. N. (2012). Metformin reduces endogenous reactive oxygen species and associated DNA damage. *Cancer Prev Res (Phila)*, *5*(4), 536-543. https://doi.org/10.1158/1940-6207.Capr-11-0536
77. Bansal, A., & Pinney, S. E. (2017). DNA methylation and its role in the pathogenesis of diabetes. *Pediatr Diabetes*, *18*(3), 167-177. https://doi.org/10.1111/pedi.12521
78. Baylin, S. B., Esteller, M., Rountree, M. R., Bachman, K. E., Schuebel, K., & Herman, J. G. (2001). Aberrant patterns of DNA methylation, chromatin formation and gene expression in cancer. *Hum Mol Genet*, *10*(7), 687-692. https://doi.org/10.1093/hmg/10.7.687
79. Blakytny, R., & Jude, E. (2006). The molecular biology of chronic wounds and delayed healing in diabetes. *Diabet Med*, *23*(6), 594-608. https://doi.org/10.1111/j.1464-5491.2006.01773.x
80. Bo-Htay, C., Shwe, T., Higgins, L., Palee, S., Shinlapawittayatorn, K., Chattipakorn, S. C., & Chattipakorn, N. (2020). Aging induced by D-galactose aggravates cardiac dysfunction via exacerbating mitochondrial dysfunction in obese insulin-resistant rats. *Geroscience*, *42*(1), 233-249. https://doi.org/10.1007/s11357-019-00132-9
81. Bolajoko, E. B., Mossanda, K. S., Adeniyi, F., Akinosun, O., Fasanmade, A., & Moropane, M. (2008). Antioxidant and oxidative stress status in type 2 diabetes and diabetic foot ulcer. *S Afr Med J*, *98*(8), 614-617. https://www.ncbi.nlm.nih.gov/pubmed/18928040
82. Bollati, V., Schwartz, J., Wright, R., Litonjua, A., Tarantini, L., Suh, H., Sparrow, D., Vokonas, P., & Baccarelli, A. (2009). Decline in genomic DNA methylation through aging in a cohort of elderly subjects. *Mech Ageing Dev*, *130*(4), 234-239. https://doi.org/10.1016/j.mad.2008.12.003
83. Brunet, A., & Berger, S. L. (2014). Epigenetics of aging and aging-related disease. *J Gerontol A Biol Sci Med Sci*, *69 Suppl 1*(Suppl 1), S17-20. https://doi.org/10.1093/gerona/glu042
84. Bryan, N., Ahswin, H., Smart, N., Bayon, Y., Wohlert, S., & Hunt, J. A. (2012). Reactive oxygen species (ROS)--a family of fate deciding molecules pivotal in constructive inflammation and wound healing. *Eur Cell Mater*, *24*, 249-265. https://www.ncbi.nlm.nih.gov/pubmed/23007910
85. Cardelli, M. (2018). The epigenetic alterations of endogenous retroelements in aging. *Mech Ageing Dev*, *174*, 30-46. https://doi.org/10.1016/j.mad.2018.02.002
86. Chalertpet, K., Pin-On, P., Aporntewan, C., Patchsung, M., Ingrungruanglert, P., Israsena, N., & Mutirangura, A. (2019). Argonaute 4 as an Effector Protein in RNA-Directed DNA Methylation in Human Cells. *Front Genet*, *10*, 645. https://doi.org/10.3389/fgene.2019.00645

87. Chomczynski, P., Mackey, K., Drews, R., & Wilfinger, W. (1997). DNAzol: a reagent for the rapid isolation of genomic DNA. *Biotechniques*, *22*(3), 550-553. https://doi.org/10.2144/97223pf01
88. Davidson, J. M., Yu, F., & Opalenik, S. R. (2013). Splinting Strategies to Overcome Confounding Wound Contraction in Experimental Animal Models. *Adv Wound Care (New Rochelle)*, *2*(4), 142-148. https://doi.org/10.1089/wound.2012.0424
89. Davis, F. M., Kimball, A., Boniakowski, A., & Gallagher, K. (2018). Dysfunctional Wound Healing in Diabetic Foot Ulcers: New Crossroads. *Curr Diab Rep*, *18*(1), 2. https://doi.org/10.1007/s11892-018-0970-z
90. de Mello, V. D., Pulkkinen, L., Lalli, M., Kolehmainen, M., Pihlajamäki, J., & Uusitupa, M. (2014). DNA methylation in obesity and type 2 diabetes. *Ann Med*, *46*(3), 103-113. https://doi.org/10.3109/07853890.2013.857259
91. den Dekker, A., Davis, F. M., Kunkel, S. L., & Gallagher, K. A. (2019). Targeting epigenetic mechanisms in diabetic wound healing. *Transl Res*, *204*, 39-50. https://doi.org/10.1016/j.trsl.2018.10.001
92. Dunnill, C., Patton, T., Brennan, J., Barrett, J., Dryden, M., Cooke, J., Leaper, D., & Georgopoulos, N. T. (2017). Reactive oxygen species (ROS) and wound healing: the functional role of ROS and emerging ROS-modulating technologies for augmentation of the healing process. *Int Wound J*, *14*(1), 89-96. https://doi.org/10.1111/iwj.12557
93. Furman, B. L. (2015a). Streptozotocin-Induced Diabetic Models in Mice and Rats. *Curr Protoc Pharmacol*, *70*, 5.47.41-45.47.20. https://doi.org/10.1002/0471141755.ph0547s70
94. Furman, B. L. (2015b). Streptozotocin-Induced Diabetic Models in Mice and Rats. *Curr Protoc Pharmacol*, *70*, 5 47 41-20. https://doi.org/10.1002/0471141755.ph0547s70
95. Grewal, S. I., & Jia, S. (2007). Heterochromatin revisited. *Nat Rev Genet*, *8*(1), 35-46. https://doi.org/10.1038/nrg2008
96. Jintaridth, P., & Mutirangura, A. (2010). Distinctive patterns of age-dependent hypomethylation in interspersed repetitive sequences. *Physiol Genomics*, *41*(2), 194-200. https://doi.org/10.1152/physiolgenomics.00146.2009
97. Jintaridth, P., Tungtrongchitr, R., Preutthipan, S., & Mutirangura, A. (2013). Hypomethylation of Alu elements in post-menopausal women with osteoporosis. *PLoS One*, *8*(8), e70386. https://doi.org/10.1371/journal.pone.0070386
98. Kerner, W., & Brückel, J. (2014). Definition, classification and diagnosis of diabetes mellitus. *Exp Clin Endocrinol Diabetes*, *122*(7), 384-386. https://doi.org/10.1055/s-0034-1366278
99. Kido, D., Mizutani, K., Takeda, K., Mikami, R., Matsuura, T., Iwasaki, K., & Izumi, Y. (2017). Impact of diabetes on gingival wound healing via oxidative stress. *PLoS One*, *12*(12), e0189601. https://doi.org/10.1371/journal.pone.0189601
100. King, A. J. (2012). The use of animal models in diabetes research. *Br J Pharmacol*, *166*(3), 877-894. https://doi.org/10.1111/j.1476-5381.2012.01911.x
101. Kongruttanachok, N., Phuangphairoj, C., Thongnak, A., Ponyeam, W., Rattanatanyong, P., Pornthanakasem, W., & Mutirangura, A. (2010). Replication independent DNA double-strand break retention may prevent genomic instability. *Mol Cancer*, *9*, 70. https://doi.org/10.1186/1476-4598-9-70
102. Kosachunhanun, N., Tongprasert, S., & Rerkasem, K. (2012). Diabetic foot problems in tertiary care diabetic clinic in Thailand. *Int J Low Extrem Wounds*, *11*(2), 124-127. https://doi.org/10.1177/1534734612446967
103. Kramerov, D. A., & Vassetzky, N. S. (2005). Short retroposons in eukaryotic genomes. *Int Rev Cytol*, *247*, 165-221. https://doi.org/10.1016/s0074-7696(05)47004-7

104. Lee, S. C., & Chan, J. C. (2015). Evidence for DNA damage as a biological link between diabetes and cancer. *Chin Med J (Engl)*, *128*(11), 1543-1548. https://doi.org/10.4103/0366-6999.157693
105. Leoni, G., Neumann, P. A., Sumagin, R., Denning, T. L., & Nusrat, A. (2015). Wound repair: role of immune-epithelial interactions. *Mucosal Immunol*, *8*(5), 959-968. https://doi.org/10.1038/mi.2015.63
106. López-Otín, C., Blasco, M. A., Partridge, L., Serrano, M., & Kroemer, G. (2013). The hallmarks of aging. *Cell*, *153*(6), 1194-1217. https://doi.org/10.1016/j.cell.2013.05.039
107. Mutirangura, A. (2019). A Hypothesis to Explain How the DNA of Elderly People Is Prone to Damage: Genome- Wide Hypomethylation Drives Genomic Instability in the Elderly by Reducing Youth-Associated Gnome-Stabilizing DNA Gaps. In. https://doi.org/10.5772/intechopen.83372
108. Naito, Y., & Ui-Tei, K. (2012). siRNA Design Software for a Target Gene-Specific RNA Interference [Review]. *Frontiers in Genetics*, *3*(102). https://doi.org/10.3389/fgene.2012.00102
109. Newsholme, P., Cruzat, V. F., Keane, K. N., Carlessi, R., & de Bittencourt, P. I., Jr. (2016). Molecular mechanisms of ROS production and oxidative stress in diabetes. *Biochem J*, *473*(24), 4527-4550. https://doi.org/10.1042/bcj20160503c
110. Nunan, R., Harding, K. G., & Martin, P. (2014). Clinical challenges of chronic wounds: searching for an optimal animal model to recapitulate their complexity. *Dis Model Mech*, *7*(11), 1205-1213. https://doi.org/10.1242/dmm.016782
111. Öhnstedt, E., Lofton Tomenius, H., Vågesjö, E., & Phillipson, M. (2019). The discovery and development of topical medicines for wound healing. *Expert Opin Drug Discov*, *14*(5), 485-497. https://doi.org/10.1080/17460441.2019.1588879
112. Palmer, A. K., Gustafson, B., Kirkland, J. L., & Smith, U. (2019). Cellular senescence: at the nexus between ageing and diabetes. *Diabetologia*, *62*(10), 1835-1841. https://doi.org/10.1007/s00125-019-4934-x
113. Palmer, A. K., Tchkonia, T., LeBrasseur, N. K., Chini, E. N., Xu, M., & Kirkland, J. L. (2015). Cellular Senescence in Type 2 Diabetes: A Therapeutic Opportunity. *Diabetes*, *64*(7), 2289-2298. https://doi.org/10.2337/db14-1820
114. Papatheodoridi, A. M., Chrysavgis, L., Koutsilieris, M., & Chatzigeorgiou, A. (2020). The Role of Senescence in the Development of Nonalcoholic Fatty Liver Disease and Progression to Nonalcoholic Steatohepatitis. *Hepatology*, *71*(1), 363-374. https://doi.org/10.1002/hep.30834
115. Pastar, I., Marjanovic, J., Stone, R. C., Chen, V., Burgess, J. L., Mervis, J. S., & Tomic-Canic, M. (2021). Epigenetic regulation of cellular functions in wound healing. *Exp Dermatol*, *30*(8), 1073-1089. https://doi.org/10.1111/exd.14325
116. Patchsung, M., Settayanon, S., Pongpanich, M., Mutirangura, D., Jintarith, P., & Mutirangura, A. (2018). Alu siRNA to increase Alu element methylation and prevent DNA damage. *Epigenomics*, *10*(2), 175-185. https://doi.org/10.2217/epi-2017-0096
117. Patel, S., Srivastava, S., Singh, M. R., & Singh, D. (2019). Mechanistic insight into diabetic wounds: Pathogenesis, molecular targets and treatment strategies to pace wound healing. *Biomed Pharmacother*, *112*, 108615. https://doi.org/10.1016/j.biopha.2019.108615
118. Pegoraro, G., Kubben, N., Wickert, U., Göhler, H., Hoffmann, K., & Misteli, T. (2009). Ageing-related chromatin defects through loss of the NURD complex. *Nat Cell Biol*, *11*(10), 1261-1267. https://doi.org/10.1038/ncb1971
119. Pongpanich, M., Patchsung, M., Thongsroy, J., & Mutirangura, A. (2014). Characteristics of replication-independent endogenous double-strand breaks in Saccharomyces cerevisiae. *BMC Genomics*, *15*(1), 750. https://doi.org/10.1186/1471-2164-15-750

120. Pornthanakasem, W., Kongruttanachok, N., Phuangphairoj, C., Suyarnsestakorn, C., Sanghangthum, T., Oonsiri, S., Ponyeam, W., Thanasupawat, T., Matangkasombut, O., & Mutirangura, A. (2008). LINE-1 methylation status of endogenous DNA double-strand breaks. *Nucleic Acids Res*, *36*(11), 3667-3675. https://doi.org/10.1093/nar/gkn261
121. Ramamoorth, M., & Narvekar, A. (2015). Non viral vectors in gene therapy- an overview. *J Clin Diagn Res*, *9*(1), Ge01-06. https://doi.org/10.7860/jcdr/2015/10443.5394
122. Reiber, G. E., Lipsky, B. A., & Gibbons, G. W. (1998). The burden of diabetic foot ulcers. *Am J Surg*, *176*(2A Suppl), 5s-10s. https://doi.org/10.1016/s0002-9610(98)00181-0
123. Rerkasem, K., Rattanatanyong, P., Rerkasem, A., Wongthanee, A., Rungruengthanakit, K., Mangklabruks, A., & Mutirangura, A. (2015). Higher Alu methylation levels in catch-up growth in twenty-year-old offsprings. *PLoS One*, *10*(3), e0120032. https://doi.org/10.1371/journal.pone.0120032
124. Riedel, U., Schüßler, E., Härtel, D., Keiler, A., Nestoris, S., & Stege, H. (2020). [Wound treatment in diabetes patients and diabetic foot ulcers]. *Hautarzt*, *71*(11), 835-842. https://doi.org/10.1007/s00105-020-04699-9 (Wundbehandlung bei Diabetes und diabetischem Fußulkus.)
125. Rogulj, D., El Aklouk, I., Konjevoda, P., Ljubić, S., Pibernik Okanović, M., Barbir, A., Luburić, M., Radman, M., Budinski, N., & Vučić Lovrenčić, M. (2017). Age-dependent systemic DNA damage in early Type 2 Diabetes mellitus. *Acta Biochim Pol*, *64*(2), 233-238. https://doi.org/10.18388/abp.2016_1313
126. Schafer, M., & Werner, S. (2008). Oxidative stress in normal and impaired wound repair. *Pharmacol Res*, *58*(2), 165-171. https://doi.org/10.1016/j.phrs.2008.06.004
127. Thewjitcharoen, Y., Sripatpong, J., Krittiyawong, S., Porramatikul, S., Srikummoon, T., Mahaudomporn, S., Butadej, S., Nakasatien, S., & Himathongkam, T. (2020). Changing the patterns of hospitalized diabetic foot ulcer (DFU) over a 5-year period in a multi-disciplinary setting in Thailand. *BMC Endocr Disord*, *20*(1), 89. https://doi.org/10.1186/s12902-020-00568-7
128. Thongsroy, J., Matangkasombut, O., Thongnak, A., Rattanatanyong, P., Jirawatnotai, S., & Mutirangura, A. (2013). Replication-independent endogenous DNA double-strand breaks in Saccharomyces cerevisiae model. *PLoS One*, *8*(8), e72706. https://doi.org/10.1371/journal.pone.0072706
129. Thongsroy, J., Patchsung, M., & Mutirangura, A. (2017). The association between Alu hypomethylation and severity of type 2 diabetes mellitus. *Clin Epigenetics*, *9*, 93. https://doi.org/10.1186/s13148-017-0395-6
130. Thongsroy, J., Patchsung, M., Pongpanich, M., Settayanon, S., & Mutirangura, A. (2018). Reduction in replication-independent endogenous DNA double-strand breaks promotes genomic instability during chronological aging in yeast. *Faseb j*, fj201800218RR. https://doi.org/10.1096/fj.201800218RR
131. Wu, H., Li, F., Shao, W., Gao, J., & Ling, D. (2019). Promoting Angiogenesis in Oxidative Diabetic Wound Microenvironment Using a Nanozyme-Reinforced Self-Protecting Hydrogel. *ACS Cent Sci*, *5*(3), 477-485. https://doi.org/10.1021/acscentsci.8b00850
132. Yao, Z., Huang, Y., Luo, G., Wu, J., & He, W. (2014). A biological membrane-based novel excisional wound-splinting model in mice (With video). *Burns Trauma*, *2*(4), 196-200. https://doi.org/10.4103/2321-3868.143625
133. Yin, H., Kanasty, R. L., Eltoukhy, A. A., Vegas, A. J., Dorkin, J. R., & Anderson, D. G. (2014). Non-viral vectors for gene-based therapy. *Nat Rev Genet*, *15*(8), 541-555. https://doi.org/10.1038/nrg3763

134. Zhang, H., & Zhu, J. K. (2011). RNA-directed DNA methylation. *Curr Opin Plant Biol*, *14*(2), 142-147. https://doi.org/10.1016/j.pbi.2011.02.003
135. Zhao, D., Wang, C. Q., Zhuo, R. X., & Cheng, S. X. (2014). Modification of nanostructured calcium carbonate for efficient gene delivery. *Colloids Surf B Biointerfaces*, *118*, 111-116. https://doi.org/10.1016/j.colsurfb.2014.03.007

จุฬาลงกรณ์มหาวิทยาลัย
CHULALONGKORN UNIVERSITY

REFERENCES

จุฬาลงกรณ์มหาวิทยาลัย
Chulalongkorn University

จุฬาลงกรณ์มหาวิทยาลัย
Chulalongkorn University

VITA

NAME	Sakawdaurn Yasom
DATE OF BIRTH	19 September 1981
PLACE OF BIRTH	Chiang Mai, Thailand
INSTITUTIONS ATTENDED	Faculty of Medical Technology, Mahidol University Faculty of Medicine, Chiang Mai University Graduate School, Chulalongkorn University
HOME ADDRESS	63/2 M2 Sankampheang Road, Sankampheang, Chiang Mai, Thailand, 50130
PUBLICATION	1. Yasom S, Khumsri W, Boonsongserm P, Kitkumthorn N, Ruangvejvorachai P, Sooksamran A, Wanotayan R, Mutirangura A. B1 siRNA increases de novo DNA methylation in B1 elements and promotes wound healing in diabetic rats. Front. Cell Dev. Biol., 19 January 2022 | https://doi.org/10.3389/fcell.2021.802024 2. Yasom S, Watcharanurak P, Bhummaphan N, Thongsroy J, Puttipanyalears C, Settayanon S, Chalertpet K, Khumsri W, Kongkaew A, Patchsung M, Siriwattanakankul C, Pongpanich M, Pin-on P, Jindatip D, Wanotayan R, Odton M, Supasai S, Tun Oo T, Arunsak B, Pratchayasakul W, Chattipakorn N, Chattipakorn S, Mutirangura A. The role of HMGB1-produced DNA gaps in DNA protection and aging biomarker reversal. FASEB BioAdvances. Accepted 1 March 2022. 3. Thiennimitr P#, Yasom S#, Tunapong W, Chunchai T, Wanchai K, et al. Lactobacillus paracasei HII01, xylooligosaccharides, and synbiotics reduce gut disturbance in obese rats. Nutrition. 2018 Oct;54: 40-47. doi: 10.1016/j.nut.2018.03.005. (#co-first author, distributed equally) 4. Wutthi-In M, Cheevadhanarak S, Yasom S, Kerdphoo S, Thiennimitr P, et al. Gut Microbiota Profiles of Treated Metabolic Syndrome Patients and their Relationship with Metabolic Health. Sci Rep. 2020 Jun 22;10(1):10085. doi: 10.1038/s41598-020-67078-3. 5. Eaimworawuthikul S, Tunapong W, Chunchai T, Yasom S, Wanchai K, et al. Effects of probiotics, prebiotics or synbiotics on jawbone in obese-insulin resistant rats. Eur J Nutr. 2019 Oct;58(7):2801-2810. doi: 10.1007/s00394-018-1829-4 6. Wanchai K, Yasom S, Tunapong W, Chunchai T, Eaimworawuthikul S, et al. Probiotic Lactobacillus paracasei HII01 protects rats against obese-insulin

จุฬาลงกรณ์มหาวิทยาลัย
Chulalongkorn University

resistance-induced kidney injury and impaired renal organic anion transporter 3 function. Clin Sci (Lond). 2018 Jul 31;132(14):1545-1563. doi: 10.1042/CS20180148.
7. Tunapong W, Apaijai N, Yasom S, Tanajak P, Wanchai K, et al. Chronic treatment with prebiotics, probiotics and synbiotics attenuated cardiac dysfunction by improving cardiac mitochondrial dysfunction in male obese insulin-resistant rats. Eur J Nutr. 2018 Sep;57(6):2091-2104. doi: 10.1007/s00394-017-1482-3.
8. Wanchai K, Yasom S, Tunapong W, Chunchai T, Thiennimitr P, et al. Prebiotic prevents impaired kidney and renal Oat3 functions in obese rats. J Endocrinol. 2018 Apr;237(1):29-42. doi: 10.1530/JOE-17-0471.
9. Chunchai T, Thunapong W, Yasom S, Wanchai K, Eaimworawuthikul S, et al. Decreased microglial activation through gut-brain axis by prebiotics, probiotics, or synbiotics effectively restored cognitive function in obese-insulin resistant rats. J Neuroinflammation. 2018 Jan 9;15(1):11. doi: 10.1186/s12974-018-1055-2.

จุฬาลงกรณ์มหาวิทยาลัย
Chulalongkorn University